Longitudinal Investigation of *In Vivo* Tibiofemoral Kinematics, Cartilage Contact, and Cartilage Composition Prior to and following Anterior Cruciate Ligament Reconstruction

By

Michael F. Vignos

A dissertation submitted in partial fulfillment of

the requirements for the degree of

Doctor of Philosophy

(Mechanical Engineering)

at the

UNIVERSITY OF WISCONSIN-MADISON

2018

Date of final oral examination: August 24, 2018

This dissertation is approved by the following members of the Final Oral Committee:

Darryl G. Thelen, Professor, Mechanical Engineering

Melih Eriten, Associate Professor, Mechanical Engineering

Corinne R. Henak, Assistant Professor, Mechanical Engineering

Geoffrey S. Baer, Associate Professor, Orthopedics and Rehabilitation

Richard Kijowski, Professor, Radiology

Acknowledgements

I would be lying if I said that writing the Acknowledgements section was not one of my favorite parts of writing my undergraduate thesis, Master's thesis, and, now, my PhD dissertation. This is because, while I have learned and grown a ton through my research and PhD coursework, the most rewarding and enriching part of my time in graduate school has been interacting and working with such a large number of motivated, talented, and helpful individuals. I could think of nothing better than having the opportunity to thank these individuals as I complete my dissertation.

First, I would like to thank my thesis committee members, Corinne Henak, Richard Kijowski, Geoffrey Baer, and Melih Eriten for their constant support and guidance throughout this research.

I would also like to thank every member of the UW Neuromuscular Biomechanics Laboratory for their constant support, assistance, and generosity throughout my time in graduate school. I would like to extend a special thank you to Jarred Kaiser for his mentorship and assistance in learning the skills needed to get this research started. I am thankful for the numerous professional development opportunities Jarred provided me early in graduate school and for the seamless transition he created with this ACL research. I would also like to extend a special thank you to everyone that has been involved in KneeMOS, including Colin Smith, Josh Roth, Rachel Lenhart, Scott Brandon, Moria Bittmann, Milad Rakhsha, Allison Clouthier, and Mariska Wesseling. Some of the best feedback I have gotten on my research has been during our weekly meetings and I will forever be thankful for the opportunity to work with all of you. I would also like to give a special thank you to Samuel Acuña, Jack Martin, Sarah Denning, Dylan Schmitz, Ana Ebrahimi, John Zunker, Emily Keuler, and Carrie Francis. Experiencing graduate school with

all of you has been a blast and I will forever be thankful for the numerous First Fridays, conference travel, and great times we had.

I would also like to thank the numerous individuals that directly helped me with my graduate research. Particularly, I would like to thank all of the former undergraduate and Master's students that were always willing to help me with data collection with a special thank you to Isaac Loegering, Maddie Pechmann, James Hermus, and Michael Schmidt. I would also like to extend a special thank you to Josh Roth for the numerous times he helped me with data collection, even when he was busy with his own work. I would also like to thank the MRI techs, Kelli Hellenbrand, Sara John, Jenelle Fuller, Haley Cilliers, and Marti Garcia, and the research coordinators, Frances Theisen, and Jan Yakey, for their numerous hours helping me with data collection, subject recruitment, and subject scheduling. I very much appreciated their flexibility whenever something went wrong during testing and their willingness to let testing run long to make sure I collected all of my data.

I would also like to thank all of the professors and students of the other UW biomechanics research labs. Having so many professors and students around that are interested in biomechanics research, willing to discuss my research, and willing to teach me about their research has been a blast. I would also like to thank you all for your willingness to take a break from your research to come hang out with me at First Fridays.

I would like to thank my family and friends for their constant love, support, and endless supply of good times during my time in graduate school. While living somewhat far away limited the amount of time we could spend together, the numerous holidays, trips, and long weekends we spent together were always a great break from my time in school.

I also need to give a special thank you to my parents for their unwavering love and support during my time in graduate school and over the past 28 years. From a young age, they have served as amazing examples of what you can accomplish through hard work, dedication, and a willingness to go the extra mile. I can honestly say that I would not be where I am today without them.

One of the most important thank yous I need to give is to my fiancée, and very soon to be wife, Erica. It would be ridiculous for me to try to put into words what her love, support, friendship, and motivation has meant to me over the past eight years we have been together. She is truly one of the hardest working, considerate, and caring people I know and she serves as a constant source of inspiration for me every day. I can honestly say that my accomplishments over the past eight years have been as much due to her hard work, as they have been my own.

Finally, I would like to thank my advisor Darryl Thelen for his countless hours of mentorship, professional development, and help with research. While Darryl has a great work-life balance, he was always willing to give a couple of extra hours to help with last minute abstract and paper submissions and to help with pressing research challenges. Additionally, I am extremely thankful for all the opportunities Darryl has given me to travel during my time in graduate school. Whether it was Columbus, OH or Brisbane, Australia, I will forever be grateful for Darryl's willingness to let me travel to conferences. As an Ohio State University graduate, choosing a Michigan State and Michigan graduate as my advisor could have been a risky move. But making that move has been one of the best decisions in my life.

Funding Support

I gratefully acknowledge the following funding support for my dissertation research and travel:

- NSF Graduate Research Fellowship Program (Grant No. DGE-1256259 and DGE-1747503)
- National Institutes of Health (Grant No. EB015410 and AR056201)
- University of Wisconsin Graduate School Physical Sciences Fellowship
- University of Wisconsin-Madison Graduate School Student Research Travel Grant
- Delsys Student Travel Grant
- OpenSim Developer's Workshop Travel Grant
- OpenSim Advanced User Workshop Travel Grant

Abstract

Anterior cruciate ligament reconstructions (ACLR) are typically successful at restoring knee stability and returning patients to previous levels of activity. However, long-term outcomes of ACLR are concerning given that 10-15 years post-surgery >50% of patients exhibit signs of osteoarthritis. It has been theorized that the high rate of osteoarthritis in ACLR knees is partially due to residual abnormal knee mechanics that exist following surgery. Indeed, previous studies have observed abnormal kinematics and cartilage contact patterns in ACLR knees. However, there is currently limited evidence of a direct link between abnormal knee mechanics and cartilage degeneration in this population. Thus, the first primary objective of this thesis was to investigate the link between abnormal knee mechanics and biomarkers of cartilage degeneration through a combination of static, dynamic, and quantitative (i.e. mcDESPOT) magnetic resonance imaging. The second primary objective was to then assess the contribution of ACLR surgical factors to abnormal post-operative knee mechanics. We first investigated the link between mcDESPOT relaxation parameters and cartilage material properties to further validate using the mcDESPOT sequence to track changes in cartilage composition. We then investigated longitudinal changes in tibiofemoral kinematics, cartilage contact, and cartilage composition in ACLR knees. We determined that, within the medial tibial plateau, reductions in the fraction of water bound to proteoglycan were correlated to increased cartilage contact. This indicated that restoring normative knee mechanics is critical to mitigate the risk of cartilage degeneration in ACLR knees. Through the use of experimental and computational modeling methods, we then determined that non-anatomic ACL graft tunnel placement can lead to abnormal kinematics and cartilage loading during functional movement. We also observed that ACL graft stiffness and initial tension may contribute to abnormal knee mechanics. However, further work is needed to assess the relative

contribution of each surgical factor to post-operative knee mechanics. Finally, we confirmed that the semi-automated algorithm used to segment articular cartilage, in this thesis, produced accurate and repeatable measures of cartilage thickness. We conclude that optimal graft tunnel placement is critical to restore normative knee mechanics, and, thus, to mitigate the risk of early osteoarthritis development in ACLR knees.

Table of Contents

List of Figures

Chapter 1

Chapter 2

Chapter 3

Chapter 4

Chapter 5

Appendix A

List of Tables

Chapter 1

Chapter 3

Chapter 4

Chapter 5

Introduction to the Thesis

The anterior cruciate ligament (ACL) is one of the four major ligaments within the knee joint and provides the primary restraint to anterior translation and secondary restraint to internal rotation of the tibia relative to the femur. Ruptures of the ACL are very common with >200,000 occurring in the United States each year [1] and with 70% of these being non-contact injuries [2]. The primary treatment for this injury is an ACL reconstruction (ACLR), which has the short-term goal of restoring knee stability and allowing patients to return to previous levels of activity. ACLR is typically successful at achieving this short-term goal with 82% to 95% of patients reporting good to excellent outcomes at 2 to 5 years post-surgery [3–6]. However, the long-term outcomes of ACLR are less successful with >50% of patients exhibiting radiographic signs of osteoarthritis (OA) at 10 to 15 years following surgery [7]. This is of great concern given that the highest incidence of ACLR is in individuals between 15 and 25 years old [8], which means these patients will have extended periods of pain and debilitation before a total knee arthroplasty becomes feasible. Additionally, even with relatively recent modifications to surgical techniques, the rate of OA development following ACL injury has not decreased over the past 25 years [9]. This suggests that there is the potential to improve the current approaches to ACLR to mitigate the risk of early OA development and improve long-term outcomes of ACL injury patients.

Surgical reconstruction of the ACL is performed arthroscopically and consists of an orthopedic surgeon drilling a tunnel in the tibia and the femur, threading an ACL graft between the tunnels, and fixing the graft in place, with the fixation method typically dependent on the type of graft used. With this procedure, there are a number of factors that can be varied including the location of the femoral and tibial tunnels, graft type, number of bundles used for the graft, amount of pretension applied to the graft, and the knee flexion angle at which the graft is fixed in place.

Previous cadaveric studies have shown that these surgical factors impact post-operative knee kinematics [10–17], although there is still extensive debate on the 'correct' choice for each factor. This is likely due, in part, to a limited understanding of how these surgical factors affect *in vivo* knee mechanics following reconstruction.

One of the commonly debated ACLR surgical factors is the ideal placement of the ACL graft tunnels based on the relationship between graft tunnel location and abnormal tibiofemoral kinematics. Cadaveric studies have shown that variations in femoral tunnel location can lead to altered anterior tibial translation [15, 18]. Additionally, the angle of the graft relative to the tibial plateau has been linked to altered passive anterior and rotational knee laxities [16, 17]. *In vivo* investigations have shown that graft tunnel location also affects tibiofemoral kinematics during functional movements [19–21]. For example, Abebe et al. observed that variations in femoral tunnel placement are associated with greater anterior tibial translation, medial tibial translation, and internal tibial rotation in ACLR knees during a quasi-static lunge [19, 22]. However, in experimental studies it is difficult to decouple the effect of ACL graft geometry from other surgical factors, such as graft type [23], stiffness [24], and initial tension [25, 26] which may also influence knee behavior.

Probabilistic musculoskeletal modeling can be used to investigate the causal influence of multiple surgical factors on internal joint mechanics [27–30]. For example, Dhaher et al. [28] used a highly detailed knee model to simulate an ACLR using a bone—patellar tendon—bone autograft. This study found that anterior joint laxity is primarily dependent on tunnel placement and secondarily on graft initial tension. Additional modeling studies found that the ACL femoral attachment location, stiffness, and initial tension influence joint laxity and ACL loading under an anteriorly applied tibial load [29, 30]. However, these previous studies did not provide a direct

comparison to experimental measurements, and it remains unclear how variations in these ACLR surgical factors influence post-operative cartilage loading.

This link between ACLR surgical factors and cartilage loading is of interest, given that it has been theorized that the high rate of OA development in ACLR knees is partially due to residual abnormal knee mechanics that exist following surgery [31, 32]. Cartilage is a multi-phasic tissue composed of water and a matrix of type II collagen, proteoglycans, and chondrocytes. It is well adapted to normal loading patterns with the thickest regions corresponding to those that are directly loaded during walking [33]. Additionally, during development, normal cartilage loading leads to increased proteoglycan content, increased cartilage thickness, and improved stiffness [34–36]. However, mature cartilage is less adaptive and, thus, altered loading patterns have been hypothesized to induce a catabolic response within the tissue and initiate OA development [31]. This theory has been supported by previous *in vitro* cartilage testing and *in vivo* animal models showing that abnormal cartilage loading can lead to the initiation and progression of cartilage degeneration [37–39]. Indeed, previous dynamic imaging studies have reported abnormal tibiofemoral kinematics and cartilage contact patterns in ACLR knees. Specifically, a bias towards external tibial rotation has been observed during a range of tasks [40–42], leading to a posterior-lateral shift in cartilage contact location on the tibial plateaus [43, 44]. However, there is currently limited evidence that these abnormal knee mechanics are directly linked to OA development in ACLR knees.

Assessing this potential link between abnormal knee mechanics and OA development is difficult due to the slow progression of changes in cartilage morphology. However, recent advancements in magnetic resonance (MR) imaging have allowed for non-invasive, quantitative assessments of cartilage composition. Given that changes in composition occur prior to

morphological changes in the cartilage tissue [45], use of quantitative MR imaging presents the potential to detect the initiation of cartilage degeneration shortly after ACLR. The most commonly utilized quantitative MR techniques aim to measure the T1ρ and T2 relaxation rates of the cartilage tissue, based on the reported relationship of these metrics with the proteoglycan content [46] and the organization of the collagen fiber network [47], respectively. A recently developed multi-component T2 mapping technique, mcDESPOT [48–50], allows for improved specificity by decomposing the T2 relaxation rate into the fast and slow relaxation components. These components are thought to be linked to the fraction of water tightly bound to proteoglycan (i.e. fraction of bound water, FBW) and the bulk water associated with the collagen matrix, respectively.

Use of these quantitative MR imaging techniques has allowed for the detection of changes in cartilage composition in ACLR knees, which occurs early in the pathogenesis of OA. For example, increases in T1ρ and T2 relaxation rates have been reported at 6 and 12 months following ACLR [51]. Additionally, Kaiser et al. found a significantly lower FBW in ACLR knees at approximately two years post-reconstruction [44]. These findings have led to numerous studies aimed at further validating the potential to assess cartilage health with MR imaging by investigating the link between quantitative MR relaxation parameters (e.g. T1, T1ρ, and T2) and cartilage mechanical properties [52–60]. While these investigations have typically shown modest associations between these quantitative MR parameters and cartilage properties, disagreement across studies has prevented the development of a clear link between these parameters and cartilage health. Given that the mcDESPOT sequence provides improved specificity for macromolecules within the cartilage tissue [61, 62] , this quantitative MR imaging technique may provide a more clear relationship with cartilage mechanical properties.

The first goal of this thesis was to directly assess the link between abnormal knee mechanics and early signs of cartilage degeneration in ACLR knees. The second goal was to then investigate the potential contribution of ACLR surgical technique to long-term patient outcomes by assessing the effect of ACLR surgical factors on post-operative knee mechanics. The first chapter provides further validation of the ability to use quantitative MR imaging as a means of assessing cartilage health by investigating the relationship between quantitative MR relaxation parameters and cartilage mechanical properties. Chapter 2 then uses a combination of quantitative and dynamic MR imaging to assess the direct link between longitudinal changes in cartilage composition and abnormal knee mechanics in ACLR knees. Chapters 3 and 4 then begin to investigate the link between ACLR surgical technique and long-term patient outcomes by providing experimental and computational modeling evidence that ACL graft tunnel placement directly influences post-operative knee mechanics. Chapter 5 then assesses the efficiency, accuracy, and reproducibility of a semi-automated segmentation algorithm that was commonly used to create 3D models of the articular cartilage geometry for this thesis. I conclude with a discussion of the primary findings of this thesis and future research directions.

References

1. Sanders TL, Maradit Kremers H, Bryan AJ, et al (2016) Incidence of Anterior Cruciate Ligament Tears and Reconstruction: A 21-Year Population-Based Study. Am J Sports Med 44:1502–1507 . doi: 10.1177/0363546516629944
2. Daniel D, Fritschy D (1994) Anterior cruciate ligament injures. In: Orthopaedic Sports Medicine: Principles and Practice., 2nd ed. Saunders, Philadelphia
3. Otto D, Pinczewski LA, Clingeleffer A, Odell R (1998) Five-year results of single-incision arthroscopic anterior cruciate ligament reconstruction with patellar tendon

autograft. Am J Sports Med 26:181–188

4. Spindler KP, Warren TA, Callison Jr. JC, et al (2005) Clinical outcome at a minimum of five years after reconstruction of the anterior cruciate ligament. J Bone Jt Surg Am 87:1673–1679
5. Bach BR, Tradonsky S, Bojchuk J, et al (1998) Arthroscopically assisted anterior cruciate ligament reconstruction using patellar tendon autograft. Five- to nine-year follow-up evaluation. Am J Sport Med 26:20–9
6. Hanypsiak BT, Spindler KP, Rothrock CR, et al (2008) Twelve-Year Follow-up on Anterior Cruciate Ligament Reconstruction: Long-term Outcomes of Prospectively Studied Osseous and Articular Injuries. Am J Sports Med 36:671–677 . doi: 10.1177/0363546508315468
7. Lohmander LS, Englund PM, Dahl LL, Roos EM (2007) The long-term consequence of anterior cruciate ligament and meniscus injuries: osteoarthritis. Am J Sports Med 35:1756–69 . doi: 10.1177/0363546507307396
8. Griffin LY, Agel J, Albohm MJ, et al (2008) Noncontact anterior cruciate ligament injuries: risk factors and prevention strategies. J Am Acad Orthop Surg 8:141–150
9. Buckwalter JA, Anderson DD, Brown TD, et al (2013) The Roles of Mechanical Stresses in the Pathogenesis of Osteoarthritis: Implications for Treatment of Joint Injuries. Cartilage 4:286–294 . doi: 10.1177/1947603513495889
10. Gulick DT, Yoder HN (2002) Anterior cruciate ligament reconstruction: clinical outcomes of patella tendon and hamstring tendon grafts. J Sports Sci Med 1:63–71
11. Rowden NJ, Sher D, Rogers GJ, Schindhelm K (1997) Anterior Cruciate Ligament Graft Fixation: Initial Comparison of Patellar Tendon and Semitendinosus Autografts in Young

Fresh Cadavers. Am J Sports Med 25:472–478 . doi: 10.1177/036354659702500409

12. Kondo E, MD P, Merican A, et al (2011) Biomechanical Comparison of Anatomic Double-Bundle, Anatomic Single-Bundle, and Nonanatomic Single-Bundle Anterior Cruciate Ligament Reconstructions. Am J Sport Med 39:279–288 . doi: 10.1177/0363546510392350
13. Boylan D, Greis PE, West JR, et al (2003) Effects of initial graft tension on knee stability after anterior cruciate ligament reconstruction using hamstring tendons: A cadaver study. Arthrosc - J Arthrosc Relat Surg 19:700–705 . doi: 10.1016/S0749-8063(03)00400-6
14. Zavras TD, Race A, Amis AA (2005) The effect of femoral attachment location on anterior cruciate ligament reconstruction: Graft tension patterns and restoration of normal anterior-posterior laxity patterns. Knee Surgery, Sport Traumatol Arthrosc 13:92–100 . doi: 10.1007/s00167-004-0541-5
15. Musahl V (2005) Varying Femoral Tunnels Between the Anatomical Footprint and Isometric Positions: Effect on Kinematics of the Anterior Cruciate Ligament-Reconstructed Knee. Am J Sports Med 33:712–718 . doi: 10.1177/0363546504271747
16. Loh JC, Fukuda Y, Tsuda E, et al (2003) Knee stability and graft function following anterior cruciate ligament reconstruction: Comparison between 11 o'clock and 10 o'clock femoral tunnel placement. 2002 Richard O'Connor Award Paper Knee. Arthrosc - J Arthrosc Relat Surg 19:297–304 . doi: 10.1053/jars.2003.50084
17. Brophy RH, Pearle AD (2009) Single-Bundle Anterior Cruciate Ligament Reconstruction: A Comparison of Conventional, Central, and Horizontal Single-Bundle Virtual Graft Positions. Am J Sports Med 37:1317–1323 . doi: 10.1177/0363546509333007
18. Zavras TD, Race A, Bull AMJ, Amis AA (2001) A comparative study of "isometric"

points for anterior cruciate ligament graft attachment. Knee Surgery, Sport Traumatol Arthrosc 9:28–33 . doi: 10.1007/s001670000170

19. Abebe E, Utturkar GM, Taylor DC, et al (2011) The effects of femoral graft placement on in vivo knee kinematics after anterior cruciate ligament reconstruction. J Biomech 44:924–929 . doi: 10.1016/j.jbiomech.2010.11.028

20. Ristanis S, Stergiou N, Siarava E, et al (2009) Effect of femoral tunnel placement for reconstruction of the anterior cruciate ligament on tibial rotation. J Bone Jt Surg - Ser A 91:2151–2158 . doi: 10.2106/JBJS.H.00940

21. Zampeli F, Ntoulia A, Giotis D, et al (2012) Correlation between anterior cruciate ligament graft obliquity and tibial rotation during dynamic pivoting activities in patients with anatomic anterior cruciate ligament reconstruction: An in vivo examination. Arthrosc - J Arthrosc Relat Surg 28:234–246 . doi: 10.1016/j.arthro.2011.08.285

22. Abebe E, Kim JP, Utturkar GM, et al (2011) The effect of femoral tunnel placement on ACL graft orientation and length during in vivo knee flexion. J Biomech 44:1914–1920 . doi: 10.1016/j.jbiomech.2011.04.030

23. Webster KE, Feller JA (2012) The knee adduction moment in hamstring and patellar tendon anterior cruciate ligament reconstructed knees. Knee Surgery, Sport Traumatol Arthrosc 20:2214–2219 . doi: 10.1007/s00167-011-1835-z

24. Suggs J, Wang C, Li G (2003) The effect of graft stiffness on knee joint biomechanics after ACL reconstruction - A 3D computational simulation. Clin Biomech 18:35–43 . doi: 10.1016/S0268-0033(02)00137-7

25. Brady MF, Bradley MP, Fleming BC, et al (2007) Effects of Initial Graft Tension on the Tibiofemoral Compressive Forces and Joint Position After Anterior Cruciate Ligament

Reconstruction. Am J Sports Med 35:395–403 . doi: 10.1177/0363546506294363

26. Nicholas SJ, D'Amato MJ, Mullaney MJ, et al (2004) A Prospectively Randomized Double-Blind Study on the Effect of Initial Graft Tension on Knee Stability After Anterior Cruciate Ligament Reconstruction. Am J Sports Med 32:1–6 . doi: 10.1177/0363546504265924
27. Barry MJ, Kwon TH, Dhaher YY (2010) Probabilistic musculoskeletal modeling of the knee: A preliminary examination of an ACL-reconstruction. 2010 Annu Int Conf IEEE Eng Med Biol Soc EMBC'10 5440–5443 . doi: 10.1109/IEMBS.2010.5626511
28. Dhaher YY, Salehghaffari S, Adouni M (2016) Anterior laxity, graft-tunnel interaction and surgical design variations during anterior cruciate ligament reconstruction: A probabilistic simulation of the surgery. J Biomech. doi: 10.1016/j.jbiomech.2016.07.019
29. Baldwin MA, Laz PJ, Stowe JQ, Rullkoetter PJ (2009) Efficient probabilistic representation of tibiofemoral soft tissue constraint. Comput Methods Biomech Biomed Engin 12:651–659 . doi: 10.1080/10255840902822550
30. Mesfar W, Shirazi-Adl A (2006) Biomechanics of changes in ACL and PCL material properties or prestrains in flexion under muscle force-implications in ligament reconstruction. Comput Methods Biomech Biomed Engin 9:201–209 . doi: 10.1080/10255840600795959
31. Chaudhari AMW, Briant PL, Bevill SL, et al (2008) Knee kinematics, cartilage morphology, and osteoarthritis after ACL injury. Med Sci Sports Exerc 40:215–222 . doi: 10.1249/mss.0b013e31815cbb0e
32. Stergiou N, Ristanis S, Moraiti C, Georgoulis AD (2007) Tibial rotation in anterior cruciate ligament (ACL)-deficient and ACL-reconstructed knees: A theoretical

proposition for the development of osteoarthritis. Sport Med 37:601–613 . doi: 10.2165/00007256-200737070-00004

33. Andriacchi TP, Mundermann AR, Smith L, et al (2004) A Framework for the in Vivo Pathomechanics of Osteoarthritis at the Knee. Ann Biomed Eng 32:447–457
34. Kiviranta I, Tammi M, Jurvelin J, et al (1988) Moderate running exercise augments glycosaminoglycans and thickness of articular cartilage in the knee joint of young beagle dogs. J Orthop Res 6:188–195 . doi: 10.1002/jor.1100060205
35. Jurvelin J, Kiviranta I, Tammi M, Helminen HJ (1986) Effect of Physical Exercise on Indentation Stiffness of Articular Cartilage in the Canine Knee. Int J Sport Med 7:106–110
36. Saamanen AM, Tammi M, Kiviranta I, Helminen HJ (1988) Running Exercise as a Modulator of Proteoglycan Matrix in the Articular Cartilage of Young Rabbits. Int J Sport Med 9:127–132
37. Griffin TM, Guilak F (2005) The Role of Mechanical Loading in the Onset and Progression of Osteoarthritis. Exerc Sport Sci Rev 33:195–200 . doi: 10.1097/00003677-200510000-00008
38. Beveridge JE, Heard BJ, Shrive NG, Frank CB (2013) Tibiofemoral centroid velocity correlates more consistently with cartilage damage than does contact path length in two ovine models of stifle injury. J Orthop Res 31:1745–1756 . doi: 10.1002/jor.22429
39. Anderst WJ, Tashman S (2009) The association between velocity of the center of closest proximity on subchondral bones and osteoarthritis progression. J Orthop Res 27:71–77 . doi: 10.1002/jor.20702
40. Tashman S, Collon D, Anderson K, et al (2004) Abnormal Rotational Knee Motion

During Running After Anterior Cruciate Ligament Reconstruction. Am J Sports Med 32:975–983 . doi: 10.1177/0363546503261709

41. Hofbauer M, Thorhauer ED, Abebe E, et al (2014) Altered Tibiofemoral Kinematics in the Affected Knee and Compensatory Changes in the Contralateral Knee After Anterior Cruciate Ligament Reconstruction. Am J Sports Med 42:2715–2721 . doi: 10.1177/0363546514549444
42. Kaiser JM, Vignos MF, Kijowski R, et al (2017) Effect of Loading on In Vivo Tibiofemoral and Patellofemoral Kinematics of Healthy and ACL-Reconstructed Knees. Am J Sports Med 45: . doi: 10.1177/0363546517724417
43. Hosseini A, Van De Velde S, Gill TJ, Li G (2012) Tibiofemoral Cartilage Contact Biomechanics in Patients after Reconstruction of a Ruptured Anterior Cruciate Ligament. 1781–1788 . doi: 10.1002/jor.22122
44. Kaiser J, Vignos MF, Liu F, et al (2016) American Society of Biomechanics Clinical Biomechanics Award 2015: MRI assessments of cartilage mechanics, morphology and composition following reconstruction of the anterior cruciate ligament. Clin Biomech 34: . doi: 10.1016/j.clinbiomech.2016.03.007
45. Buckwalter JA, Lane NE (1997) Current Concepts: Athletics and Osteoarthritis. Am J Sports Med 25:873–881
46. Duvvuri U, Kudchodkar S, Reddy R, Leigh JS (2002) T1rho relaxation can assess longitudinal proteoglycan loss from articular cartilage in vitro. Osteoarthr Cartil 10:838–844 . doi: 10.1053/joca.2002.0826
47. Mosher TJ, Dardzinski BJ, Smith MB (2000) Human Articular Cartilage: Influence of Aging and Early Symptomatic Degenetation on the Spatial Variation of T2 - Preliminary

Findings at 3T. Radiology 214:256–266

48. Deoni SCL, Rutt BK, Arun T, et al (2008) Gleaning Multicomponent T1 and T2 Information From Steady-State Imaging Data. Magn Reson Med 60:1372–1387 . doi: 10.1002/mrm.21704

49. Liu F, Chaudhary R, Hurley SA, et al (2014) Rapid Multicomponent T2 Analysis of the Articular Cartilage of the Human Knee Joint at 3.0T. J Magn Reson Imaging 39:1191–1197 . doi: 10.1002/jmri.24290

50. Liu F, Choi KW, Samsonov A, et al (2015) Articular Cartilage of the Human Knee Joint: In Vivo Multicomponent T2 Analysis at 3.0 T. Radiology 277:477–488 . doi: https://doi-org.ezproxy.library.wisc.edu/10.1148/radiol.2015142201

51. Pedoia V, Su F, Amano K, et al (2017) Analysis of the articular cartilage T1ρ and T2 relaxation times changes after ACL reconstruction in injured and contralateral knees and relationships with bone shape. J Orthop Res 35:707–717 . doi: 10.1002/jor.23398

52. Kurkijärvi JE, Nissi MJ, Kiviranta I, et al (2004) Delayed gadolinium-enhanced MRI of cartilage (dGEMRIC) and T2 characteristics of human knee articular cartilage: Topographical variation and relationships to mechanical properties. Magn Reson Med 52:41–46 . doi: 10.1002/mrm.20104

53. Nieminen MT, Töyräs J, Laasanen MS, et al (2004) Prediction of biomechanical properties of articular cartilage with quantitative magnetic resonance imaging. J Biomech 37:321–328 . doi: 10.1016/S0021-9290(03)00291-4

54. Samosky JT, Burstein D, Grimson WE, et al (2005) Spatially-localized correlation of dGEMRIC-measured GAG distribution and mechanical stiffness in the human tibial plateau. J Orthop Res 23:93–101 . doi: 10.1016/j.orthres.2004.05.008

55. Lammentausta E, Kiviranta P, Nissi M., et al (2006) T2 Relaxation Time and Delayed Gadolinium-Enhanced MRI of Cartilage (dGEMRIC) of Human Patellar Cartilage at 1.5 T and 9.4 T: Relationships with Tissue Mechanical Properties. J Orthop Res MARCH 366–374 . doi: 10.1002/jor

56. Wheaton AJ, Dodge GR, Elliott DM, et al (2005) Quantification of cartilage biomechanical and biochemical properties via T1rho magnetic resonance imaging. Magn Reson Med 54:1087–1093 . doi: 10.1002/mrm.20678

57. Miyata S, Numano T, Homma K, et al (2007) Feasibility of noninvasive evaluation of biophysical properties of tissue-engineered cartilage by using quantitative MRI. J Biomech 40:2990–2998 . doi: 10.1016/j.jbiomech.2007.02.002

58. Nissi MJ, Rieppo J, Töyräs J, et al (2007) Estimation of mechanical properties of articular cartilage with MRI - dGEMRIC, T2 and T1 imaging in different species with variable stages of maturation. Osteoarthr Cartil 15:1141–1148 . doi: 10.1016/j.joca.2007.03.018

59. Tang SY, Souza RB, Ries M, et al (2011) Local tissue properties of human osteoarthritic cartilage correlate with magnetic resonance T1rho relaxation times. J Orthop Res 29:1312–9 . doi: 10.1002/jor.21381

60. Rautiainen J, Nissi MJ, Salo E-N, et al (2014) Multiparametric MRI assessment of human articular cartilage degeneration: Correlation with quantitative histology and mechanical properties. Magn Reson Med 00:249–259 . doi: 10.1002/mrm.25401

61. Reiter DA, Roque RA, Lin PC, et al (2011) Mapping proteoglycan-bound water in cartilage: Improved specificity of matrix assessment using multiexponential transverse relaxation analysis. Magn Reson Med 65:377–384 . doi: 10.1002/mrm.22673

62. Reiter DA, Roque RA, Lin P, et al (2011) Improved specificity of cartilage matrix

evaluation using multiexponential transverse relaxation analysis applied to pathomimetically degraded cartilage. NMR Biomed 24:1286–1294 . doi: 10.1002/nbm.1690.Improved

63. DeFrate LE (2017) The effects of ACL graft placement on in vivo knee function and cartilage thickness distributions. J Orthop Res 1–34 . doi: 10.1002/jor.23541

64. Defrate LE, Papannagari R, Gill TJ, et al (2006) The 6 degrees of freedom kinematics of the knee after anterior cruciate ligament deficiency: An in vivo imaging analysis. Am J Sports Med 34:1240–1246 . doi: 10.1177/0363546506287299

65. Georgoulis AD, Papadonikolakis A, Papageorgiou CD, et al (2003) Three-dimensional tibiofemoral kinematics of the anterior cruciate ligament-deficient and reconstructed knee during walking. Am J Sports Med 31:75–9

66. Scanlan SF, Chaudhari AMW, Dyrby CO, Andriacchi TP (2010) Differences in tibial rotation during walking in ACL reconstructed and healthy contralateral knees. J Biomech 43:1817–1822 . doi: 10.1016/j.jbiomech.2010.02.010

67. Li X, Kuo D, Theologis A, et al (2011) Cartilage in anterior cruciate ligament-reconstructed knees: MR imaging T1rho and T2--initial experience with 1-year follow-up. Radiology 258:505–14 . doi: 10.1148/radiol.10101006

Chapter 1: Cartilage Biphasic Material Properties are Correlated with Measures of Cartilage Composition Assessed via Quantitative MR Imaging at 3.0T

Michael F. Vignos, Matthew Grondin, Fang Liu, Richard Kijowski, Darryl G. Thelen, Corinne R. Henak

Abstract

High-fidelity computational models of articular cartilage are becoming increasingly popular for studying the initiation and progression of osteoarthritis. However, the predictions of such models are sensitive to the assigned cartilage material properties. Thus, the primary goal of this work was to assess the potential of using quantitative magnetic resonance (MR) imaging within a 3.0T scanner, specifically with a multicomponent-driven equilibrium single-shot observation of T1 and T2 (mcDESPOT) sequence, as a non-invasive method to measure cartilage biphasic material properties. In this study, we performed MR imaging with a mcDESPOT sequence of tibial and femoral cartilage resections from one cadaveric knee to generate maps of the T2 relaxation parameters (i.e. T2, $T2_{short}$, and $T2_{long}$) and the fraction of water bound to proteoglycan. We then extracted 12 cartilage samples from the resections and tested each in confined compression to assess the aggregate compressive modulus and hydraulic permeability. We then computed the correlation between the mcDESPOT parameters and the material properties of the cartilage samples ($\alpha = 0.05$). We found that the aggregate modulus was associated with the fraction of water bound to proteoglycan ($R = 0.67$, $P = 0.018$) and the hydraulic permeability was associated with the each of the T2 components (i.e. T2, $T2_{short}$, and $T2_{long}$, $R = 0.64$, 0.53, and 0.68, respectively, and $P = 0.025$, 0.027, and 0.015, respectively). The ability to assess these relationships within a clinical MR scanner suggests that the mcDESPOT sequence may be useful

when developing subject-specific models of human articular cartilage and, thus, may improve our ability to study osteoarthritis development.

1. Introduction

Osteoarthritis (OA) is a painful and debilitating degenerative joint that leads to disability and a reduced quality of life. Recent estimates indicate that the incidence of OA is on the rise, with an increase from 21 million US adults with OA in 1995 to an estimated 27 million in 2005.[1] While it was previously thought that OA was simply a 'wear and tear' disease, it is now known that the initiation and progression of OA is multifactorial and, thus, dependent on a wide range of mechanical,[2,3] inflammatory,[4] and age-related[5–7] changes that give rise to articular cartilage degeneration. These system level changes give rise to the degeneration of the cartilage microstructure, with loss of proteoglycan content and disorganization of the collagen matrix,[8] leading to a loss in the load-bearing capacity of the articular cartilage and, in turn, leading to further degeneration. This complexity and multi-scale nature of the pathogenesis of OA motivates the need to investigate the sensitivity of cartilage microstructure damage to changes in these individual factors. However, in *in vivo* experiments, it is difficult to isolate the effect of these individual factors on the initiation and progression of cartilage degeneration.

Recent developments in computational modeling have provided the ability to investigate the effect of system-level changes on cartilage mechanics and the risk for cartilage degeneration. For example, previous studies have coupled highly-detailed finite element models with a cartilage damage algorithm to show that changes in body weight and cartilage loading patterns can induce cartilage degeneration patterns observed in OA.[9,10] Additional modeling studies have shown that simulated reductions in proteoglycan content and collagen organization, which occur with aging,[7]

can induce OA progression.[11] However, previous work has also shown that the predictions of cartilage finite element models are sensitive to the assigned mechanical properties.[12–14] Thus, accurate characterization of these properties is necessary to extend these general insights to patient-specific investigations. This presents a need for a non-invasive method to accurately measure cartilage mechanical properties.

Quantitative magnetic resonance (MR) imaging has become an increasingly common means for non-invasively assessing cartilage composition. This has led to many investigations of the potential of using quantitative MR imaging to predict cartilage mechanical properties. Numerous studies have investigated the correlation between cartilage mechanical properties and quantitative MR relaxation parameters, with T1, T1ρ, T2, and delayed gadolinium-enhanced MRI of cartilage (dGEMRIC) mapping being the most commonly used.[15–23] While these investigations have typically shown modest predictions of mechanical properties, disagreement across studies have limited the feasibility to use these quantitative MR techniques for assessing subject-specific material properties. A recently developed multi-component T2 mapping technique (i.e. a multicomponent-driven equilibrium single-shot observation of T1 and T2 sequence, mcDESPOT[24–26]), allows for improved specificity by decomposing the T2 relaxation rate into fast- and slow-relaxation components. These components are thought to be linked to the water tightly bound to proteoglycan and the bulk water loosely associated with the collagen matrix. Additionally, this technique provides a measure of the fraction of water bound to proteoglycan (i.e. fraction of bound water, FBW), which has been used to detect compositional changes in cartilage tissue.[27] Thus, this sequence may allow for more accurate characterization of the cartilage mechanical properties. Additionally, previous studies have typically been performed at high MR field strengths, thus limiting the potential to apply these findings to a human subject population.

The goal of this study was to investigate the capability of predicting mechanical properties of human cartilage tissue using quantitative MR relaxation parameters assessed within a 3.0 T clinical MR scanner. Accordingly, the first objective was to obtain measures of the single component T2 relaxation parameter (i.e. T2), the multi-component T2 relaxation parameters (i.e. $T2_{short}$ and $T2_{long}$), the fraction of water bound to proteoglycan (i.e. fraction of bound water, FBW), and the biphasic material properties assessed via confined compression of cartilage tissue samples. The second objective was to then investigate the correlation between the quantitative MR parameters and the measured cartilage material properties. We hypothesized that the aggregate compressive modulus of the cartilage would be most tightly linked to the FBW, due to its association with the proteoglycan content, and that the hydraulic permeability would be most tightly linked to single component T2 parameter, due to its association with collagen organization.

2. Methods

2.1 Static MR Imaging

The distal femoral condyles and tibial plateau were resected from one fresh, frozen human cadaveric knee (M, 59 years, 69.9 kg, 1.88 m); (Science Care, Inc., Phoenix, AZ, USA). The cartilage resections were placed into individual plastic containers with a solution of phosphate-buffered saline (PBS) and protease inhibitor (PI) to maintain cartilage tissue hydration and matrix integrity during MR imaging. Each resection was then imaged using an 8-channel phased array wrist coil (InVivo, Orlando, FL) within a 3.0 T clinical MR scanner (Discovery MR750, GE Healthcare, Waukesha, WI). The mcDESPOT sequence[24–26] was performed on each cartilage resection (in-plane resolution = 0.1367 x 0.1367 mm, slice thickness = 2 mm). This sequence consisted of eight SPGR scans with TR/TE = 4.6/2.2 ms over a range of flip angles (α = 3, 4, 5, 6,

7, 9, 13, and 18º) and eight bSSFP scans with TR/TE = 5.0/2.4 ms over a range of flip angles (α = 2, 5, 10, 15, 20, 30, 40, and 50º). The bSSFP scans were repeated with radiofrequency phase cycling ψ = 0º and 180º for each of the flip angles to remove the effects of bSSFP banding artifacts and to provide an estimate of the B0 field. An additional inversion recovery IR-SPGR scan with TR/TE = 4.6/2.2 ms, TI = 450 ms, and α = 5º was acquired to estimate the transmit B1 field .[24,28–32] The mcDESPOT imaging data was then used to reconstruct the single-component T2 relaxation parameter (T2), $T2_{short}$, $T2_{long}$, and the FBW within each voxel using custom MATLAB code[25] (Figure 1) (MathWorks, Natick, MA, USA).

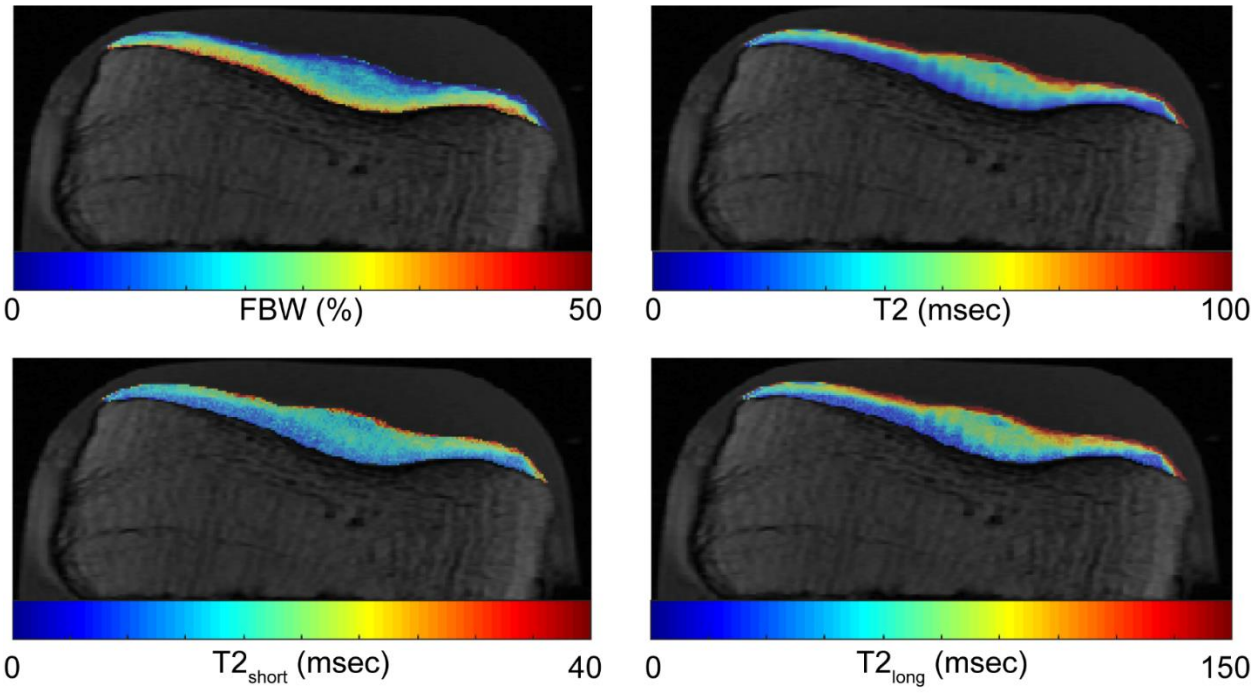

Figure 1: Representative maps of T2, $T2_{short}$, $T2_{long}$, and FBW within a single slice of the medial tibial plateau cartilage tissue. These mcDESPOT parameters were computed throughout the entire tibial and distal femoral cartilage surfaces.

2.2. Cartilage Samples

After MR imaging, full thickness cartilage samples (diameter = 4.1 mm) were obtained from the medial and lateral tibial plateaus and from the weight-bearing region of the distal femoral

condyles using a cylindrical biopsy punch (12 cartilage samples total) (Figure 2). Prior to mechanical testing, each cartilage sample was trimmed using a hand microtome such that the bottom surface of the sample was approximately parallel to the top surface. Thickness of each sample was then measured using a custom-built resistive micrometer (thickness = 2.479 ± 0.460 mm).

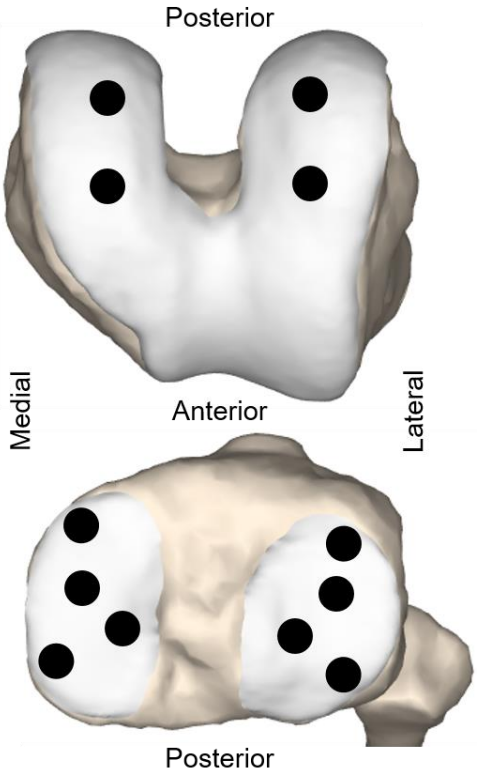

Figure 2: Image shows the region from which each of the cartilage samples was extracted from the distal femoral (top) and tibial (bottom) cartilage surfaces for mechanical testing.

2.3. Biomechanical Evaluation

Confined compression testing of each sample was performed on a table top mechanical testing machine (ElectroForce 3200, TA Instruments, New Castle, DE, USA). Each sample was placed in a custom-built cylindrical (inner diameter = 4.1 mm) rigid confined compression chamber with impervious side walls. The confining chamber was then placed into a well containing

a rigid steel porous bottom and filled with a solution of PBS and PI. This allowed the cartilage sample to remain hydrated and prevent collagen matrix degeneration throughout the entirety of the experiment. The sample was allowed to equilibrate within this confining chamber for 5 min prior to being loaded on the articular surface using a rigid aluminum indenter.

Incremental stress-relaxation tests were performed (Figure 3). A tare load of at least 10 g (13.0 ± 2.7 g) was applied to the sample until less than a 5% change in the load was observed for 10 minutes. This ensured full surface contact between the platen and the sample. The sample was then loaded at a rate of 0.01%/sec for 5 increments of 10% strain each. After each 10% strain step, the indenter displacement was held constant and the sample was allowed to relax for 30 min. Force and displacement data were sampled at 1 Hz throughout entire the experiment.

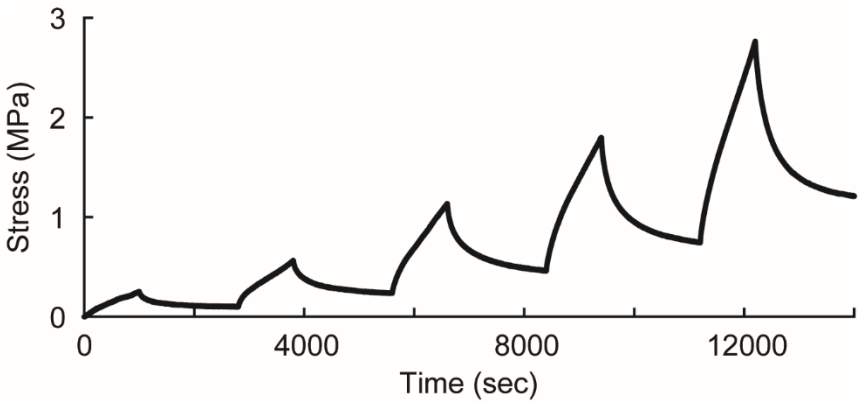

Figure 3: Axial stress versus time plot for a representative cartilage sample. Each stress-relaxation step consisted of a 10% strain step loaded at a rate of 0.01%/sec followed by a 30 min relaxation phase.

After completion of the experiments, the aggregate compressive modulus (H_{A0}) and compressive stiffening coefficient (β) were computed from the equilibrium response of each cartilage sample. To do this, the axial compressive stress and stretch were computed from the force-displacement data using the known cross-sectional area (13.2025 mm^2) and measured thickness of each sample. Equilibrium axial stress and stretch were then computed at the end of

each hold phase of the stress-relaxation experiments. H_{A0} and β were determined by performing a non-linear least squares regression of a hyperelastic constitutive model to the equilibrium stress-stretch data[33,34] (Eq. 1 and Figure 4),

$$\sigma^e = \frac{1}{2} H_{A0} \left(\frac{\lambda^2 - 1}{\lambda^{2\beta+1}} \right) e^{\beta(\lambda^2 - 1)}, \tag{1}$$

where σ^e is the equilibrium axial stress and λ is the equilibrium axial stretch.

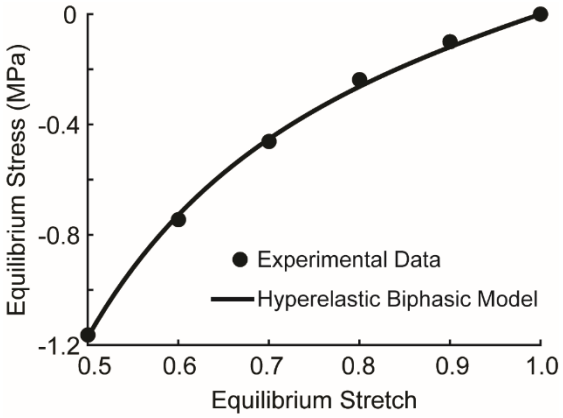

Figure 4: Plot shows the equilibrium stress-stretch data for a representative cartilage sample measured at the end of each hold phase of the stress-relaxation steps. Additionally, the nonlinear least squares fit of a hyperelastic biphasic constitutive model to these data is shown. The equilibrium stress is shown as negative to indicate the sample is being compressed.

The nonlinear strain dependent permeability coefficients (k_0, M) were determined for each sample using inverse finite element modeling (FEBio, Musculoskeletal Research Laboratories, Salt Lake City, UT, USA). A plain strain finite element model was built for each sample that included cartilage (400 elements per model), the indenter (10 elements), and sliding interface contact[35] between the cartilage and indenter. The indenter was modeled as a rigid body and cartilage was modeled with biphasic hexahedral elements consisting of a Holmes-Mow elastic solid and strain-dependent permeability[34] with an assumed solid fraction (φ_0) of 0.2.[33,36] The material properties of the Holmes-Mow solid (i.e. Young's modulus, Poisson's ratio, and the

exponential stiffening coefficient) were determined by performing a nonlinear regression of this constitutive model to the experimental equilibrium stress-stretch data. For the strain-dependent permeability, the power-law exponent (α) was assumed to be 2.[37] The permeability coefficients (k_0, M) were then optimized by minimizing the sum of squared differences between the predicted and measured compressive stress while simulating the indenter displacement from the stress-relaxation experiment (Figure 3).

2.4. Extracting Quantitative MR Parameters for Cartilage Samples

Following removal of the cartilage samples, imaging of the cartilage resections was again performed using one of the SPGR sequences from the mcDESPOT protocol (in-plane resolution = 0.1367 x 0.1367 mm, slice thickness = 2 mm, TR/TE = 4.6/2.2 ms, flip angle =18º). Regions of interest (ROIs) were segmented (MATLAB, The Mathworks, Inc., Natick, MA) within these images to indicate the section of cartilage that was removed for each sample. Additionally, the bone was manually segmented from both the new images and the SPGR images obtained prior to extracting the cartilage samples. These bone masks were registered (Elastix[38], Image Sciences Institute, Utrecht, Netherlands) to compute the transformation between the first set and second set of MR images. This transformation was then used to register the cartilage sample ROIs to the mcDESPOT parameter maps. The T2, $T2_{short}$, $T2_{long}$, and FBW parameters were then averaged within each ROI.

2.5. Statistical Analysis

Pearson correlation coefficients were computed to determine the association between the quantitative MR relaxation parameters (i.e. T2, $T2_{short}$, $T2_{long}$, and FBW) and the cartilage material properties of interest (i.e. H_{A0} and k_0). Significance was set at $P < 0.05$.

3. Results

The material properties and mcDESPOT parameters were determined for each cartilage sample (Table 1). We found that the aggregate compressive modulus was significantly correlated with the FBW (Figure 5), but not the T2, $T2_{short}$, or $T2_{long}$ relaxation rates (R = -0.45, -0.45, and -0.56, respectively and P = 0.14, 0.15, and 0.06, respectively). The hydraulic permeability was not significantly correlated with the FBW, (Figure 5). However, the hydraulic permeability was significantly correlated with the T2, $T2_{short}$, and $T2_{long}$ relaxation rates (Figure 6).

Table 1: Mean (+/- standard deviation) mcDESPOT parameters and material properties across all cartilage samples.

Material Properties		**mcDESPOT Parameters**			
H_{A0} (MPa)	k_0 ($mm^4/Ns \times 10^{-3}$)	FBW (%)	T2 (ms)	$T2_{short}$ (ms)	$T2_{long}$ (ms)
0.78 ± 0.50	0.00198 ± 0.0011	26.1 ± 2.9	46.4 ± 7.1	18.8 ± 2.2	77.9 ± 12.3

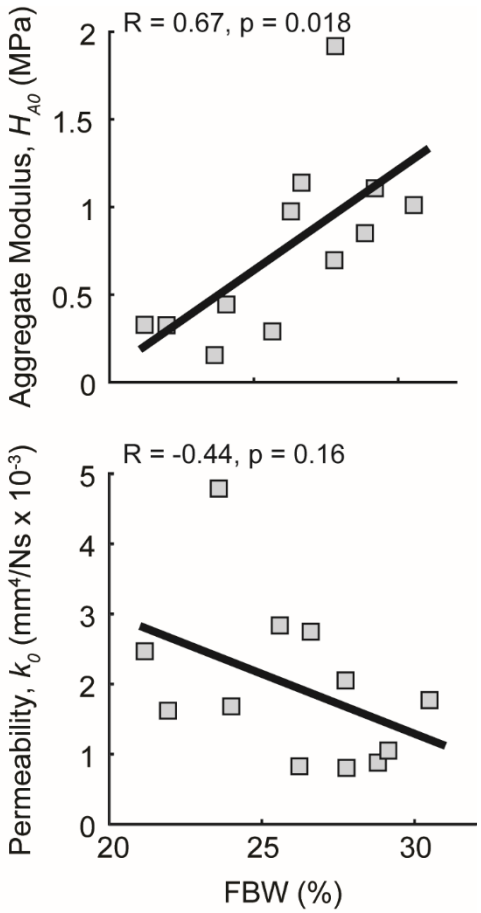

Figure 5: Relationship between the cartilage material properties (H_{A0}, top and k_0, bottom) and the FBW. A significant relationship (P <0.05) was observed between H_{A0} and the FBW.

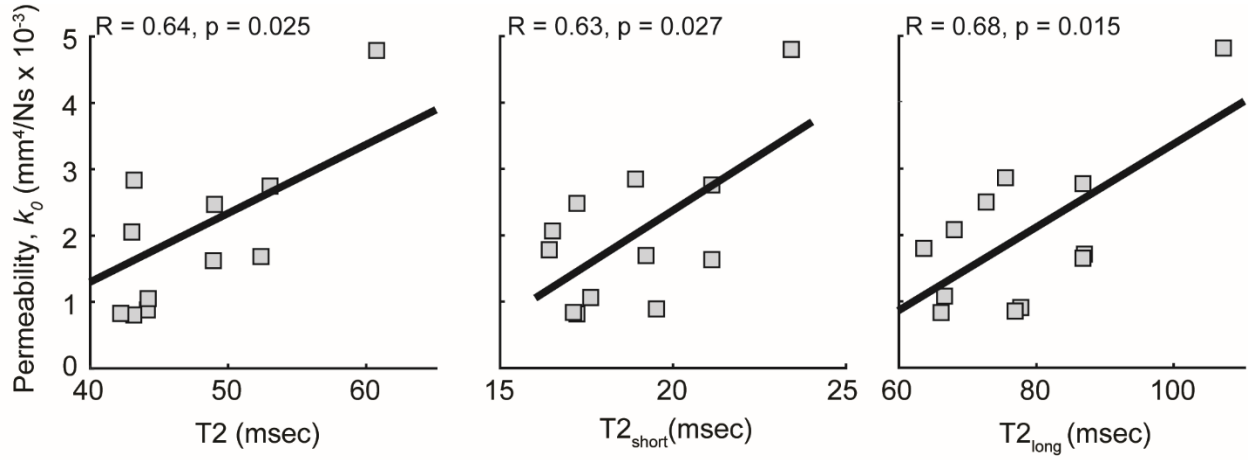

Figure 6: Relationships between k_0 and T2 (left), $T2_{short}$ (middle), and $T2_{long}$ (right). A significant relationship was (P <0.05) between k_0 and each of these parameters.

4. Discussion

In this study, we assessed the potential of using quantitative MR imaging to non-invasively assess *in vivo* cartilage material properties. Specifically, this was done by investigating the association between quantitative MR relaxation parameters obtained via a mcDESPOT sequence within a 3.0T MR scanner and cartilage material properties measured through confined compression. This was motivated by the potential improvement in the predictive capabilities of computational models by incorporating subject-specific material properties. We found that cartilage material properties were significantly correlated to mcDESPOT parameters, with the aggregate modulus associated with the FBW and the hydraulic permeability associated with the slow-relaxing component of the T2 signal. The ability to measure these correlations within a 3.0T MR scanner highlights the potential of using the mcDESPOT sequence to non-invasively determine subject-specific cartilage material properties within a clinical environment.

Previous studies have observed similar relationships between quantitative MR parameters and cartilage material properties to those found in this study. For example, significant correlations have been observed between T1ρ values, which have been associated with proteoglycan content,[39,40] and the aggregate modulus.[19] Additionally, previous studies have measured a link between the cartilage proteoglycan content and aggregate modulus.[41–43] Agreement across these studies highlights the potential of using these quantitative MR techniques to assess proteoglycan content and material properties of cartilage. However, previous work has also observed a significant relationship between T1ρ values and hydraulic permeability.[19] In the current study, no association was observed between the FBW and hydraulic permeability, thus indicating that the FBW metric may have improved specificity in measuring the cartilage aggregate compressive modulus.

One of the previously cited benefits of the mcDESPOT sequence is the ability to decompose the T2 signal into short- and long-relaxation components.[44–46] We found that this feature improved the predictive capability of this sequence. While the cartilage hydraulic permeability was correlated to the single component T2 relaxation parameter, this material property was more strongly correlated to the long-relaxation T2 component (Figure 6). Given the association between the long-relaxation T2 component and the relative amount of bulk water,[44,46] this finding agrees with previous studies that observed a link between the hydraulic permeability and hydration of cartilage tissue.[47] Additionally, we observed a significant relationship between the hydraulic permeability and the short-relaxation T2 component. This T2 component is believed to be associated with the water tightly bound to proteoglycan.[45,46] Therefore, these findings agree with previous studies that suggest a link between hydraulic permeability and proteoglycan content.[48] However, we also observed a relatively small range in permeability across the cartilage samples, which may not account for the permeability of highly degenerated cartilage.[41] Future studies with greater variability in health of the cartilage samples, and, thus, permeability, is needed to assess the robustness of this relationship between permeability and the T2 relaxation components.

The most salient finding of this study was that mcDESPOT relaxation parameters assessed within a clinical 3.0T MR scanner showed the potential to predict subject-specific cartilage material properties. This is important given that previous studies have shown that the incorporation of subject-specific parameters improves the accuracy of computational model predictions.[49–52] Some previous studies have shown similar abilities to predict cartilage material properties using different quantitative MR sequences.[15,16,18,19,21,23] However, these studies were primarily performed using MR scanners with a field-strength >3.0T, which are not commonly found within

a clinical setting. Additionally, many of these studies have used MR sequences that require contrast-enhancement (i.e. dGEMRIC), which is not ideal for regular use on human subjects. Thus, this is one of the first studies to confirm the ability to measure cartilage material properties using a contrast-free quantitative MR sequence imaged within a clinical MR scanner. However, it is important to note that the mcDESPOT parameters did not describe all the variability in cartilage material properties. While future studies with a larger set of cartilage samples may help improve the robustness of this measurement framework, further work is also needed to assess the effect of these 'errors' on the accuracy of computational model predictions.

There are three primary limitations to consider when interpreting the findings of this study. First, the cartilage samples used in this study came from the knee of a single cadaveric specimen. Further work is needed to determine if these correlations persist when including additional cadaveric specimen and to determine if the relationship between the quantitative MR parameters and cartilage material properties varies across specimen. However, the findings of this study provide the basis and motivation for these future investigations. Second, only confined compression testing was used to assess the cartilage material properties. Additional material properties can be determined for cartilage using other material testing techniques (e.g. unconfined compression and microindentation) and are needed to needed to fully assess the loading response of the cartilage tissue. Thus, future investigations will incorporate these additional testing techniques to help obtain a more complete understanding of the link between quantitative MR parameters and material properties. Third, all the samples were grouped together in this analysis even though the samples were extracted from different regions of the cartilage tissue and different cartilage surfaces (i.e. femur and tibia). While this suggests that the relationships observed in this study can be generalized to any cartilage surface within the knee, previous studies have shown that

the association between cartilage material properties and quantitative MR parameters varies when only considering samples from similarly loaded regions within the knee (e.g. weight-bearing versus sub-meniscal in the tibial cartilage).[17] Future investigations with larger numbers of samples will allow for a regional analysis of the link between cartilage mechanics and mcDESPOT relaxation parameters.

In conclusion, the findings of this study show the potential to use a mcDESPOT sequence to measure subject-specific knee articular cartilage material properties. The ability to collect these images within a clinical MR scanner and within a reasonable scan time suggests that this MR sequence may be useful when developing highly detailed cartilage models of human subjects. Given that the use of subject-specific material properties may allow for more accurate computational model predictions, use of this quantitative MR technique may improve our ability to study the initiation and progression of OA development.

Acknowledgements

The authors gratefully acknowledge the contributions of Kelly Vazquez. This material is based upon work supported by the National Science Foundation Graduate Research Fellowship Program under Grant No. DGE-1747503 and the National Institutes of Health (EB015410). Any opinions, findings, and conclusions or recommendations expressed in this material are those of the author(s) and do not necessarily reflect the views of the NSF or NIH. Support was also provided by the Graduate School and the Office of the Vice Chancellor for Research and Graduate Education at the University of Wisconsin-Madison with funding from the Wisconsin Alumni Research Foundation.

References

1. Lawrence RC, Felson DT, Helmick CG, et al. 2008. Estimates of the prevalence of arthritis and other rheumatic conditions in the United States. Part II. Arthritis Rheum. 58(1):26–35.
2. Griffin TM, Guilak F. 2005. The Role of Mechanical Loading in the Onset and Progression of Osteoarthritis. Exerc. Sport Sci. Rev. 33(4):195–200 Available from: http://content.wkhealth.com/linkback/openurl?sid=WKPTLP:landingpage&an=00003677-200510000-00008.
3. Buckwalter JA, Anderson DD, Brown TD, et al. 2013. The Roles of Mechanical Stresses in the Pathogenesis of Osteoarthritis: Implications for Treatment of Joint Injuries. Cartilage 4(4):286–294.
4. Goldring MB, Otero M. 2011. Inflammation in osteoarthritis. Curr. Opin. Rheumatol. 23(5):471–478.
5. Loeser RF. 2011. Aging and Osteoarthritis. Curr. Opin. Rheumatol. 23(5):492–496.
6. Loeser RF. 2009. Aging and osteoarthritis: the role of chondrocyte senescence and aging changes in the cartilage matrix. Osteoarthr. Cartil. 17(8):971–979 Available from: http://dx.doi.org/10.1016/j.joca.2009.03.002.
7. Martin JA, Buckwalter JA. 2002. Aging, articular cartilage chondrocyte senscence and osteoarthritis. Biogerontology. 3_ _(5):257–264 Available from: http://www.ncbi.nlm.nih.gov/entrez/query.fcgi?cmd=Retrieve&db=pubmed&dopt=Abstract&list_uids=12237562.
8. Buckwalter JA, Lane NE. 1997. Current Concepts: Athletics and Osteoarthritis. Am. J. Sports Med. 25(6):873–881.

9. Mononen ME, Tanska P, Isaksson H, Korhonen RK. 2016. A Novel Method to Simulate the Progression of Collagen Degeneration of Cartilage in the Knee : Data from the Osteoarthritis Initiative. Nat. Publ. Gr. (February):1–14 Available from: http://dx.doi.org/10.1038/srep21415.

10. Andriacchi TP, Briant PL, Bevill SL, Koo S. 2006. Rotational Changes at the Knee after ACL Injury Cause Cartilage Thinning. Clin. Orthop. Relat. Res. 442:39–44.

11. Mononen ME, Tanska P, Isaksson H, Korhonen RK. 2017. New Algorithm for Simulation of Proteoglycan Loss and Collagen Degeneration in the Knee Joint: Data from the Osteoarthritis Initiative. J. Orthop. Res. (June):24–26 Available from: http://doi.wiley.com/10.1002/jor.23811.

12. Anderson AE, Ellis BJ, Maas S a, et al. 2010. Validation of Finite Element Predictions of Cartilage Contact Pressure in the Human Hip Joint. J. Biomech. Eng. 130(5):1–25.

13. Li G, Lopez O, Rubash H. 2001. Variability of a Three-Dimensional Finite Element Model Constructed Using Magnetic Resonance Images of a Knee for Joint Contact Stress Analysis. J. Biomech. Eng. 123(4):341 Available from: http://biomechanical.asmedigitalcollection.asme.org/article.aspx?articleid=1405981.

14. Henak CR, Kapron AL, Anderson AE, et al. 2014. Specimen-specific predictions of contact stress under physiological loading in the human hip: Validation and sensitivity studies. Biomech. Model. Mechanobiol. 13(2):387–400.

15. Kurkijärvi JE, Nissi MJ, Kiviranta I, et al. 2004. Delayed gadolinium-enhanced MRI of cartilage (dGEMRIC) and T2 characteristics of human knee articular cartilage: Topographical variation and relationships to mechanical properties. Magn. Reson. Med. 52(1):41–46.

16. Nieminen MT, Töyräs J, Laasanen MS, et al. 2004. Prediction of biomechanical properties of articular cartilage with quantitative magnetic resonance imaging. J. Biomech. 37(3):321–328.

17. Samosky JT, Burstein D, Grimson WE, et al. 2005. Spatially-localized correlation of dGEMRIC-measured GAG distribution and mechanical stiffness in the human tibial plateau. J. Orthop. Res. 23(1):93–101.

18. Lammentausta E, Kiviranta P, Nissi M., et al. 2006. T2 Relaxation Time and Delayed Gadolinium-Enhanced MRI of Cartilage (dGEMRIC) of Human Patellar Cartilage at 1.5 T and 9.4 T: Relationships with Tissue Mechanical Properties. J. Orthop. Res. MARCH (24):366–374.

19. Wheaton AJ, Dodge GR, Elliott DM, et al. 2005. Quantification of cartilage biomechanical and biochemical properties via T1rho magnetic resonance imaging. Magn. Reson. Med. 54(5):1087–1093.

20. Miyata S, Numano T, Homma K, et al. 2007. Feasibility of noninvasive evaluation of biophysical properties of tissue-engineered cartilage by using quantitative MRI. J. Biomech. 40(13):2990–2998.

21. Nissi MJ, Rieppo J, Töyräs J, et al. 2007. Estimation of mechanical properties of articular cartilage with MRI - dGEMRIC, T2 and T1 imaging in different species with variable stages of maturation. Osteoarthr. Cartil. 15(10):1141–1148.

22. Tang SY, Souza RB, Ries M, et al. 2011. Local tissue properties of human osteoarthritic cartilage correlate with magnetic resonance T1rho relaxation times. J. Orthop. Res. 29(9):1312–9 Available from: http://www.pubmedcentral.nih.gov/articlerender.fcgi?artid=4092115&tool=pmcentrez&re

ndertype=abstract.

23. Rautiainen J, Nissi MJ, Salo E-N, et al. 2014. Multiparametric MRI assessment of human articular cartilage degeneration: Correlation with quantitative histology and mechanical properties. Magn. Reson. Med. 00(May):249–259 Available from: http://www.ncbi.nlm.nih.gov/pubmed/25104181.

24. Deoni SCL, Rutt BK, Arun T, et al. 2008. Gleaning Multicomponent T1 and T2 Information From Steady-State Imaging Data. Magn. Reson. Med. 60:1372–1387.

25. Liu F, Chaudhary R, Hurley SA, et al. 2014. Rapid Multicomponent T2 Analysis of the Articular Cartilage of the Human Knee Joint at 3.0T. J. Magn. Reson. Imaging 39:1191–1197.

26. Liu F, Choi KW, Samsonov A, et al. 2015. Articular Cartilage of the Human Knee Joint: In Vivo Multicomponent T2 Analysis at 3.0 T. Radiology 277(2):477–488.

27. Kaiser J, Vignos MF, Liu F, et al. 2016. American Society of Biomechanics Clinical Biomechanics Award 2015: MRI assessments of cartilage mechanics, morphology and composition following reconstruction of the anterior cruciate ligament. Clin. Biomech. 34.

28. Deoni SCL, Rutt BK, Jones DK. 2007. Investigating the effect of exchange and multicomponent T1 relaxation on the short repetition time spoiled steady-state signal and the DESPOT1 T1 quantification method. J. Magn. Reson. Imaging 25(3):570–578.

29. Deoni SCL, Peters TM, Rutt BK. 2005. High-resolution T1 and T2 mapping of the brain in a clinically acceptable time with DESPOT1 and DESPOT2. Magn. Reson. Med. 53(1):237–241.

30. Deoni SCL. 2007. High-resolution T1 mapping of the brain at 3T with driven equilibrium single pulse observation of T1 with high-speed incorporation of RF field inhomogeneities

(DESPOT1-HIFI). J. Magn. Reson. Imaging 26(4):1106–1111.

31. Deoni SCL. 2009. Transverse relaxation time (T2) mapping in the brain with off-resonance correction using phase-cycled steady-state free precession imaging. J. Magn. Reson. Imaging 30(2):411–417.

32. Deoni SCL. 2011. Correction of main and transmit magnetic field (B0 and B 1) inhomogeneity effects in multicomponent-driven equilibrium single-pulse observation of T1 and T2. Magn. Reson. Med. 65(4):1021–1035.

33. Ateshian GA, Warden WH, Kim JJ, et al. 1997. Finite deformation biphasic material properties of bovine articular cartilage from confined compression experiments. J. Biomech. 30(11–12):1157–1164.

34. Holmes, M.H.; Mow VC. 1990. The nonlinear characteristics of hydrated gels and hydrated connective tissues in ultrafiltration. J. Biomech. 23(11):1145–1156.

35. Laursen TA, Maker BN. 1995. An augmented Lagrangian quasi-Newton solver for constrained nonlinear finite element applications. Int. J. Numer. Methods Eng. 38(21):3571–3590.

36. Torzilli PA. 1985. Influence of cartilage conformation on its equilibrium water partition. J. Orthop. Res. 3(4):473–483.

37. Ateshian GA, Maas S, Weiss JA. 2013. Multiphasic Finite Element Framework for Modeling Hydrated Mixtures With Multiple Neutral and Charged Solutes. J. Biomech. Eng. 135(11):111001 Available from: http://biomechanical.asmedigitalcollection.asme.org/article.aspx?doi=10.1115/1.4024823.

38. Klein S, Staring M, Murphy K, et al. 2010. elastix: A Toolbox for Intensity-Based Medical Image Registration. IEEE Trans. Med. Imaging 29(1):196–205.

39. Duvvuri U, Kudchodkar S, Reddy R, Leigh JS. 2002. T1rho relaxation can assess longitudinal proteoglycan loss from articular cartilage in vitro. Osteoarthr. Cartil. 10(11):838–844.

40. Duvvuri U, Reddy R, Patel SD, et al. 1997. T1rho-relaxation in articular cartilage: effects of enzymatic degradation. Magn Reson Med 38(6):863–867 Available from: http://www.ncbi.nlm.nih.gov/entrez/query.fcgi?cmd=Retrieve&db=PubMed&dopt=Citation&list_uids=9402184.

41. Sah RL, Yang AS, Chen AC, et al. 1997. Physical properties of rabbit articular cartilage after transection of the anterior cruciate ligament. J. Orthop. Res. 15(2):197–203 Available from: http://www.ncbi.nlm.nih.gov/pubmed/9167621.

42. Rivers PA, Rosenwasser MP, Mow VC, et al. 2000. Osteoarthritic changes in the biochemical composition of thumb carpometacarpal joint cartilage and correlation with biomechanical properties. J. Hand Surg. Am. 25(5):889–898.

43. Lyyra T, Arokoski J, Oksala N, et al. 1999. Experimental validation of arthroscopic cartilage stiffness measurement using enzymatically degraded cartilage samples measurement using enzymatically degraded cartilage samples. Phys. Med. Biol. 44:525–535.

44. Reiter DA, Lin PC, Fishbein KW, Spencer RG. 2009. Multicomponent T2 relaxation analysis in cartilage. Magn. Reson. Med. 61(4):803–809.

45. Reiter DA, Roque RA, Lin PC, et al. 2011. Mapping proteoglycan-bound water in cartilage: Improved specificity of matrix assessment using multiexponential transverse relaxation analysis. Magn. Reson. Med. 65(2):377–384.

46. Reiter DA, Roque RA, Lin P, et al. 2011. Improved specificity of cartilage matrix

evaluation using multiexponential transverse relaxation analysis applied to pathomimetically degraded cartilage. NMR Biomed. 24(10):1286–1294.

47. Setton LA, Mow VC, Muller FJ, et al. 1994. Mechanical-Properties of Canine Articular-Cartilage Are Significantly Altered Following Transection of the Anterior Cruciate Ligament. J. Orthop. Res. 12(4):451–463.

48. Maroudas A. 1968. Physicochemical Properties of Cartilage in the Light of Ion Exchange Theory. Biophys. J. 8(5):575–595.

49. Schileo E, Dall'Ara E, Taddei F, et al. 2008. An accurate estimation of bone density improves the accuracy of subject-specific finite element models. J. Biomech. 41(11):2483–2491.

50. Kent DM, Hayward RA. 2007. Limitations of Applying Summary Results of Clinical Trials to Individual Patients. Jama 298(10):1209 Available from: http://jama.jamanetwork.com/article.aspx?doi=10.1001/jama.298.10.1209.

51. Neal ML, Kerckhoffs R. 2009. Current progress in patient-specific modeling. Brief. Bioinform. 11(1):111–126.

52. Gerus P, Sartori M, Besier TF, et al. 2013. Subject-specific knee joint geometry improves predictions of medial tibiofemoral contact forces. J. Biomech. 46(16):2778–2786 Available from: http://dx.doi.org/10.1016/j.jbiomech.2013.09.005.

Chapter 2: Longitudinal Changes in Cartilage Composition are Associated with Abnormal *In Vivo* Knee Mechanics following ACL Reconstruction

Michael F. Vignos, Jarred M. Kaiser, Geoffrey S. Baer, Richard Kijowski, Darryl G. Thelen

(This chapter was prepared for submission to the *Journal of Orthopaedic Research*)

Abstract

It has been theorized that the high rate of osteoarthritis development in anterior cruciate ligament reconstructed (ACLR) knees is partially due to residual, abnormal knee mechanics that remain following reconstruction. However, there is currently limited evidence of a direct link between abnormal knee mechanics and cartilage degeneration in ACLR subjects. Thus, the objectives of this work were (1) to assess longitudinal changes in knee kinematics, cartilage contact, and cartilage composition in ACLR knees and (2) to investigate the relationship between abnormal knee mechanics and changes in cartilage composition. We tested 10 subjects undergoing a primary, unilateral ACLR. Prior to ACLR and following completion of post-ACLR rehabilitation, subjects underwent bilateral static and dynamic MR imaging to assess tibiofemoral kinematics and cartilage contact during active knee flexion-extension for the ACL deficient (ACLD), ACLR, and contralateral knees. At these same time-points and at one year following completion of rehabilitation, quantitative MR imaging (mcDESPOT) was used to assess the fraction of water bound to proteoglycan (FBW) in the tibial cartilage of the ACL injured knees. Two-factor repeated measures ANOVAs were used to determine longitudinal changes in knee mechanics and FBW across each time-point ($P < 0.05$). Additionally, geospatial analysis (BiLISA) was used to investigate the correlation between abnormal cartilage contact and changes in the FBW ($P < 0.05$). Abnormal kinematics were observed in the ACLD and ACLR knees, relative to the

contralateral knees, which gave rise to increased cartilage contact on the medial tibial plateau in both ACL conditions. Additionally, progressive reductions in the FBW were observed on the medial tibial plateau of the ACL injured knees across all time-points. Geospatial analysis indicated that these reductions in FBW were correlated with increased cartilage contact on the medial plateaus. These findings provide a direct link between abnormal *in vivo* cartilage contact and early signs of cartilage degeneration in ACLR knees.

1. Introduction

The anterior cruciate ligament (ACL) is one of the most commonly injured ligaments in sporting activities with over 200,000 ACL ruptures occurring in the US each year.[1] Typically, ACL ruptures are treated with an ACL reconstruction (ACLR), with the short-term goal of restoring knee stability and allowing patients to return to previous levels of activity. ACLR is generally successful at achieving this goal with >90% of patients reporting good to excellent outcomes at 2 to 5 years following surgery.[2–4] However, the long-term outcomes of ACLR are concerning with >50% of patients exhibiting early signs of osteoarthritis (OA) at 10 to 15 years following surgery.[5] While it is well known that ACLR patients are at a high risk of early OA, there is limited evidence of the direct cause of cartilage degeneration in this patient population.

Recent advancements in magnetic resonance (MR) imaging have allowed for non-invasive, quantitative assessments of cartilage composition. The most commonly utilized techniques aim to measure the T1ρ and T2 relaxation rates of the cartilage tissue, based on the reported relationship of these metrics with the proteoglycan content[6] and the organization of the collagen fiber network[7], respectively. A recently developed multi-component T2 mapping technique, mcDESPOT,[8–10] allows for improved specificity by decomposing the T2 relaxation rate into the fast and slow

relaxation components. These components are thought to be linked to the fraction of water tightly bound to proteoglycan (i.e. fraction of bound water, FBW) and the bulk water associated with the collagen matrix, respectively. Use of these quantitative MR imaging techniques has allowed for the detection of changes in cartilage composition in ACLR knees, which occurs early in the development of OA. For example, increases in T1ρ and T2 relaxation rates have been reported at 6 and 12 months following ACLR.[11] Additionally, Kaiser et al. found a significantly lower FBW in ACLR knees at approximately two years post-reconstruction.[12]

It has been theorized that these early changes in cartilage composition are partially due to residual abnormal knee mechanics that remain following ACLR.[13,14] This theory has been supported by *in vitro* cartilage testing and *in vivo* animal models showing that abnormal cartilage loading can lead to the initiation and progression of cartilage degeneration.[15–17] Indeed, previous dynamic imaging studies have reported abnormal tibiofemoral kinematics and cartilage contact patterns in ACLR knees. Specifically, a bias towards external tibial rotation has been observed during a range of tasks,[18–20] leading to a posterior-lateral shift in cartilage contact location on the tibial plateaus.[12,21] However, these previous studies have primarily been cross-sectional in design, thus limiting the ability to isolate the effect of ACLR on post-operative knee mechanics. Additionally, there is currently limited evidence of a direct link between abnormal knee mechanics and early signs of cartilage degeneration in ACLR knees.

The purpose of this study was to investigate the relationship between altered knee mechanics and changes in cartilage composition following ACLR. Accordingly, the first objective was to investigate longitudinal changes in tibiofemoral kinematics, cartilage contact, and cartilage composition following ACL injury and subsequent ACLR through the use of dynamic and

quantitative MR imaging. The second objective was to then assess the link between abnormal cartilage contact and the observed changes in cartilage composition.

2. Methods

2.1. Subjects

Ten subjects were recruited and tested after providing informed consent according to the University of Wisconsin-Madison Institutional Review Board-approved protocol (5 females, 25.9 ± 7.7 years, 75.7 ± 13.6 kg). Each subject had no other concurrent ligament damage, post-operative complications, and history of surgery, injury, pain, or inflammatory or crystalline-induced arthritis in the contralateral knee. ACL reconstructions were performed by four fellowship-trained sports medicine surgeons through independent tunnel drilling techniques (5 bone—patellar tendon—bone and 5 hamstrings tendon grafts). Two subjects had minor meniscal damage (one with small medial and lateral meniscal repairs and one with a small medial meniscectomy). All subjects were tested at two separate time points: (1) following ACL injury (time point 1, TP1; 48 ± 20 days post-injury) and (2) following completion of post-ACLR rehabilitation (time point 2, TP2; 13.4 ± 4.2 months post-surgery) (Figure 1). Seven of the subjects were tested at a third time point of at least one year after completion of rehabilitation (time point 3, TP3; 2.4 ± 0.4 years post-surgery), with three subjects lost at long-term follow-up.

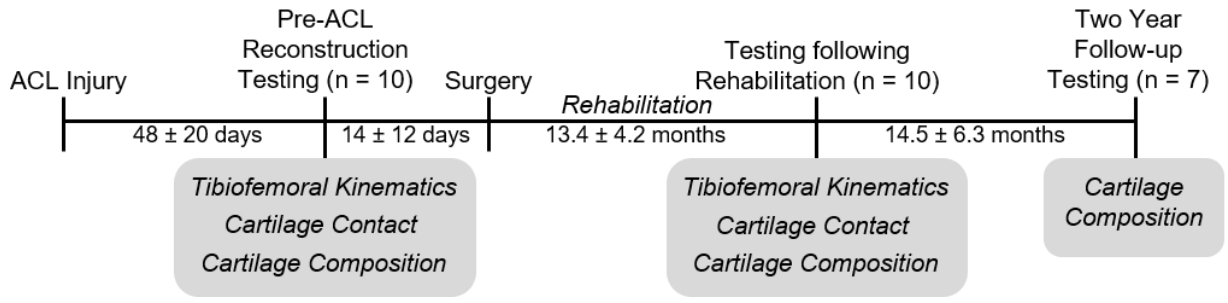

Figure 1: Timeline shows the three separate time points at which subjects were tested. Gray boxes indicate the data collected at each time point.

2.2. Static and Dynamic MR Imaging

At the first two testing time-points (i.e. TP1 and TP2), each subject underwent a bilateral static MR imaging protocol using an 8-channel phased array extremity coil (InVivo, Orlando, FL) within a 3.0 T clinical MR scanner (Discovery MR750, GE Healthcare, Waukesha, WI). High-resolution images (in-plane resolution=0.37 x 0.37 mm; slice thickness=0.9 mm) of the knee were obtained using an IDEAL SPGR sequence (iterative least squares estimation of fat-water separation using a spoiled gradient recall-echo sequence) to characterize bone geometry. Additionally, a 3D FSE Cube sequence (fast spin-echo; in-plane resolution=0.39 x 0.39 mm; slice thickness=1.0 mm) was used to characterize cartilage geometry. The IDEAL SPGR and 3D FSE Cube images were manually segmented to create 3D models of the femoral and tibial bone and cartilage geometries, respectively, of the ACL deficient (ACLD), contralateral, and ACLR knees of each subject (MIMICS, Materialise Group, Leuven, Belgium). All models were smoothed and converted into triangular meshes (7000 triangles/surface for bones and approximately 0.33 mm^2/triangle for cartilage and ACL meshes); (Geomagic Studio, 3D Systems, Rock Hill, SC, USA and MeshLab, Visual Computing Lab-ISTI-CNR, Pisa, Italy). Anatomic coordinate systems were defined for the femoral and tibial bone models using an automated algorithm to determine the axes for each bone independently based on its geometric and inertial properties.[22] The bone and cartilage models were subsequently co-registered to create subject-specific morphological knee models.

Each subject then underwent bilateral dynamic MR imaging to characterize knee mechanics during active movement. Subjects lied supine with their lower leg secured to a custom-built, MR-compatible knee-loading device.[23] Voluntary knee flexion-extension was performed at 0.5 Hz with an audible metronome used to assist subjects in maintaining this rate. During this motion, the device induced stretch-shortening quadriceps contractions by applying a load to the

subjects' lower leg via a set of rotating disks.[24] This quadriceps loading is comparable to that experienced during the loading-response phase of walking.[25,26]

The subjects performed active knee flexion-extension for 5 min while a 3D SPGR sequence with vastly under-sampled isotropic projections (3D SPGR-VIPR) continuously acquired volumetric MR data[24] (Figure 2); (1.5-mm isotropic resolution; repetition time, 4 ms; echo time, 1.4 ms; flip angle, 8°; receiver bandwidth, 32.5 kHz; unique radial lines, 93,922; field of view, 48 cm). An MRI-compatible rotary encoder was used to track the device arm angle during this motion to determine the beginning of each flexion-extension cycle. The SPGR-VIPR projections were then sorted into equally spaced bins and reconstructed into 60 volumetric image frames over the flexion-extension motion.[24]

2.3. Quantitative MR Imaging

At all three time points, each subject underwent quantitative MR imaging of the ACL injured knee using an mcDESPOT sequence[8–10] (multicomponent-driven equilibrium single-shot observation of T1 and T2; in-plane resolution = 0.62 x 0.62 mm; slice thickness = 3.0 mm). The mcDESPOT imaging data was then used to reconstruct the fraction of water bound to proteoglycan (i.e. fraction of bound water, FBW) within each voxel using custom MATLAB code[9] (MathWorks, Natick, MA, USA). The cartilage masks, segmented from the 3D FSE Cube images, were then registered (Elastix[27], Image Sciences Institute, Utrecht, Netherlands) and interpolated to the mcDESPOT images to extract the FBW throughout the tibial cartilage volume. The voxels were separated into superficial and deep portions by dividing the full cartilage thickness in half. The FBW was then averaged through the superficial half of the cartilage and through the full cartilage thickness to obtain superficial and full thickness FBW maps, respectively (Figure 2).

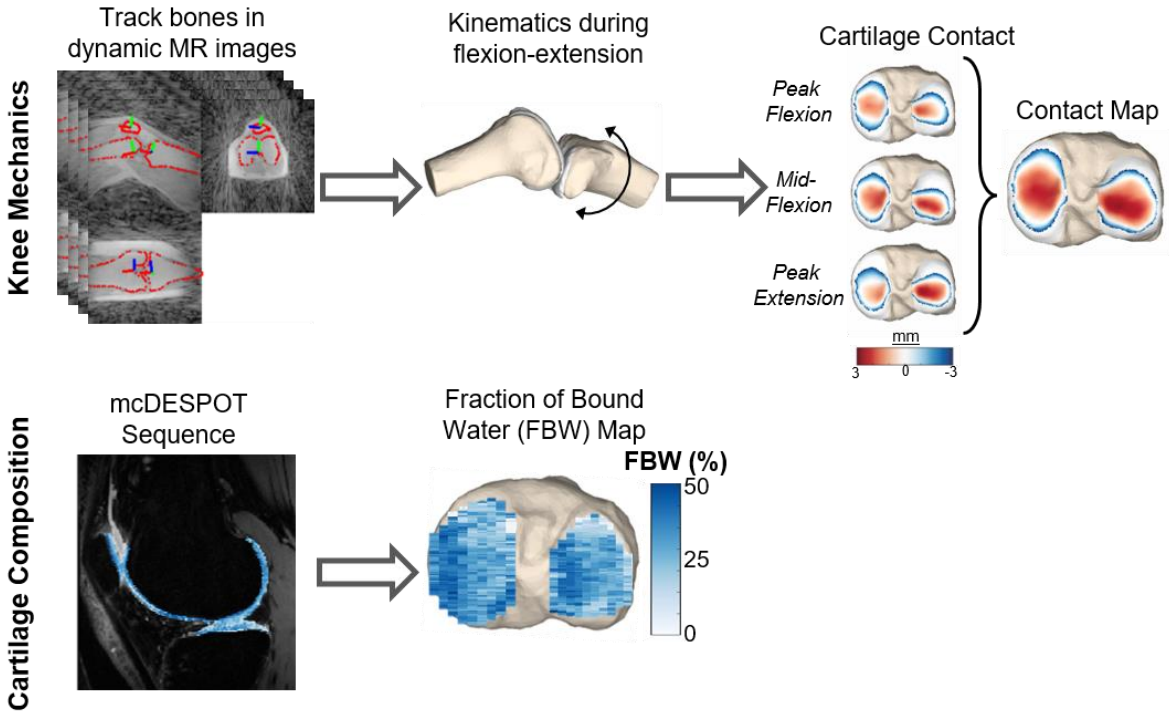

Figure 2: Composite figure shows the methods used to measure tibiofemoral kinematics, cartilage contact, and cartilage composition. (top row) Tibiofemoral kinematics were measured during active knee flexion-extension by tracking the bones in dynamic MR images collected during this motion. Cartilage contact was then computed by measuring the cartilage overlap during the flexion-extension motion. Contact maps were characterized as the maximum overlap of each triangle in the tibial cartilage mesh during the extension phase of the motion. (bottom row) Cartilage composition was characterized using a mcDESPOT sequence, which generated a measure of the FBW within the superficial layer and through the full thickness of the tibial cartilage.

2.4. MR Image Processing

Three-dimensional tibiofemoral motion was measured by tracking the position and orientation of the femur and tibia in the dynamic MR images (Figure 2). To do this, the position and orientation of the femoral and tibial bone models were optimized in each frame of the 3D dynamic MR images by minimizing the sum of squared intensities at the bone model vertices.[24,28] This model-based tracking method provides kinematics with precisions of <0.8º and 0.5 mm.[29]

Tibiofemoral kinematics were then computed as the position and orientation of the tibia relative to the femur throughout the flexion-extension motion[30] and filtered at a cutoff frequency of 5 Hz.[24]

Cartilage contact was then characterized based on the proximity of the cartilage meshes throughout the flexion-extension motion (Figure 2). The measured tibiofemoral kinematics were prescribed to the femoral and tibial cartilage meshes and the proximity of each triangle in the tibial mesh to the femoral mesh was determined by projecting a vector along the triangle normal from its center. The proximity was computed as the distance between the triangle center and the point of intersection of the vector on the femoral mesh.[31] A positive proximity was indicative of the meshes overlapping and, thus, cartilage contact. Cartilage contact maps were then generated by computing the maximum contact for each triangle in the tibial cartilage mesh during the extension phase of the motion (Figure 2).

A region of interest (ROI) analysis was used to discretize the cartilage contact and FBW maps. This allowed for direct comparisons across subjects and between the contact and FBW data. The cartilage meshes of each knee were divided into forty regions of interest—twenty medial and twenty lateral.[32] The contact and FBW maps were then averaged within each ROI.

2.5. Statistical Analysis

Six separate, two-factor repeated-measures analysis of variance (ANOVA) were used to assess differences in tibiofemoral kinematics, cartilage contact, and superficial and full thickness FBW across the multiple time points (objective 1). The first ANOVA tested for differences in tibiofemoral kinematics during knee extension between ACL conditions (ACLD, contralateral, and ACLR) and across knee flexion angle (interpolated at every 2.5º of extension). The second ANOVA tested for differences in tibiofemoral cartilage contact between ACL conditions and

across each ROI. The third and fourth ANOVAs tested for differences in the superficial and full-thickness FBW in the ACL injured knees between the first two time points and across each ROI. The fifth and sixth ANOVAs tested for differences in superficial and full-thickness FBW in the ACL injured knees between the first and third time points (TP1 and TP3) and across each ROI. For each of the ANOVAs, if a significant main effect was detected ($P < 0.05$), then post-hoc comparisons with a Bonferroni correction were performed to determine the knee flexion angle or ROI at which the group-based differences occurred.

A geospatial statistical analysis technique (bivariate local indicator of spatial association, i.e. BiLISA[33]) was used to determine correlations between abnormal cartilage contact in the ACL reconstructed knees and longitudinal changes in the FBW (objective 2). Side-to-side differences (reconstructed minus contralateral) and longitudinal changes in the superficial and full thickness FBW (TP2 minus TP1, n =10 and TP3 minus TP1, n = 7) were computed within each ROI for each subject. The BiLISA technique was then used to compute correlations between these contact and FBW differences across all the ROIs with significance set at $P < 0.05$.

3. Results

Differences in tibiofemoral kinematics were observed between the ACLD, ACLR, and contralateral knees during knee extension (Figure 3). ACLD knees exhibited greater anterior tibial translation, lateral tibial translation, and internal tibial rotation relative to the contralateral knees ($P < 0.0001$, $P = 0.04$, $P < 0.0001$, respectively). Additionally, ACLD knees were inferiorly translated relative to the contralateral knees ($P < 0.0001$). Following reconstruction, the ACLR knees exhibited a shift in kinematics such that differences were observed relative to both the ACLD and contralateral knees. A significant reduction in anterior tibial translation was observed in the

ACLR knees compared to the ACLD knees (P < 0.0001), but it was not restored to that of the contralateral knees (P < 0.0001). We also observed an overcorrection of the internal tibial rotation and lateral tibial translation of the ACLD knees, resulting in an externally rotated and medially translated tibia in the ACLR knees relative to the ACLD (*P* < 0.0001 for both) and contralateral knees (*P* < 0.0001, P = 0.007, respectively). The ACLR knees were also inferiorly translated relative to the contralateral knees (*P* < 0.0001).

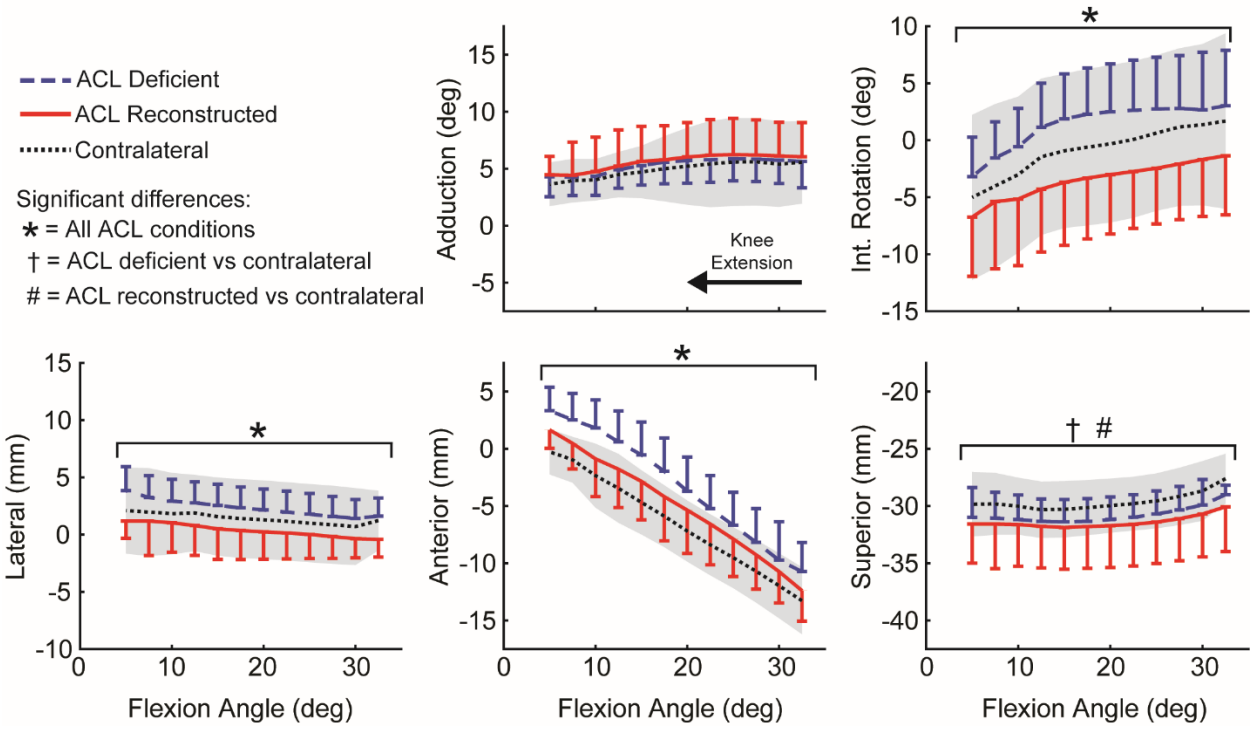

Figure 3: Composite figure shows tibiofemoral kinematics (mean ± standard deviation) measured during knee extension for the ACLD, ACLR, and contralateral knees. Significant differences were observed in internal tibial rotation, anterior tibial translation, and lateral tibial translation between all ACL conditions.

These kinematic abnormalities corresponded to differences in cartilage contact patterns across the ACL conditions (Figure 4). A significant difference in cartilage contact was observed between the ACLD, ACLR, and contralateral knees on the medial tibial plateau (ACLD: -2.0 ±

2.6, ACLR: -0.88 ± 3.4, contralateral: -2.1 ± 2.7, $P < 0.0001$ for all comparisons) and between the ACLD and the other ACL conditions on the lateral tibial plateau (ACLD: -2.4 ± 2.8 , ACLR: -1.8 ± 3.4, contralateral: -1.8 ± 3.4, $P = 0.0003$ for ACLD versus contralateral and ACLR). Post-hoc analyses indicated that, relative to the contralateral knee, ACLD knees exhibited significantly greater contact on the posterior aspect of the weight-bearing region of the medial plateau and less contact on the anterior aspect of the lateral plateau. ACLR knees exhibited greater contact on the posterior lateral-aspect of the medial tibial plateau, relative to the contralateral knees.

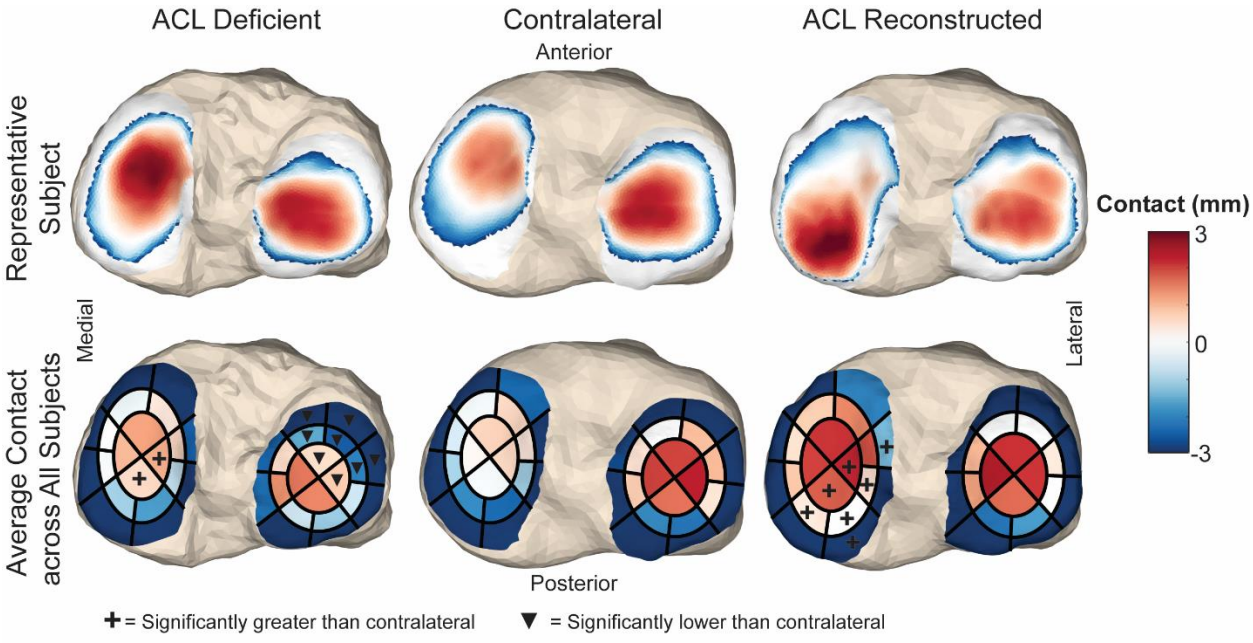

Figure 4: Composite figure shows significant differences in cartilage contact observed across the ACL conditions. (top row) Contact maps for the ACLD, contralateral, and ACLR knee of one subject that are representative of the average changes observed across all subjects. (bottom row) Average contact within each ROI measured across the ACLD, contralateral, and ACLR knees of all subjects.

Longitudinal changes in the FBW in the superficial cartilage layer and through the full thickness were observed across the three testing time points (Figure 5). Specifically, a progressive decrease in the superficial and full thickness FBW was observed in the medial tibial plateau of the

ACLR knees, relative to the ACLD knees (superficial, TP1: 27 ± 3%, TP2: 24 ± 4%, TP3: 21 ± 3%; full thickness, TP1: 26 ± 2%, TP2: 23 ± 3%, TP3: 22 ± 2%; $P < 0.0001$ for all comparisons). Post-hoc analyses revealed that the number of ROIs with a significant reduction in the FBW increased temporally. Additionally, reductions in the FBW occurred more commonly in the superficial layer than through the full cartilage thickness.

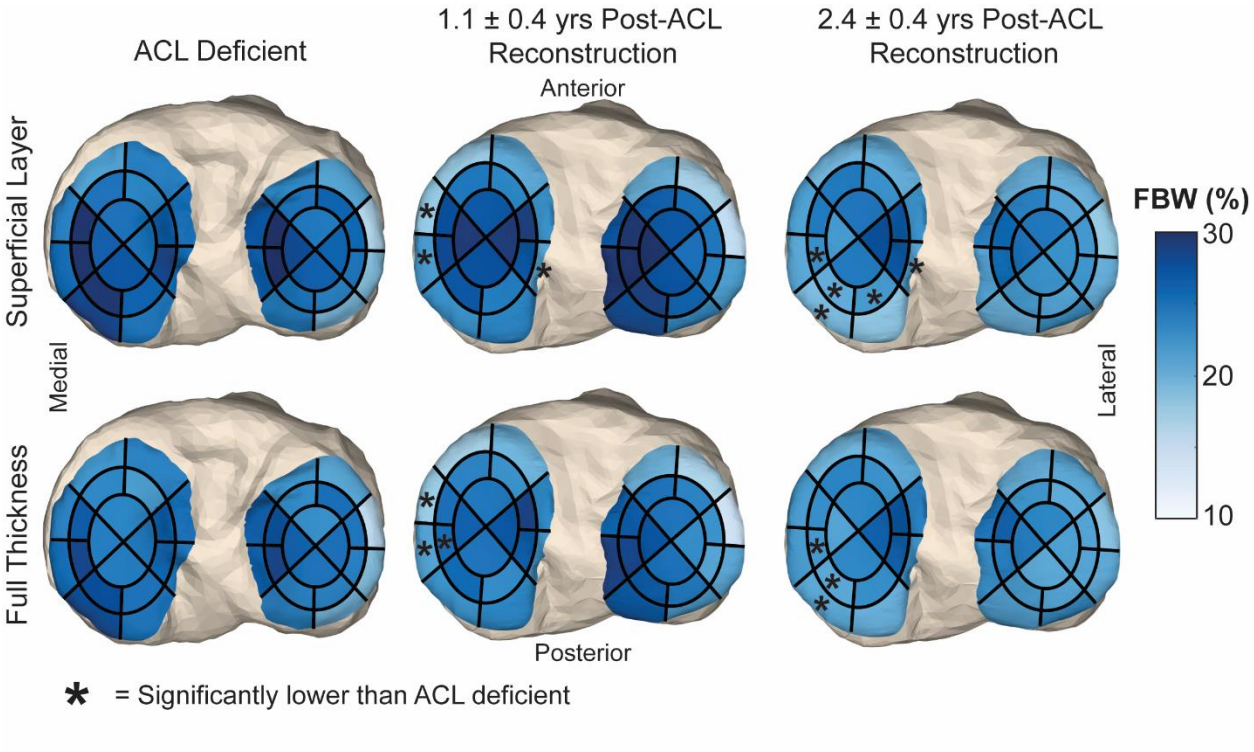

Figure 5: Composite figure shows the average FBW across all subjects within the superficial layer (top row) and through the full thickness (bottom row) of the tibial cartilage within each ROI at each time point. * indicates regions with significant reductions in the FBW, relative to the ACLD knees.

Significant correlations between abnormal cartilage contact and longitudinal changes in the FBW were observed in the ACLR knees (Figure 6). Following the completion of post-ACLR rehabilitation (i.e. TP2), greater cartilage contact in the reconstructed knee was significantly

correlated to changes in the superficial and full thickness FBW within most of the regions in which a reduction in the FBW was observed. Additionally, greater cartilage contact in the reconstructed knee at TP2 was correlated to reductions in the superficial and full thickness FBW measured at one year after TP2 (i.e. TP3).

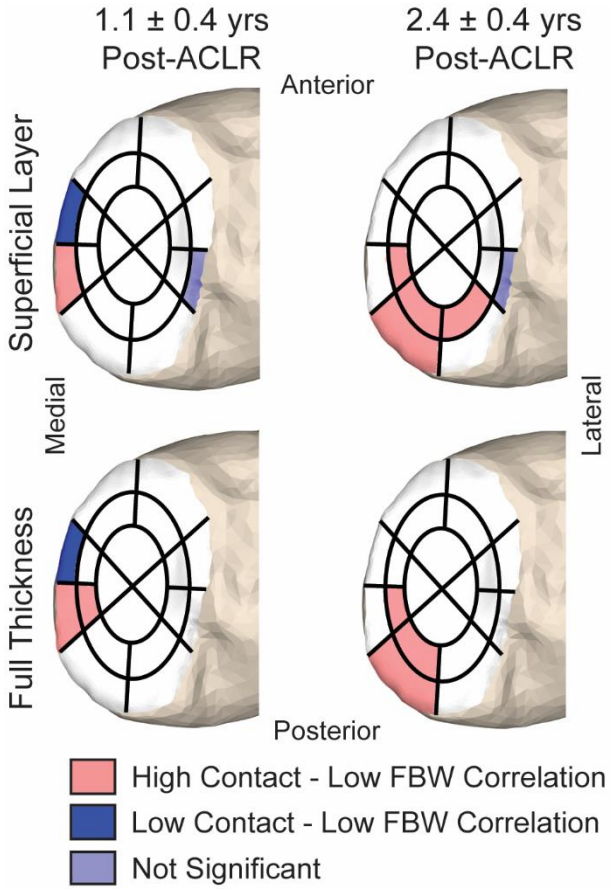

Figure 6: Composite figure shows the results of the geospatial analysis for those ROIs within which a significant reduction in the superficial layer (top row) and full thickness (bottom row) FBW were observed at approximately 1 year (left column) and 2.5 years (right column) post-ACLR. Red regions indicate those within which the reduction in FBW was significantly correlated with greater cartilage contact.

4. Discussion

This study aimed to investigate the theory that abnormal knee mechanics leads to the initiation and early development of OA in ACLR knees. To do this, we longitudinally assessed

changes in tibiofemoral kinematics, cartilage contact, and cartilage composition with dynamic and quantitative MR imaging. Our results demonstrate that, on average, ACLR is unable to restore normative tibiofemoral kinematics and cartilage contact patterns and, thus, results in elevated contact on the medial tibial plateau. Additionally, we found that these abnormal cartilage contact patterns were correlated with progressive changes in the cartilage composition at approximately 1 year and 2.5 years post-ACLR. To our knowledge, this is one of the first studies that has observed a direct link between abnormal cartilage contact patterns and early indicators of cartilage degeneration following ACLR.

Previous dynamic imaging studies have reported similar kinematic and cartilage contact abnormalities to those reported in this study. It has been observed that ACLD knees exhibit greater anterior tibial translation and internal tibial rotation relative to contralateral knees.[34] Additionally, it has commonly been reported that ACLR knees exhibit greater external tibial rotation during a range of tasks.[18–20] These kinematics abnormalities both lead to a posterior-lateral shift in the cartilage contact location on the tibial plateau.[21,35] We observed similar trends in this longitudinal investigation (Figure 3), thus suggesting that these shifts in knee mechanics are directly induced by surgical reconstruction of the ACL. However, we also observed a residual increase in anterior tibial translation in the ACLR knees. While it has been reported that ACLR typically restores anterior tibial translation during functional motion,[18] there is evidence of a progressive increase in anterior translation from 5 to 12 months post-ACLR,[19] potentially due to graft relaxation. Additionally, previous studies have shown that an active, open-chain knee extension task, similar to the one used in this study, induces greater anterior tibial translation than that observed during a closed-chain task.[36] Given that subjects were tested an average of 13.4 months following surgery,

this observed increase in anterior tibial translation may reflect an interaction of progressive changes in knee kinematics with the open-chain motion.

Quantitative MR imaging has become increasingly popular for use as a non-invasive technique for tracking changes in cartilage composition. This has been supported through previous work showing that quantitative MR relaxation parameters are related to the macromolecular content of the cartilage tissue[6,7] and that changes in these parameters have been linked to the severity of cartilage degeneration in OA patients.[37] Using T2, T1ρ, and mcDESPOT mapping, changes in the cartilage composition of ACLR knees has been detected within 6 months to 2 years following surgery.[11,35,38] In this study, we similarly used a quantitative MR imaging technique to track changes in cartilage composition and detected longitudinal reductions in the fraction of water bound to proteoglycan in the medial tibial plateau (Figure 5). Proteoglycan is critical for producing the hydrostatic compressive stiffness of cartilage tissue and a reduction in the proteoglycan content is commonly cited as an indicator of OA development.[39,40] Thus, the changes in the FBW observed in this study may be reflective of early cartilage degeneration. We also found that the greatest changes in the FBW occurred in the superficial cartilage layer. Localized fibrillation or disruption of the superficial layer of the cartilage surface is one of the earliest visible signs of articular cartilage degeneration.[39] Thus, the changes in FBW observed in the superficial cartilage layer may be a precursor to macroscopic cartilage tissue damage in these subjects. However, longer-term studies are needed to determine if changes in these quantitative MR parameters are predictive of future OA development.

It has commonly been theorized that residual abnormal knees mechanics following ACLR contribute to the initiation and progression of OA in this population.[13,14] In this study we detected significant correlations between increased cartilage contact and early signs of cartilage

degeneration (Figure 6), which support this theory. Previous studies have investigated similar relationships with cross-sectional designs and shown that greater anterior tibial positioning and abnormal cartilage contact paths are correlated with quantitative MR biomarkers of cartilage degeneration at a single time point post-ACLR.[41,42] However, to our knowledge, this is the first study to establish a direct link between abnormal cartilage contact and longitudinal changes in cartilage composition across specific regions of the cartilage tissue. Interestingly, we found that the correlations between contact and significant changes in cartilage composition most commonly occurred in the superficial cartilage tissue. This suggests that abnormal cartilage contact may contribute to the damage that occurs to the superficial cartilage layer early in OA development.[39] Future investigations are needed to determine if these altered knee mechanics are linked to long-term development of radiographic OA

There are three primary limitations to consider when interpreting the findings of this study. First, we focused our analysis on differences in cartilage contact and changes in FBW across only the tibial cartilage surface. Early changes in cartilage composition, as measured via quantitative MRI, have also been detected in the femoral and patellar cartilage and, thus, have relevance for long-term patient outcomes.[11,38] The dynamic and quantitative MR imaging techniques used in this study can also measure cartilage contact patterns and cartilage composition for these additional cartilage surfaces. This allows the potential to extend these analyses to investigate the link between knee mechanics and cartilage composition for the entire knee joint. Second, the cartilage contact metric used in this study does not account for the complex mechanical environment typically experienced by cartilage tissue. During movement, cartilage experiences a combination of compressive and shear stresses, which are resisted by a hydrostatic pressure created within the cartilage tissue by a complex interaction of collagen fibers, proteoglycan, and water.[39] The contact

metric used in this study is likely most comparable to the compressive pressure within the tissue and could be coupled with a more complex model of the cartilage to gain a better understanding of how these subtle shifts in knee mechanics affect the cartilage microstructure. Third, in this study we primarily considered cartilage contact as a potential cause of the observed changes in cartilage composition. However, previous studies have indicated multiple other factors that may also contribute to early cartilage degeneration in these patients, including acute cartilage damage sustained at injury,[43], subchondral bone bruising,[44] and inflammation within the joint capsule.[45,46] Future investigations are needed to assess the interaction of these additional factors with changes in knee mechanics to gain a more complete understanding of the pathogenesis of OA in ACLR patients.

In conclusion, the findings of this study indicate that residual abnormal knee mechanics that remain following ACLR are directly linked to changes in cartilage composition. These findings suggest that restoring normative cartilage loading is critical to reduce the high rate of OA development in this population. Future investigations are needed to assess the sensitivity of cartilage tissue degeneration to abnormal knee mechanics to gain a better understating of the accuracy needed in ACLR to improve long-term patient outcomes.

Acknowledgements

The authors gratefully acknowledge the contributions of Josh Roth, Colin Smith, Isaac Loegering, Oliver Wieben, Kevin Johnson, Kelli Hellenbrand, Frances Theisen, Sara John, and Jenelle Fuller. This material is based upon work supported by the National Science Foundation Graduate Research Fellowship Program under Grant No. DGE-1747503 and the National Institutes of Health (EB015410). Any opinions, findings, and conclusions or recommendations expressed in this material are those of the author(s) and do not necessarily reflect the views of the NSF or NIH.

Support was also provided by the Graduate School and the Office of the Vice Chancellor for Research and Graduate Education at the University of Wisconsin-Madison with funding from the Wisconsin Alumni Research Foundation.

References

1. Sanders TL, Maradit Kremers H, Bryan AJ, et al. 2016. Incidence of Anterior Cruciate Ligament Tears and Reconstruction: A 21-Year Population-Based Study. Am. J. Sports Med. 44(6):1502–1507.
2. Corry IS, Webb JM, Clingeleffer AJ, Pinczewski LA. 1999. Arthroscopic reconstruction of the anterior cruciate ligament. A comparison of patellar tendon autograft and four-strand hamstring tendon autograft. Am. J. Sports Med. 27(3):444–54.
3. O'Neill DB. 2001. Arthroscopically Assisted Reconstruction of the Anterior Cruciate Ligament: A Follow-Up Report. J. Bone Jt. Surg. 83a(9):1329–1332.
4. Otero AL, Hutcheson L. 1993. A comparison of the doubled semitendinosus/gracilis and central third of the patellar tendon autografts in arthroscopic anterior cruciate ligament reconstruction. Arthroscopy 9(2):143–148.
5. Lohmander LS, Englund PM, Dahl LL, Roos EM. 2007. The long-term consequence of anterior cruciate ligament and meniscus injuries: osteoarthritis. Am. J. Sports Med. 35(10):1756–69.
6. Duvvuri U, Kudchodkar S, Reddy R, Leigh JS. 2002. T1rho relaxation can assess longitudinal proteoglycan loss from articular cartilage in vitro. Osteoarthr. Cartil. 10(11):838–844.
7. Mosher TJ, Dardzinski BJ, Smith MB. 2000. Human Articular Cartilage: Influence of

Aging and Early Symptomatic Degenetation on the Spatial Variation of T2 - Preliminary Findings at 3T. Radiology 214(1):256–266.

8. Deoni SCL, Rutt BK, Arun T, et al. 2008. Gleaning Multicomponent T1 and T2 Information From Steady-State Imaging Data. Magn. Reson. Med. 60:1372–1387.
9. Liu F, Chaudhary R, Hurley SA, et al. 2014. Rapid Multicomponent T2 Analysis of the Articular Cartilage of the Human Knee Joint at 3.0T. J. Magn. Reson. Imaging 39:1191–1197.
10. Liu F, Choi KW, Samsonov A, et al. 2015. Articular Cartilage of the Human Knee Joint: In Vivo Multicomponent T2 Analysis at 3.0 T. Radiology 277(2):477–488.
11. Pedoia V, Su F, Amano K, et al. 2017. Analysis of the articular cartilage T1ρ and T2 relaxation times changes after ACL reconstruction in injured and contralateral knees and relationships with bone shape. J. Orthop. Res. 35(3):707–717.
12. Kaiser J, Vignos MF, Liu F, et al. 2016. American Society of Biomechanics Clinical Biomechanics Award 2015: MRI assessments of cartilage mechanics, morphology and composition following reconstruction of the anterior cruciate ligament. Clin. Biomech. 34.
13. Chaudhari AMW, Briant PL, Bevill SL, et al. 2008. Knee kinematics, cartilage morphology, and osteoarthritis after ACL injury. Med. Sci. Sports Exerc. 40(2):215–222.
14. Stergiou N, Ristanis S, Moraiti C, Georgoulis AD. 2007. Tibial rotation in anterior cruciate ligament (ACL)-deficient and ACL-reconstructed knees: A theoretical proposition for the development of osteoarthritis. Sport. Med. 37(7):601–613.
15. Beveridge JE, Heard BJ, Shrive NG, Frank CB. 2013. Tibiofemoral centroid velocity correlates more consistently with cartilage damage than does contact path length in two ovine models of stifle injury. J. Orthop. Res. 31(11):1745–1756.

16. Anderst WJ, Tashman S. 2009. The association between velocity of the center of closest proximity on subchondral bones and osteoarthritis progression. J. Orthop. Res. 27(1):71–77.

17. Griffin TM, Guilak F. 2005. The Role of Mechanical Loading in the Onset and Progression of Osteoarthritis. Exerc. Sport Sci. Rev. 33(4):195–200 Available from: http://content.wkhealth.com/linkback/openurl?sid=WKPTLP:landingpage&an=00003677-200510000-00008.

18. Tashman S, Collon D, Anderson K, et al. 2004. Abnormal Rotational Knee Motion During Running After Anterior Cruciate Ligament Reconstruction. Am. J. Sports Med. 32(4):975–983.

19. Hofbauer M, Thorhauer ED, Abebe E, et al. 2014. Altered Tibiofemoral Kinematics in the Affected Knee and Compensatory Changes in the Contralateral Knee After Anterior Cruciate Ligament Reconstruction. Am. J. Sports Med. 42(11):2715–2721.

20. Kaiser JM, Vignos MF, Kijowski R, et al. 2017. Effect of Loading on In Vivo Tibiofemoral and Patellofemoral Kinematics of Healthy and ACL-Reconstructed Knees. Am. J. Sports Med. 45(14).

21. Hosseini A, Van De Velde S, Gill TJ, Li G. 2012. Tibiofemoral Cartilage Contact Biomechanics in Patients after Reconstruction of a Ruptured Anterior Cruciate Ligament.(March):1781–1788.

22. Miranda DL, Rainbow MJ, Leventhal EL, et al. 2010. Automatic determination of anatomical coordinate systems for three- dimensional bone models of the isolated human knee. J. Biomech. 43(8):1623–1626.

23. Westphal CJ, Schmitz A, Reeder SB, Thelen DG. 2013. Load-dependent variations in

knee kinematics measured with dynamic MRI. J. Biomech. 46(12):2045–2052 Available from: http://dx.doi.org/10.1016/j.jbiomech.2013.05.027.

24. Kaiser J, Bradford R, Johnson K, et al. 2013. Measurement of Tibiofemoral Kinematics Using Highly Accelerated 3D Radial Sampling. Magn. Reson. Med. 69:1310–1316.

25. Besier TF, Fredericson M, Gold GE, et al. 2009. Knee muscle forces during walking and running in patellofemoral pain patients and pain-free controls. J. Biomech. 42(7):898–905.

26. Whittington B, Silder A, Heiderscheit B, Thelen DG. 2008. The contribution of passive-elastic mechanisms to lower extremity joint kinetics during human walking. Gait Posture 27(4):628–634.

27. Klein S, Staring M, Murphy K, et al. 2010. <emphasis emphasistype="mono">elastix</emphasis>: A Toolbox for Intensity-Based Medical Image Registration. IEEE Trans. Med. Imaging 29(1):196–205.

28. Powell M. 1964. An efficient method for finding the minimum of a function of several variables without calculating derivatives. Comput. J. 7(2):155–162.

29. Kaiser J, Monawer A, Chaudhary R, et al. 2016. Accuracy of model-based tracking of knee kinematics and cartilage contact measured by dynamic volumetric MRI. Med. Eng. Phys. 38:1–5 Available from: http://dx.doi.org/10.1016/j.medengphy.2016.06.016.

30. Grood ES, Suntay WJ. 1983. A joint coordinate system for the clinical description of three-dimensional motions: application to the knee. J. Biomech. Eng. 105(2):136–44.

31. Smith CR, Won Choi K, Negrut D, Thelen DG. 2016. Efficient computation of cartilage contact pressures within dynamic simulations of movement. Comput. Methods Biomech. Biomed. Eng. Imaging Vis. 1163(March):1–8 Available from: http://www.tandfonline.com/doi/full/10.1080/21681163.2016.1172346.

32. Wirth W, Eckstein F. 2008. A Technique for Regional Analysis of Femorotibial Cartilage Thickness Based on Quantitative Magnetic Resonance Imaging.27(6):737–744.

33. Anselin L, Syabri I, Kho Y. 2006. GeoDa: An introduction to spatial data analysis. Geogr. Anal. 38(1):5–22.

34. DeFrate LE. 2006. The 6 Degrees of Freedom Kinematics of the Knee After Anterior Cruciate Ligament Deficiency: An In Vivo Imaging Analysis. Am. J. Sports Med. 34(8):1240–1246 Available from: http://ajs.sagepub.com/lookup/doi/10.1177/0363546506287299.

35. Kaiser J, Vignos MF, Liu F, et al. 2016. American Society of Biomechanics Clinical Biomechanics Award 2015: MRI assessments of cartilage mechanics, morphology and composition following reconstruction of the anterior cruciate ligament. Clin. Biomech. 34:38–44.

36. Yack HJ, Collins CE, Whieldon TJ. 1993. Comparison of closed and open kinetic chain exercise in the anterior cruciate ligament-deficient knee. Am. J. Sport. Med. 21:49–53.

37. Li X, Ma CB, Link TM, et al. 2007. in Vivo T1Rho and T2 Mapping of Articular Cartilage in Osteoarthritis of the Knee Using 3 Tesla Mri. Osteoarthr. Cart. 15(7):789–797.

38. Li X, Kuo D, Theologis A, et al. 2011. Cartilage in anterior cruciate ligament-reconstructed knees: MR imaging T1rho and T2--initial experience with 1-year follow-up. Radiology 258(2):505–14.

39. Buckwalter JA, Lane NE. 1997. Current Concepts: Athletics and Osteoarthritis. Am. J. Sports Med. 25(6):873–881.

40. Rizkalla G, Reiner A, Bogoch E, Poole AR. 1992. Studies of the articular cartilage

proteoglycan aggrecan in health and osteoarthritis. Evidence for molecular heterogeneity and extensive molecular changes in disease. J. Clin. Invest. 90(6):2268–2277.

41. Li G, Li J-S, Torriani M, Hosseini A. 2018. Short-Term Contact Kinematic Changes and Longer-Term Biochemical Changes in the Cartilage After ACL Reconstruction: A Pilot Study. Ann. Biomed. Eng. Available from: http://link.springer.com/10.1007/s10439-018-2079-6.

42. Haughoms B, Schairer W, Souza BR, et al. 2012. Abnormal Tibiofemoral Kinematics Following ACL Reconstruction are Associated with Early Cartilage Matrix. Knee 19(4):482–487.

43. Bolbos RI, Ma CB, Link TM, et al. 2008. In vivo T1rho quantitative assessment of knee cartilage after anterior cruciate ligament injury using 3 Tesla magnetic resonance imaging. Invest. Radiol. 43(11):782–788.

44. Johnson DL, Bealle DP, Brand Jr. JC, et al. 2000. The effect of a geographic lateral bone bruise on knee inflammation after acute anterior cruciate ligament rupture. Am J Sport. Med 28(2):152–155 Available from: http://www.ncbi.nlm.nih.gov/pubmed/10750989.

45. Elsaid KA, Fleming BC, Oksendahl HL, et al. 2008. Decreased lubricin concentrations and markers of joint inflammation in the synovial fluid of patients with anterior cruciate ligament injury. Arthritis Rheum. 58(6):1707–1715.

46. Marks PH, Donaldson MLC. 2005. Inflammatory Cytokine Profiles Associated With Chondral Damage in the Anterior Cruciate Ligament-Deficient Knee. Arthrosc. J. Arthrosc. Relat. Surg. 21(11):1342–1347.

Chapter 3: American Society of Biomechanics Clinical Biomechanics Award 2017: Non-Anatomic Graft Geometry is Linked with Asymmetric Tibiofemoral Kinematics and Cartilage Contact Following Anterior Cruciate Ligament Reconstruction

Michael F. Vignos, Jarred Kaiser, Geoffrey S. Baer, Richard Kijowski, Darryl G. Thelen

(This chapter is published in *Clinical Biomechanics* as the recipient of the *2017 American Society of Biomechanics Clinical Biomechanics Award*)

Abstract

Background

Abnormal knee mechanics may contribute to early cartilage degeneration following anterior cruciate ligament reconstruction. Anterior cruciate ligament graft geometry has previously been linked to abnormal tibiofemoral kinematics, suggesting this parameter may be important in restoring normative cartilage loading. However, the relationship between graft geometry and cartilage contact is unknown.

Methods

Static MR images were collected and segmented for eighteen subjects to obtain bone, cartilage, and anterior cruciate ligament geometries for their reconstructed and contralateral knees. The footprint locations and orientation of the anterior cruciate ligament were calculated. Volumetric, dynamic MR imaging was also performed to measure tibiofemoral kinematics, cartilage contact location, and contact sliding velocity while subjects performed loaded knee flexion-extension. Multiple linear regression was used to determine the relationship between non-anatomic graft geometry and asymmetric knee mechanics.

Findings

Non-anatomic graft geometry was related to asymmetric knee mechanics, with the sagittal plane graft angle being the best predictor of asymmetry. A more vertical sagittal graft angle was associated with greater anterior tibial translation (β=0.11$^{mm}/_{deg}$, P=0.049, R^2=0.22), internal tibial rotation (β=0.27$^{deg}/_{deg}$, P=0.042, R^2=0.23), and adduction angle (β=0.15$^{deg}/_{deg}$, P=0.013, R^2=0.44) at peak knee flexion. A non-anatomic sagittal graft orientation was also linked to asymmetries in tibial contact location and sliding velocity on the medial (β=-4.2$^{mm/s}/_{deg}$, P=0.002, R^2=0.58) and lateral tibial plateaus (β=5.7$^{mm/s}/_{deg}$, P=0.006, R^2=0.54).

Interpretation

This study provides evidence that non-anatomic graft geometry is linked to asymmetric knee mechanics, suggesting that restoring native anterior cruciate ligament geometry may be important to mitigate the risk of early cartilage degeneration in these patients.

Key words: knee; anterior cruciate ligament reconstruction; cartilage; anterior cruciate ligament graft; MRI; osteoarthritis

1. Introduction

Anterior cruciate ligament reconstruction (ACLR) procedures are common, with over 150,000 occurring in the United States each year (Sanders et al., 2016). The primary goal of ACLR is to restore knee stability such that patients can return to previous levels of activity. ACLR is generally successful at meeting this short-term goal, with good or excellent outcomes reported in 90% or more of patients (Corry et al., 1999; O'Neill, 2001; Otero and Hutcheson, 1993). However, the long-term prognosis after ACLR is not as favorable, with greater than 50% of patients exhibiting radiographic evidence of post-traumatic osteoarthritis (PTOA) at 10 to 15 year follow-up (Lohmander et al., 2007).

It is theorized that osteoarthritis in ACLR patients may arise, in part, from abnormal cartilage tissue loading after surgery (Chaudhari et al., 2008; Stergiou et al., 2007). Indeed, prior studies have identified asymmetries in ACLR knee kinematics that would affect the location of cartilage contact (Decker et al., 2011; Hofbauer et al., 2014; Kaiser et al., 2017; Scanlan et al., 2010; Tashman et al., 2006). Additionally, *in vitro* studies have shown that cartilage damage can be initiated by altering the load on cartilage tissue from its homeostatic condition (Griffin and Guilak, 2005). Animal studies have also shown that abnormal cartilage loading, specifically increased tibiofemoral sliding velocity, can initiate cartilage degeneration patterns seen in PTOA (Anderst and Tashman, 2009; Beveridge et al., 2013). Thus, identifying surgical factors that can be modified to restore normal knee mechanics may help improve long-term outcomes of ACLR.

ACL graft tunnel location has been linked to abnormal post-operative tibiofemoral kinematics, suggesting that it may be an important surgical factor in ACLR. Cadaveric studies have shown that variations in femoral tunnel location lead to altered anterior tibial translation (Musahl et al., 2011; Zavras et al., 2005). Additionally, a more vertical graft increases the passive

anterior and rotational laxities of the knee (Brophy and Pearle, 2009; Loh et al., 2003). *In vivo* investigations have found that graft tunnel location also affects tibiofemoral mechanics during functional movement (Abebe et al., 2011b; Ristanis et al., 2009; Zampeli et al., 2012). For example, variations in femoral tunnel placement have been associated with greater anterior tibial translation, medial tibial translation, and internal tibial rotation in ACL reconstructed knees during a quasi-static lunge (Abebe et al., 2011a, 2011b). However, the effects of these kinematic asymmetries on cartilage loading patterns are less understood, though important to understand implications for PTOA after ACLR.

The objective of this study was to investigate the relationship between ACL graft tunnel location, graft orientation, and tibiofemoral kinematics and cartilage contact in ACLR subjects. To do this, we utilized a combination of static and dynamic magnetic resonance imaging to obtain *in vivo* measurements of ACL graft geometry and post-operative knee mechanics during loaded knee flexion-extension. We first investigated whether there was evidence of systematic bias in ACL graft geometry, tibiofemoral kinematics, or tibial cartilage contact in ACLR knees when compared to the contralateral knees. We then tested the hypothesis that a more vertically oriented ACL graft would be related to greater anterior tibial translation and internal tibial rotation and would also be related to abnormal cartilage contact location and sliding velocity on the tibial plateau.

2. Methods

2.1 Subjects

The bilateral knees of 18 subjects that underwent a primary unilateral, isolated ACLR were tested (9 male, 9 female, mean: 24.8 (SD: 5.7) yrs, 78.9 (SD: 16.5) kg, 20.2 (SD: 8.7) months post-op). The surgeon performing the procedure and the graft type used in the ACLR were not

controlled (9 bone-patellar tendon-bone grafts, 9 hamstrings tendon grafts, 1 subject with small, stable medial and lateral meniscal tears, 2 subjects with small partial, lateral meniscectomies). Subjects provided informed consent according to a University of Wisconsin-Madison Institutional Review Board approved protocol. The subjects' reconstructed knees had no history of septic, inflammatory, or crystalline-induced arthritis, and no post-operative complications. The contralateral knees had no history of pain, injury, or surgery and no history of septic, inflammatory, or crystalline-induced arthritis. At the time of testing, all subjects had been released to return to full participation in sporting activities based on successful completion of post-operative physical therapy.

2.2 Static and Dynamic MR Imaging

The subjects underwent a bilateral static magnetic resonance (MR) imaging protocol consisting of a three-dimensional intermediate-weighted fast spin-echo sequence (3D FSE Cube) and a three-dimensional spoiled gradient recall-echo sequence with iterative decomposition with echo asymmetry and least squares estimation fat-water separation sequence (IDEAL-SPGR) (Fig. 1) (Kaiser et al., 2013). MR scans were performed in a 3.0 T clinical scanner (Discovery MR750, GE Healthcare, Waukesha, WI, USA) using an 8-channel phased array extremity coil (InVivo, Orlando, FL, USA) positioned around the knee. The 3D FSE Cube sequence was used to obtain images for characterizing ligament and cartilage morphology (in-plane sagittal resolution, 0.39 x 0.39 mm; slice thickness, 1.0 mm; matrix, 384 x 384 x 96; repetition time, 2066.7 ms; echo time, 19.8 ms; flip angle, 90°). The IDEAL-SPGR sequence was used to obtain images for characterizing bone morphology (in-plane axial resolution, 0.37 x 0.37 mm; slice thickness, 0.9 mm; matrix, 512 x 512 x 304; repetition time, 10 ms; echo times, 4.5/5.5/6.1 ms; flip angle, 14°).

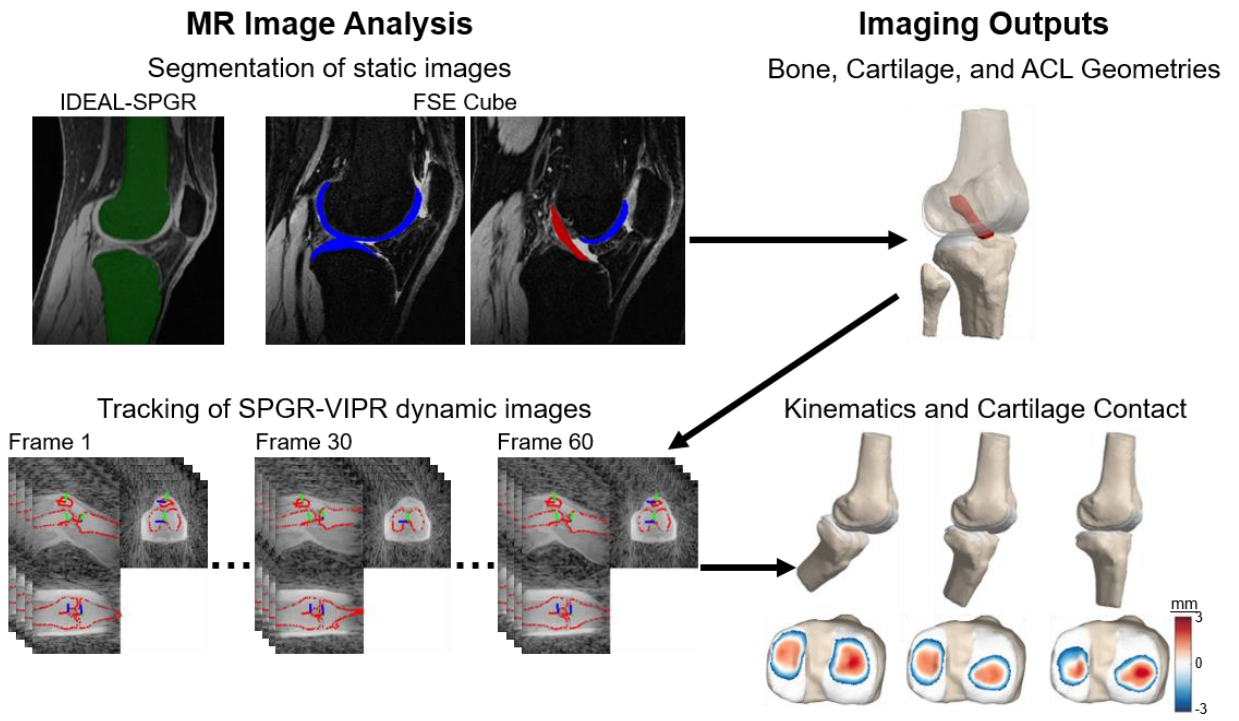

Figure 1: Workflow for MR Image Analysis. (Top row) Subject-specific bone, cartilage, and ACL geometries were created by segmenting IDEAL-SPGR and 3D FSE Cube MR images of both knees of each subject. (Bottom row) Subjects performed an active flexion-extension motion against an inertial load while volumetric, dynamic MR images were collected with an SPGR-VIPR sequence. The bones were tracked in the dynamic images using the bone geometries. Tibiofemoral kinematics were then computed using the position and orientation of the tibia relative to the femur (Grood and Suntay, 1983). Cartilage contact was computed by prescribing the tibiofemoral kinematics to the femoral and tibial cartilage geometries and measuring the overlap of the cartilage surfaces.

Following completion of static MR imaging, subjects underwent a bilateral dynamic MR imaging protocol with their lower leg secured to the lever arm of an MR-compatible knee-loading device (Westphal et al., 2013). Subjects performed cyclic knee flexion-extension at 0.5 Hz with the rate denoted by an audible metronome. During this task, the device induced active stretch-shortening quadriceps contractions by applying an inertial load to the subjects' lower leg via a set of rotating disks (Westphal et al., 2013). This quadriceps loading paradigm mimics the loading-response phase of walking (Besier et al., 2009; Whittington et al., 2008).

Subjects performed this knee flexion-extension motion for 5 minutes while a 3D SPGR sequence with vastly under-sampled isotropic projections (3D SPGR-VIPR) continuously acquired volumetric data (Fig. 1) (1.5-mm isotropic resolution; repetition time, 4 ms; echo time, 1.4 ms; flip angle, 8°; receiver bandwidth, 32.5 kHz; unique radial lines, 93,922; field of view, 48 cm). During this motion, an MRI-compatible rotary encoder tracked the lever arm angle (Micronor Inc., Camarillo, CA, USA). This angle was used to determine the beginning of each flexion-extension cycle. The SPGR-VIPR projections were then sorted into 60 equally-spaced bins based on percent of the total cycle (Kaiser et al., 2013). The sorted projections were reconstructed into 60 volumetric image sets over the flexion-extension motion using conjugate gradient least squares minimization (Pruessmann et al., 2001). Each of these image frames consisted of an average of the MR data collected during 1.67%, or 33.3 ms, of the 2 sec flexion-extension cycle.

2.3 MR Image Processing

Distal femur and proximal tibia bone geometries were manually segmented from the IDEAL-SPGR images (Fig. 1) (MIMICS, Materialise Group, Leuven, Belgium). Femoral and tibial articular cartilage, native ACL, and ACL reconstruction graft geometries were manually segmented from the 3D FSE Cube images and registered to the bone geometries. Bone, cartilage, and ACL geometries were smoothed and converted into triangular meshes (7000 triangles/surface for bones and approximately 0.33 mm^2/triangle for cartilage and ACL meshes); (Geomagic Studio, 3D Systems, Rock Hill, SC, USA and MeshLab, Visual Computing Lab-ISTI-CNR, Pisa, Italy). Anatomical references frames were independently established for each femur and tibia using an algorithm that automatically determined the coordinate systems based on the geometric and inertial properties of the bone (Miranda et al., 2010).

The segmented bone and ACL meshes were used to characterize ACL geometry (Fig. 2A). The ACL femoral and tibial footprints were defined as the intersection of the ACL mesh with the femoral and tibial meshes, respectively. We then computed the location of the center of the femoral and tibial footprints relative to anatomical landmarks and expressed the location in the femoral and tibial reference frames, respectively. Femoral footprint location was measured relative to the most anterior point of the trochlear groove and the most inferior point of the lateral femoral condyle. The tibial footprint location was measured relative to the most anterior and most medial points of the tibial plateau. A cylinder was then fit to the mid-substance of the ACL and ACL graft and a plane was fit to the tibial plateau. The long axis of the cylinder was used to compute the ACL orientation in the frontal and sagittal planes relative to the best-fit plane. Non-anatomic ACL graft geometry metrics were computed as the side-to-side differences (reconstructed minus contralateral) in the femoral and tibial footprint locations, the ACL frontal plane orientation, and the ACL sagittal plane orientation.

Tibiofemoral kinematics were measured by tracking the femur and tibia in the 3D dynamic MR images (Fig. 1). To do this, the femoral and tibial bone meshes were manually placed in the first dynamic image frame. The bones' position and orientation were then determined by minimizing the sum of squared intensities at each vertex of the bone meshes (Kaiser et al., 2013; Powell, 1964). The solution for this frame was then used as the initial guess for the next frame and the optimization proceeded until the bones were tracked in all remaining dynamic MR image frames. This model-based tracking method provides kinematics with precisions of less than 0.8° and 0.5 mm (Kaiser et al., 2016a). Tibiofemoral kinematics were computed as the position and orientation of the tibia relative to the femur in each dynamic image frame (Grood and Suntay,

1983). Kinematics were low-pass filtered at a cutoff frequency of 5 Hz, which is 10 times greater than the flexion-extension cycle rate performed by subjects.

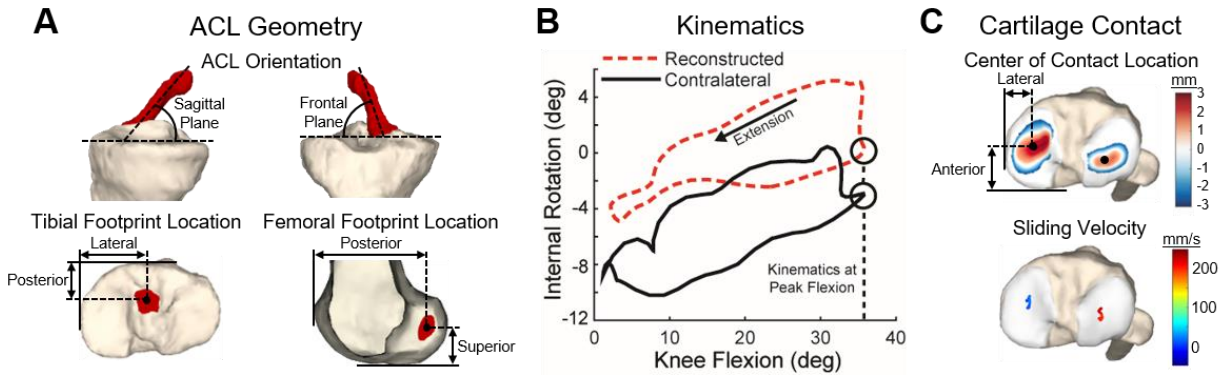

Figure 2: ACL Geometry, Kinematics, and Cartilage Contact Metrics. (A) The orientation of the ACL relative to the tibial plateau in the sagittal and frontal planes, the location of the tibial footprint in the axial plane, and the location of the femoral footprint in the sagittal plane were computed for both knees of each subject. (B) Representative plot showing internal tibial rotation throughout the flexion-extension motion for both knees of one subject. The extension phase of the motion is denoted with an arrow. Similar plots were created for the other five degrees of freedom of the tibiofemoral joint. Kinematics metrics were then computed as the kinematics at peak knee flexion and the range in kinematics during knee extension. (C) Top row shows the proximity of the tibial cartilage to the femoral cartilage at peak knee flexion for the contralateral knee of a representative subject. Red is indicative of cartilage contact. Similar maps were generated for both knees of each subject and used to compute the center of contact location on the tibial plateaus. Bottom row shows the cartilage surface sliding velocity on the medial and lateral tibial plateaus during knee extension for the contralateral knee of a representative subject. The mean absolute sliding velocity during extension and the sliding velocity at peak knee flexion were computed for both knees of each subject.

Cartilage contact was characterized based on the proximity between the femoral and tibial cartilage meshes at each frame of the cyclic motion. For each triangle in the tibial mesh, proximity was computed by projecting along the triangle normal, and then computing the distance between the triangle center and the point of intersection on the femoral mesh (Smith et al., 2016). A positive proximity was indicative of mesh overlap and, thus, cartilage contact (Fig. 1). The proximity of the tibial cartilage mesh was re-zeroed such that at least one triangle was in contact at each frame of the flexion-extension motion in both the medial and lateral compartments (Borotikar and

Sheehan, 2013; Kaiser et al., 2016b). The center of contact locations on the medial and lateral tibial plateaus and the medial and lateral femoral condyles were computed as the weighted-average position of the contact region, with the position of each triangle weighted by its proximity. This method of measuring the center of contact location from the SPGR-VIPR images has precisions less than 0.25 mm and 0.49 mm in the anterior-posterior and medial-lateral directions, respectively (Kaiser et al., 2016a).

A first-order central finite difference approximation was used to compute the center of contact velocities for the medial and lateral compartments of the femur and tibia (Beveridge et al., 2013). The femoral center of contact velocities were then subtracted from the corresponding velocities of the tibia to determine the sliding velocity vectors. The sliding velocity vectors were then projected onto a tangent plane at the center of contact, and the magnitudes of the projected velocity vectors were computed. This metric has previously been used as a measure of cartilage contact sliding velocity (Anderst and Tashman, 2009; Beveridge et al., 2013).

Kinematic and cartilage contact metrics were computed for the reconstructed and contralateral knees. Kinematic metrics were defined as the tibiofemoral kinematics (i.e. internal tibial rotation, adduction angle, and anterior, lateral, and superior tibial translations) at peak knee flexion and the range in tibiofemoral kinematics during the extension phase of the flexion-extension motion (Fig. 2B). Cartilage contact location metrics were defined as the anterior and lateral location of the center of contact on the medial and lateral tibial plateaus at peak knee flexion (Fig. 2C). Cartilage contact sliding velocity metrics were computed as the sliding velocity at peak knee flexion and the mean absolute sliding velocity during knee extension for the medial and lateral compartments. Asymmetric kinematics and cartilage contact were computed as the side-to-side differences (reconstructed minus contralateral) in these metrics.

2.4 Statistical Analysis

Paired t-tests were used to determine if there was a bias in the ACL graft footprint locations or orientations relative to the native ACLs ($\alpha = 0.05$). Paired t-tests were also used to test for differences in the kinematics and contact metrics between reconstructed and contralateral knees ($\alpha = 0.05$). A multiple linear regression analysis was used to determine the relationship between non-anatomic ACL graft geometry and asymmetric tibiofemoral kinematics and cartilage contact. In this linear regression analysis, the independent variables were the non-anatomic ACL graft geometry metrics and the dependent variables were the asymmetric tibiofemoral kinematics, cartilage contact location, and cartilage contact sliding velocity metrics. When a significant relationship was found ($\alpha = 0.05$), the coefficient of the linear regression model (β) was used to determine the sensitivity of kinematics and cartilage contact to non-anatomic graft geometry.

3. Results

The tibial footprints of the reconstructed knees were significantly more posterior than that of the contralateral knees (reconstructed mean: 21.6 (SD: 3.3) mm, contralateral mean: 19.3 (SD: 2.5) mm, P=0.001, Cohen's d=0.92) (Table 1). No other ACL geometry metrics were significantly different between the reconstructed and contralateral knees.

Table 1: Side-to-side comparisons of ACL graft geometry. The location of the femoral footprint in the sagittal plane, location of the tibial footprint in the axial plane, and orientation of the ACL in the sagittal and frontal planes for the reconstructed and contralateral knees. *P*-values are the result of paired t-tests. Effect size computed as Cohen's *d* coefficient.

		Reconstructed mean (SD)	Contralateral mean (SD)	*P*-value	Effect Size
Femoral Footprint Location (mm)	Superior	21.1 (5.1)	21.6 (2.4)	0.75	-0.075
	Posterior	49.1 (4.4)	49.8 (3.8)	0.37	-0.22
Tibial Footprint Location (mm)	Lateral	40.3 (2.6)	40.5 (2.9)	0.77	-0.070
	Posterior	21.6 (3.3)	19.3 (2.5)	**0.001**	**0.92**
ACL Orientation (deg)	Sagittal Plane	51.2 (6.0)	53.8 (7.4)	0.22	-0.30
	Frontal Plane	73.5 (5.7)	72.8 (5.7)	0.65	0.11

Reconstructed knees exhibited altered kinematics and cartilage contact relative to the contralateral knees. Specifically, reconstructed knees were more externally rotated (side-to-side difference: 2.9º (SD: 5.4º), *P*=0.04, Cohen's *d*=0.53) and medially translated (1.6 (SD: 2.5) mm, *P*=0.01, Cohen's *d*=0.65) at peak knee flexion. Additionally, reconstructed knees exhibited a greater range in knee adduction during extension (0.81º (SD: 1.4º), *P*=0.03, Cohen's *d*=0.56). The center of contact was more posterior in reconstructed knees on both plateaus at peak knee flexion (side-to-side difference medial: 2.0 (SD: 3.4) mm, *P*=0.02, Cohen's *d*=0.60; side-to-side difference lateral: 1.2 (SD: 2.2) mm, *P* = 0.04, Cohen's *d*=0.53).

Non-anatomic ACL graft geometry was associated with asymmetric tibiofemoral kinematics, with the sagittal plane orientation of the ACL being the best predictor of asymmetric motion (Table 2). Specifically, a more vertical graft in the sagittal plane (i.e. a greater sagittal plane angle) was significantly linked with greater anterior tibial translation (β=0.11 $^{mm}/_{deg}$, *P*=0.049, R^2=0.22), internal tibial rotation (β=0.27 $^{deg}/_{deg}$, *P*=0.042, R^2=0.23), and adduction angle

(β=0.15 $^{deg}/_{deg}$, P=0.013, R^2=0.44) at peak knee flexion (Fig. 3). Additionally, a more vertical graft in the frontal plane (i.e. a greater frontal plane angle) was related to a reduced range in lateral tibial translation during extension (β=-0.089 $^{mm}/_{deg}$, P=0.046, R^2=0.23). The tibial footprint location was also related to asymmetric kinematics, with a more lateral tibial footprint associated with a greater range in anterior translation (β=0.49 $^{mm}/_{mm}$, P=0.0089, R^2=0.36) and a more posterior tibial footprint related to a less adducted knee at peak knee flexion (β=-0.44 $^{deg}/_{mm}$, P=0.032, R^2=0.44). A more superior femoral footprint was linked to greater lateral tibial translation (β=0.26 $^{mm}/_{mm}$, P=0.021, R^2=0.29).

Table 2: Relationships between Kinematics and ACL Graft Geometry. Coefficients of the linear regression model (β) for those relationships between asymmetric kinematics and non-anatomic ACL graft geometry that were statistically significant (*P<0.05, **P<0.01).

		ACL Orientation (deg)		Tibial Footprint Location (mm)		Femoral Footprint Location (mm)	
		Sagittal Plane	Frontal Plane	Lateral	Posterior	Superior	Posterior
Anterior Translation (mm)	At Peak Flexion	0.11 $^{mm}/_{deg}$*	–	–	–	–	–
	Range	–	–	0.49 $^{mm}/_{mm}$**	–	–	–
Lateral Translation (mm)	At Peak Flexion	–	–	–	–	0.26 $^{mm}/_{mm}$*	–
	Range	–	-0.087 $^{mm}/_{deg}$*	–	–	–	–
Internal Rotation (deg)	At Peak Flexion	0.27 $^{deg}/_{deg}$*	–	–	–	–	–
Adduction Angle (deg)	At Peak Flexion	0.15 $^{deg}/_{deg}$*	–	–	-0.44 $^{deg}/_{mm}$*	–	–

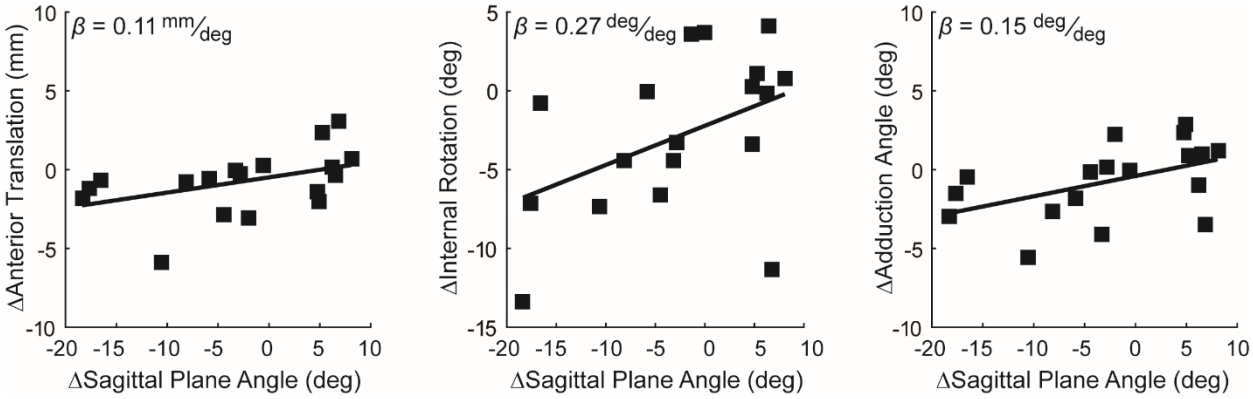

Figure 3: Relationship between Kinematics and ACL Sagittal Plane Angle. Scatter plots show the relationship between asymmetric kinematics and non-anatomic graft sagittal plane angles for anterior tibial translation, internal tibial rotation, and adduction angle at peak knee flexion. The coefficient of the linear regression model (β) is shown for each relationship.

Non-anatomic ACL graft geometry was also associated with asymmetric tibiofemoral cartilage contact (Table 3). Similar to kinematics, the graft sagittal plane orientation was most often significantly related to asymmetries in the center of contact location and cartilage contact sliding velocity. A greater sagittal plane angle was associated with a more medial center of contact on both the medial (β=-0.32$^{mm}/_{deg}$, P=0.003, R^2=0.43) and lateral (β=-0.27 $^{mm}/_{deg}$, P=0.002, R^2=0.45) tibial plateaus and a more posterior center of contact on the lateral plateau at peak knee flexion (β=-0.11$^{mm}/_{deg}$, P=0.030, R^2=0.45) (Fig. 4A). During extension, a greater sagittal plane angle was related to lower mean absolute contact sliding velocity in the medial compartment (β=-4.2 $^{mm/s}\big/_{deg}$, P=0.002, R^2=0.58), but greater mean absolute sliding velocity in the lateral compartment (β=5.7 $^{mm/s}\big/_{deg}$, P=0.006, R^2=0.54) (Fig. 4B).

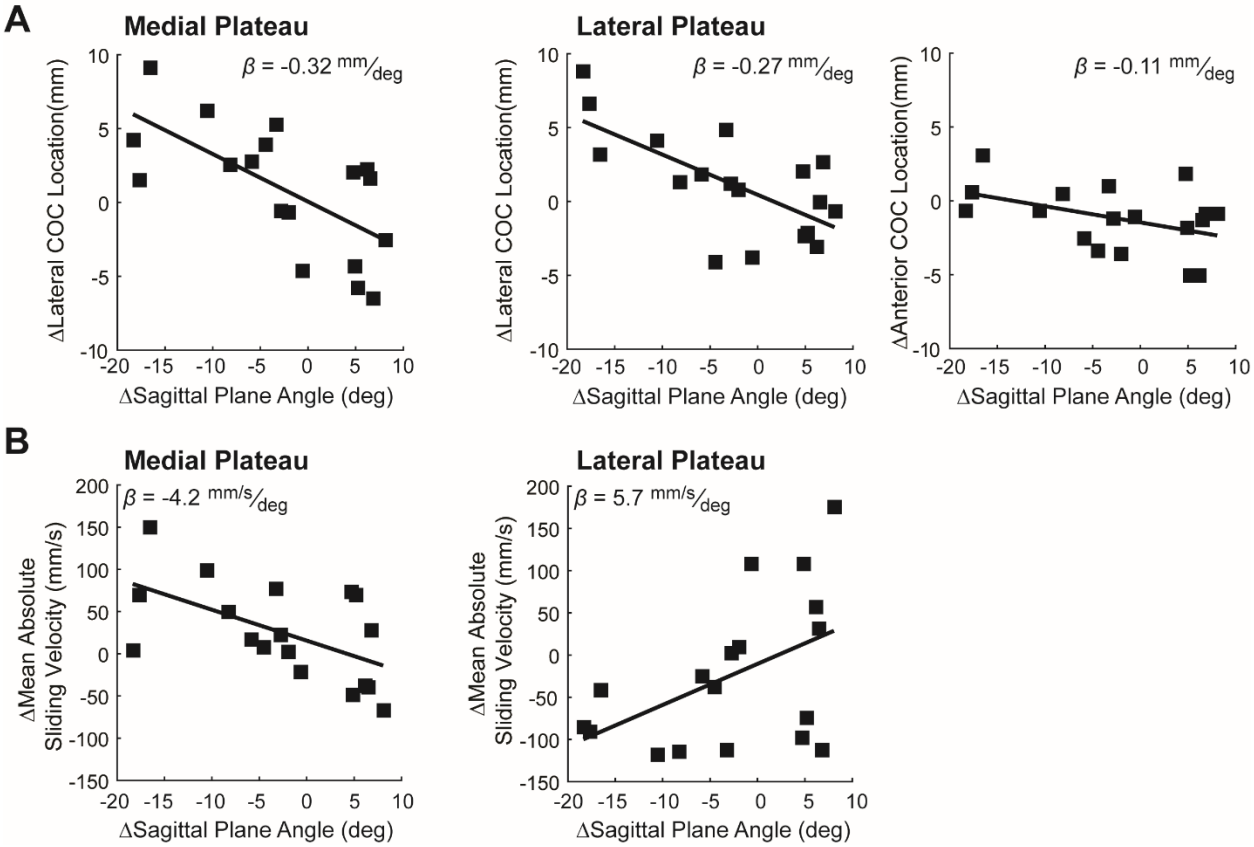

Figure 4: Relationship between Cartilage Contact and ACL Sagittal Plane Angle. Scatter plots show the relationships between asymmetric cartilage contact and non-anatomic graft sagittal plane angles for (A) the center of contact location and (B) the mean absolute contact sliding velocity for the medial and lateral tibial plateaus. The coefficient of the linear regression model (β) is shown for each relationship.

The tibial and femoral footprint locations were also frequently associated with asymmetric cartilage contact (Table 3). A more lateral tibial footprint was related to a more posterior center of contact on the lateral plateau (β=-0.51 $^{mm}/_{mm}$, P=0.018, R^2=0.45). Additionally, a more posterior tibial footprint was related to lower mean absolute contact sliding velocity during extension (β=-12 $^{mm/s}/_{mm}$, P=0.008, R^2=0.58) and at peak knee flexion (β=-37 $^{mm/s}/_{mm}$, P=0.020, R^2=0.29) in the medial compartment, but greater sliding velocity in the lateral compartment (β=20 $^{mm/s}/_{mm}$, P=0.006, R^2=0.54). A more posterior femoral footprint was

associated with reduced sliding velocity in the lateral compartment at peak knee flexion (β=-33 $^{mm}/_{s}/_{mm}$, P=0.049, R^2=0.22).

Table 3: Relationships between Cartilage Contact and ACL Graft Geometry. Coefficients of the linear regression model (β) for those relationships between asymmetric cartilage contact and non-anatomic ACL graft geometry that were statistically significant (*P<0.05, **P<0.01).

			ACL Orientation (deg)		Tibial Footprint Location (mm)		Femoral Footprint Location (mm)	
			Sagittal Plane	Frontal Plane	Lateral	Posterior	Superior	Posterior
Center of Contact Location (mm)	Medial Tibial Plateau	Anterior	–	–	–	–	–	–
		Lateral	-0.32 $^{mm}/_{deg}$**	–	–	–	–	–
	Lateral Tibial Plateau	Anterior	-0.11 $^{mm}/_{deg}$*	–	-0.51 $^{mm}/_{mm}$*	–	–	–
		Lateral	-0.27 $^{mm}/_{deg}$**	–	–	–	–	–
Sliding Velocity (mm/s)	Medial Tibial Plateau	Mean Absolute	-4.2 $^{mm/s}/_{deg}$**	–	–	-11.9 $^{mm/s}/_{mm}$**	–	–
		At Peak Flexion	–	–	–	-36.9 $^{mm/s}/_{mm}$*	–	–
	Lateral Tibial Plateau	Mean Absolute	5.7 $^{mm/s}/_{deg}$**	–	–	20.2 $^{mm/s}/_{mm}$**	–	–
		At Peak Flexion	–	–	–	–	–	-33.0 $^{mm/s}/_{mm}$*

4. Discussion

Current ACLR surgical techniques do not substantially mitigate the risk of early cartilage degeneration, with greater than 50% of patients exhibiting radiographic evidence of PTOA at 10 to 15 years post-surgery (Lohmander et al., 2007). Based on the link between altered loading and cartilage damage (Griffin and Guilak, 2005), it is theorized that abnormal knee mechanics that remain after ACLR play a role in the pathogenesis of PTOA (Chaudhari et al., 2008). Thus, identifying surgical factors to better restore normative cartilage loading may reduce the risk of PTOA in these patients. In this study, we found that there was a posterior bias in positioning of the

tibial tunnel, relative to the native ACL footprint. We also observed abnormal tibiofemoral kinematics and an altered center of contact location in ACL reconstructed knees, relative to the contralateral knee. Further, we found that non-anatomic graft geometry was linked to side-to-side differences in tibiofemoral kinematics, cartilage contact location, and cartilage contact sliding velocity.

Our kinematic observations are generally consistent with previously observed links between ACL graft geometry and kinematics. Prior studies found that a more vertical graft was associated with increased anterior and rotational laxities (Brophy and Pearle, 2009; Loh et al., 2003) and greater anterior tibial translation, medial tibial translation, and internal tibial rotation during a quasi-static lunge (Abebe et al., 2011b). Given that the ACL provides the primary restraint to anterior tibial translation and a secondary restraint to internal tibial rotation (Andersen and Dyhre-Poulsen, 1997; Fukubayashi et al., 1982; Gabriel et al., 2004; Sakane et al., 1997), these results suggest that the functionality of an ACL graft is potentially related to its sagittal plane orientation. Additionally, the similarities between our findings and previous studies suggest that graft geometry can affect knee behavior across a range of open- and closed-chain tasks.

We have shown that side-to-side differences in kinematics give rise to altered cartilage contact patterns, which are also linked to ACL graft geometry. Specifically, the graft sagittal plane orientation and the posterior location of the tibial footprint were linked to asymmetries in cartilage contact location and sliding velocity (Table 3). The observed trends suggest a subject with a graft sagittal plane angle that is greater than that of the contralateral ACL is likely to exhibit more anterior tibial translation, internal tibial rotation, and adduction in their reconstructed knee (Fig. 5). On the medial plateau, this same subject would exhibit a more medial center of contact and a decreased contact sliding velocity. On the lateral plateau, this subject would exhibit a more medial

and posterior center of contact and an increased contact sliding velocity. These effects are important because a shift in contact location and contact sliding velocity can load cartilage in a manner that the composition and microstructure may not be well adapted for, potentially initiating a degenerative pathway that leads to PTOA (Beveridge et al., 2013; Chaudhari et al., 2008).

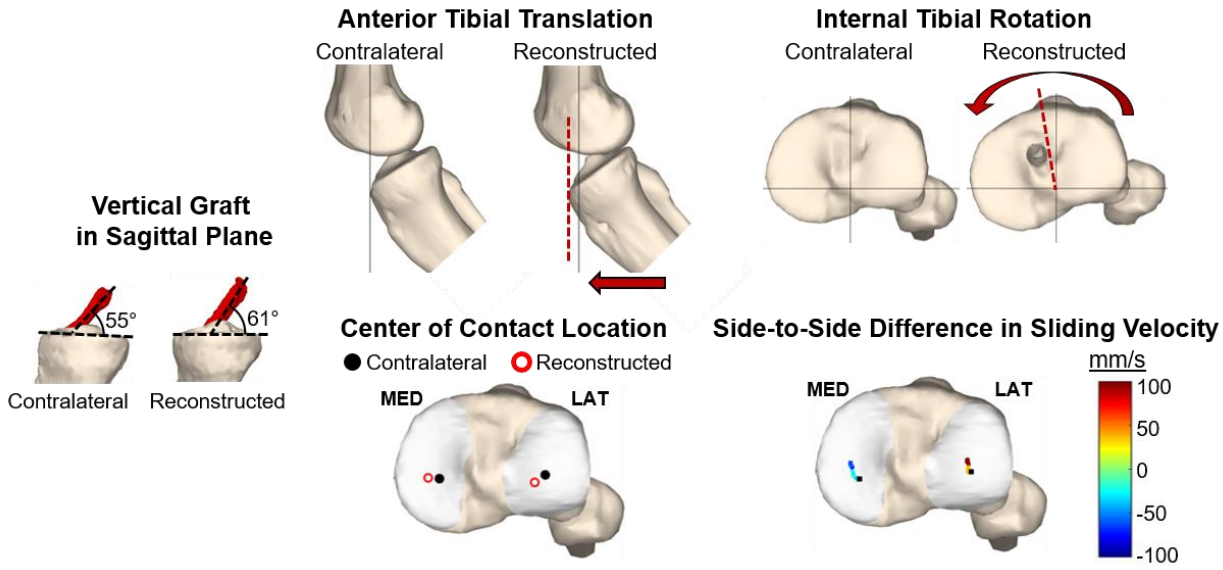

Figure 5: Representative subject with a vertical ACL graft. Graphic shows the anterior tibial translation, internal tibial rotation, and center of contact location at peak knee flexion and the side-to-side difference in contact sliding velocity during knee extension for a subject with a more vertical ACL graft in the sagittal plane, relative to the native ACL. The asymmetries in kinematics and cartilage contact measured in this subject are representative of the relationship between asymmetric knee mechanics and non-anatomic ACL graft sagittal plane orientation observed across all subjects.

Femoral and tibial tunnel placement are primary determinants of ACL graft orientation. However, surgical placement of ACL graft tunnels remains technically challenging. Using a transtibial drilling technique, experienced surgeons placed the femoral tunnel an average of 8 to 9 mm from the native ACL footprint center (Abebe et al., 2009; Kaseta et al., 2008; Kopf et al., 2010). These tunnels were typically placed anterior and superior to the femoral footprint center, resulting in a more vertical graft in the sagittal plane. Femoral tunnel placement accuracy improved

to 2 to 3 mm when drilling the femoral and tibial tunnels independently. While this improvement in accuracy would result in knee mechanics significantly closer to that of the contralateral knee, our results suggest that small, residual abnormalities in kinematics and contact location and a relatively large difference in contact sliding velocity would still remain in the reconstructed knee (Tables 2 and 3). We also observed a posterior bias in the tibial footprint location (Table 1). This bias towards a posterior tibial tunnel position may be intentional to prevent graft impingement against the superior notch during knee extension (Amis and Jakob, 1998; Bedi et al., 2011). While further work is needed to assess the threshold for an acceptable difference in tunnel location relative to the native ACL footprints, the accuracy of current techniques may limit surgeons' ability to adequately restore normative knee mechanics. Advancements in the treatment of ACL injury through computer-assisted reconstruction (Dessenne et al., 1995; Jalliard et al., 1998; Kaseta et al., 2008; Picard et al., 2001) and a more thorough understanding of the link between slight alterations in tunnel position and knee kinematics may allow surgeons to accurately recreate the native ACL geometry needed to restore normative knee mechanics and improve long-term outcomes of ACLR.

There are three primary limitations to consider in this study. First, knee mechanics were studied during an open-chain task, in contrast to the closed-chain loading that occurs during locomotion. However, in our previous work, we found that small, subtle shifts in tibiofemoral kinematics detected during this open-chain task are similar to those observed during downhill running (Kaiser et al., 2017). Additionally, strain in the ACL is similar between open-chain and closed-chain knee flexion (Beynnon et al., 1997), which suggests the experimentally measured relationships in this study may extend to locomotion. Using a simple task may also reduce the variability in neuromuscular coordination between ACLR subjects that exists during functional motions (Ciccotti et al., 1994; Gokeler et al., 2010) and can influence knee mechanics

(Chmielewski et al., 2005; Zeller et al., 2003). The open-chain motion used in this study may then more readily isolate the effect of graft geometry on post-operative knee mechanics. Second, the kinematics and cartilage contact data throughout the flexion-extension motion were reduced to metrics at peak knee flexion and during knee extension. Peak knee flexion corresponds with peak quadriceps loading during this cyclic motion (Westphal et al., 2013). The quadriceps loading during the extension phase of this motion mimics the loading-response phase of walking, in which the quadriceps brake knee flexion and then induce knee extension (Besier et al., 2009; Whittington et al., 2008). Thus, these portions of the flexion-extension motion were selected based on their potential functional relevance. Third, we did not control graft type or initial graft tension in these subjects. Previous work has shown that graft type is related to differences in knee kinetics during walking (Webster et al., 2005) and initial graft tension is related to differences in passive knee mechanics under simple loading conditions (Boylan et al., 2003; Brady et al., 2007; Nicholas et al., 2004). Further work is needed to assess the effect of these surgical parameters on cartilage loading during active knee motion and to assess their interaction with graft geometry when attempting to restore normative knee mechanics with ACLR.

In conclusion, the findings of this study provide evidence that non-anatomic ACL graft geometry is related to asymmetric tibiofemoral kinematics and cartilage contact. Given that abnormal cartilage loading may precipitate cartilage degeneration, these findings suggest that replicating native ACL geometry may be critical for normalizing mechanics and mitigating the risk of PTOA following ACLR. Future longitudinal studies are needed to determine whether the changes in cartilage contact and contact sliding velocity due to non-anatomic graft geometry are directly related to early cartilage degeneration within abnormally loaded regions of the knee.

Conflict of Interest Statement

The authors have no conflicts of interest to disclose.

Acknowledgements

We gratefully acknowledge the contributions of Oliver Wieben, Kevin Johnson, Kelli Hellenbrand, Frances Theisen, Sara John, and Jenelle Fuller. This material is based upon work supported by the National Science Foundation Graduate Research Fellowship Program [grant number DGE-1747503] and the National Institutes of Health [grant number EB015410]. Any opinions, findings, and conclusions or recommendations expressed in this material are those of the author(s) and do not necessarily reflect the views of the NSF or NIH. Support was also provided by the Graduate School and the Office of the Vice Chancellor for Research and Graduate Education at the University of Wisconsin-Madison with funding from the Wisconsin Alumni Research Foundation.

References

Abebe, E., Kim, J.P., Utturkar, G.M., Taylor, D.C., Spritzer, C.E., Moorman, C.T., Garrett, W.E., DeFrate, L.E., 2011a. The effect of femoral tunnel placement on ACL graft orientation and length during in vivo knee flexion. J. Biomech. 44, 1914–1920. doi:10.1016/j.jbiomech.2011.04.030

Abebe, E., Utturkar, G.M., Taylor, D.C., Spritzer, C.E., Kim, J.P., Moorman, C.T., Garrett, W.E., DeFrate, L.E., 2011b. The effects of femoral graft placement on in vivo knee kinematics after anterior cruciate ligament reconstruction. J. Biomech. 44, 924–929. doi:10.1016/j.jbiomech.2010.11.028

Abebe, E.S., Moorman, C.T., Dziedzic, T.S., Spritzer, C.E., Cothran, R.L., Taylor, D.C., Garrett, W.E., DeFrate, L.E., 2009. Femoral Tunnel Placement During Anterior Cruciate Ligament Reconstruction An In Vivo Imaging Analysis Comparing Transtibial and 2-Incision Tibial Tunnel–Independent Techniques. Am. J. Sports Med. 37, 1904–1911. doi:10.1177/0363546509340768

Amis, A.A., Jakob, R.P., 1998. Anterior cruciate ligament graft positioning , tensioning and twisting. Knee Surgery, Sport. Traumatol. Arthrosc. 6 [Suppl 1, S2–S12.

doi:10.1007/s001670050215

Andersen, H.N., Dyhre-Poulsen, P., 1997. The anterior cruciate ligament does play a role in controlling axial rotation in the knee. Knee 5, 145–149. doi:10.1007/s001670050042

Anderst, W.J., Tashman, S., 2009. The association between velocity of the center of closest proximity on subchondral bones and osteoarthritis progression. J. Orthop. Res. 27, 71–77. doi:10.1002/jor.20702

Bedi, A., Maak, T., Musahl, V., Citak, M., O'Loughlin, P.F., Choi, D., Pearle, A.D., 2011. Effect of tibial tunnel position on stability of the knee after anterior cruciate ligament reconstruction: is the tibial tunnel position most important? Am. J. Sports Med. 39, 366–373. doi:10.1177/0363546510388157

Besier, T.F., Fredericson, M., Gold, G.E., Beaupré, G.S., Delp, S.L., 2009. Knee muscle forces during walking and running in patellofemoral pain patients and pain-free controls. J. Biomech. 42, 898–905. doi:10.1016/j.jbiomech.2009.01.032

Beveridge, J.E., Heard, B.J., Shrive, N.G., Frank, C.B., 2013. Tibiofemoral centroid velocity correlates more consistently with cartilage damage than does contact path length in two ovine models of stifle injury. J. Orthop. Res. 31, 1745–1756. doi:10.1002/jor.22429

Beynnon, B.D., Johnson, R.J., Fleming, B.C., Stankewich, C.J., Renstrom, P.A., Nichols, C.E., 1997. The strain behavior of the anterior cruciate ligament during squatting and active flexion-extension. A comparison of an open and a closed kinetic chain exercise. Am J Sport. Med 25, 823–9. doi:10.1177/036354659702500616

Borotikar, B.S., Sheehan, F.T., 2013. In vivo patellofemoral contact mechanics during active extension using a novel dynamic MRI-based methodology. Osteoarthr. Cartil. 21, 1886–1894. doi:10.1016/j.joca.2013.08.023

Boylan, D., Greis, P.E., West, J.R., Bachus, K.N., Burks, R.T., 2003. Effects of initial graft tension on knee stability after anterior cruciate ligament reconstruction using hamstring tendons: A cadaver study. Arthrosc. - J. Arthrosc. Relat. Surg. 19, 700–705. doi:10.1016/S0749-8063(03)00400-6

Brady, M.F., Bradley, M.P., Fleming, B.C., Fadale, P.D., Hulstyn, M.J., Banerjee, R., 2007. Effects of Initial Graft Tension on the Tibiofemoral Compressive Forces and Joint Position After Anterior Cruciate Ligament Reconstruction. Am. J. Sports Med. 35, 395–403. doi:10.1177/0363546506294363

Brophy, R.H., Pearle, A.D., 2009. Single-Bundle Anterior Cruciate Ligament Reconstruction: A Comparison of Conventional, Central, and Horizontal Single-Bundle Virtual Graft Positions. Am. J. Sports Med. 37, 1317–1323. doi:10.1177/0363546509333007

Chaudhari, A.M.W., Briant, P.L., Bevill, S.L., Koo, S., Andriacchi, T.P., 2008. Knee kinematics, cartilage morphology, and osteoarthritis after ACL injury. Med. Sci. Sports Exerc. 40, 215–222. doi:10.1249/mss.0b013e31815cbb0e

Chmielewski, T.L., Hurd, W.J., Rudolph, K.S., Axe, M.J., Snyder-mackler, L., 2005. Perturbation Training Improves Knee Kinematics and Reduces Muscle Co-contraction After Complete Unilateral Anterior Cruciate Ligament Rupture. Phys. Ther. 85, 740–754. doi:10.1093/ptj/85.8.740

Ciccotti, M.G., Kerlan, R.K., Perry, J., Pink, M., 1994. An Electromyographic Analysis of the Knee During Functional Activities: II. The Anterior Cruciate Ligament-deficient and -reconstructed Profiles. Am. J. Sports Med. 22, 651–658. doi:10.1177/036354659402200513

Corry, I.S., Webb, J.M., Clingeleffer, A.J., Pinczewski, L.A., 1999. Arthroscopic reconstruction of the anterior cruciate ligament. A comparison of patellar tendon autograft and four-strand hamstring tendon autograft. Am. J. Sports Med. 27, 444–54. doi:10.1177/03635465990270040701

Decker, L.M., Moraiti, C., Stergiou, N., Georgoulis, A.D., 2011. New insights into anterior cruciate ligament deficiency and reconstruction through the assessment of knee kinematic variability in terms of nonlinear dynamics. Knee Surgery, Sport. Traumatol. Arthrosc. 19, 1620–1633. doi:10.1007/s00167-011-1484-2

Dessenne, V., Lavallée, S., Julliard, R., Orti, R., Martelli, S., Cinquin, P., 1995. Computer-Assisted Knee Anterior Cruciate Ligament Reconstruction: *First Clinical Tests*. Comput. Aided Surg. 1, 59–64. doi:10.3109/10929089509106827

Fukubayashi, T., Torzilli, P.A., Sherman, M.F., Warren, R.F., 1982. An in Vivo Biomechanical Evaluation of Anterior-Posterior Motion of the Knee. J. Bone Jt. Surg. 64, 258–264.

Gabriel, M.T., Wong, E.K., Woo, S.L.Y., Yagi, M., Debski, R.E., 2004. Distribution of in situ forces in the anterior cruciate ligament in response to rotatory loads. J. Orthop. Res. 22, 85–89. doi:10.1016/S0736-0266(03)00133-5

Gokeler, A., Hof, A.L., Arnold, M.P., Dijkstra, P.U., Postema, K., Otten, E., 2010. Abnormal landing strategies after ACL reconstruction. Scand. J. Med. Sci. Sport. 20, 12–19. doi:10.1111/j.1600-0838.2008.00873.x

Griffin, T.M., Guilak, F., 2005. The Role of Mechanical Loading in the Onset and Progression of Osteoarthritis. Exerc. Sport Sci. Rev. 33, 195–200. doi:10.1097/00003677-200510000-00008

Grood, E.S., Suntay, W.J., 1983. A joint coordinate system for the clinical description of three-dimensional motions: application to the knee. J. Biomech. Eng. 105, 136–44. doi:10.1115/1.3138397

Hofbauer, M., Thorhauer, E.D., Abebe, E., Bey, M., Tashman, S., 2014. Altered Tibiofemoral Kinematics in the Affected Knee and Compensatory Changes in the Contralateral Knee After Anterior Cruciate Ligament Reconstruction. Am. J. Sports Med. 42, 2715–2721. doi:10.1177/0363546514549444

Jalliard, R., Lavallee, S., Dessenne, V., 1998. Computer assisted reconstruction of the anterior cruciate ligament. Clin. Orthop. Relat. Res. 57–64.

Kaiser, J., Bradford, R., Johnson, K., Wieben, O., Thelen, D.G., 2013. Measurement of Tibiofemoral Kinematics Using Highly Accelerated 3D Radial Sampling. Magn. Reson. Med. 69, 1310–1316. doi:10.1002/mrm.24362

Kaiser, J., Monawer, A., Chaudhary, R., Johnson, K.M., Wieben, O., Kijowski, R., Thelen, D.G., 2016a. Accuracy of model-based tracking of knee kinematics and cartilage contact measured by dynamic volumetric MRI. Med. Eng. Phys. 38, 1–5. doi:10.1016/j.medengphy.2016.06.016

Kaiser, J., Vignos, M.F., Liu, F., Kijowski, R., Thelen, D.G., 2016b. American Society of Biomechanics Clinical Biomechanics Award 2015: MRI assessments of cartilage mechanics, morphology and composition following reconstruction of the anterior cruciate ligament. Clin. Biomech. 34, 38–44. doi:10.1016/j.clinbiomech.2016.03.007

Kaiser, J.M., Vignos, M.F., Kijowski, R., Baer, G., Thelen, D.G., 2017. Effect of Loading on In Vivo Tibiofemoral and Patellofemoral Kinematics of Healthy and ACL-Reconstructed Knees. Am. J. Sports Med. 36354651772441. doi:10.1177/0363546517724417

Kaseta, M.K., DeFrate, L.E., Charnock, B.L., Sullivan, R.T., Garrett, W.E., 2008. Reconstruction technique affects femoral tunnel placement in ACL reconstruction. Clin. Orthop. Relat. Res. 466, 1467–1474. doi:10.1007/s11999-008-0238-z

Kopf, S., Forsythe, B., Wong, A.K., Tashman, S., Anderst, W., Irrgang, J.J., Fu, F.H., 2010. Nonanatomic Tunnel Position in Traditional Transtibial Single-Bundle Anterior Cruciate Ligament Reconstruction Evaluated by Three-Dimensional Computed Tomography. J. Bone Jt. Surgery-American Vol. 92, 1427–1431. doi:10.2106/JBJS.I.00655

Loh, J.C., Fukuda, Y., Tsuda, E., Steadman, R.J., Fu, F.H., Woo, S.L.Y., 2003. Knee stability and graft function following anterior cruciate ligament reconstruction: Comparison between 11 o'clock and 10 o'clock femoral tunnel placement. Arthrosc. - J. Arthrosc. Relat. Surg. 19, 297–304. doi:10.1053/jars.2003.50084

Lohmander, L.S., Englund, P.M., Dahl, L.L., Roos, E.M., 2007. The long-term consequence of anterior cruciate ligament and meniscus injuries: osteoarthritis. Am. J. Sports Med. 35, 1756–69. doi:10.1177/0363546507307396

Miranda, D.L., Rainbow, M.J., Leventhal, E.L., Crisco, J.J., Fleming, B.C., 2010. Automatic determination of anatomical coordinate systems for three- dimensional bone models of the isolated human knee. J. Biomech. 43, 1623–1626. doi:10.1016/j.jbiomech.2010.01.036

Musahl, V., Bedi, A., Citak, M., O'Loughlin, P., Choi, D., Pearle, A.D., 2011. Effect of single-bundle and double-bundle anterior cruciate ligament reconstructions on pivot-shift kinematics in anterior cruciate ligament- and meniscus-deficient knees. Am. J. Sports Med. 39, 289–295. doi:10.1177/0363546510385422

Nicholas, S.J., D'Amato, M.J., Mullaney, M.J., Tyler, T.F., Kolstad, K., McHugh, M.P., 2004. A Prospectively Randomized Double-Blind Study on the Effect of Initial Graft Tension on Knee Stability After Anterior Cruciate Ligament Reconstruction. Am. J. Sports Med. 32, 1–6. doi:10.1177/0363546504265924

O'Neill, D.B., 2001. Arthroscopically Assisted Reconstruction of the Anterior Cruciate Ligament: A Follow-Up Report. J. Bone Jt. Surg. 83a, 1329–1332.

Otero, A.L., Hutcheson, L., 1993. A comparison of the doubled semitendinosus/gracilis and central third of the patellar tendon autografts in arthroscopic anterior cruciate ligament reconstruction. Arthroscopy 9, 143–148. doi:10.1016/S0749-8063(05)80363-9

Picard, F., DiGioia, A.M., Moody, J., Martinek, V., Fu, F.H., Rytel, M., Nikou, C., LaBarca, R.S., Jaramaz, B., 2001. Accuracy in tunnel placement for ACL reconstruction. Comparison of traditional arthroscopic and computer-assisted navigation techniques. Comput. Aided Surg. 6, 279–289. doi:10.1002/igs.10014

Powell, M., 1964. An efficient method for finding the minimum of a function of several variables without calculating derivatives. Comput. J. 7, 155–162. doi:10.1093/comjnl/7.2.155

Pruessmann, K.P., Weiger, M., Bornert, P., Boesiger, P., 2001. Advances in Sensitivity Encoding With Arbitrary k-Space Trajectories. Magn. Reson. Med. 46, 638–651.

Ristanis, S., Stergiou, N., Siarava, E., Ntoulia, A., Mitsionis, G., Georgoulis, A.D., 2009. Effect of femoral tunnel placement for reconstruction of the anterior cruciate ligament on tibial rotation. J. Bone Jt. Surg. - Ser. A 91, 2151–2158. doi:10.2106/JBJS.H.00940

Sakane, M., Fox, R.J., Woo, S.L.Y., Livesay, G.A., Li, G., Fu, F.H., 1997. In situ forces in the anterior cruciate ligament and its bundles in response to anterior tibial loads. J. Orthop. Res. 15, 285–293. doi:10.1002/jor.1100150219

Sanders, T.L., Maradit Kremers, H., Bryan, A.J., Larson, D.R., Dahm, D.L., Levy, B.A., Stuart, M.J., Krych, A.J., 2016. Incidence of Anterior Cruciate Ligament Tears and Reconstruction: A 21-Year Population-Based Study. Am. J. Sports Med. 44, 1502–1507. doi:10.1177/0363546516629944

Scanlan, S.F., Chaudhari, A.M.W., Dyrby, C.O., Andriacchi, T.P., 2010. Differences in tibial rotation during walking in ACL reconstructed and healthy contralateral knees. J. Biomech. 43, 1817–1822. doi:10.1016/j.jbiomech.2010.02.010

Smith, C.R., Won Choi, K., Negrut, D., Thelen, D.G., 2016. Efficient computation of cartilage contact pressures within dynamic simulations of movement. Comput. Methods Biomech. Biomed. Eng. Imaging Vis. 1163, 1–8. doi:10.1080/21681163.2016.1172346

Stergiou, N., Ristanis, S., Moraiti, C., Georgoulis, A.D., 2007. Tibial rotation in anterior cruciate ligament (ACL)-deficient and ACL-reconstructed knees: A theoretical proposition for the development of osteoarthritis. Sport. Med. 37, 601–613. doi:10.2165/00007256-200737070-00004

Tashman, S., Kolowich, P., Collon, D., Anderson, K., Anderst, W., 2006. Dynamic Function of the ACL-reconstructed Knee during Running. Clin. Orthop. Relat. Res. 454, 66–73. doi:10.1097/BLO.0b013e31802bab3e

Webster, K.E., Wittwer, J.E., Brien, J.O., Feller, J.A., 2005. Gait Patterns After Anterior Cruciate Ligament Reconstruction Are Related to Graft Type. Am. J. Sports Med. 33, 247–254. doi:10.1177/0363546504266483

Westphal, C.J., Schmitz, A., Reeder, S.B., Thelen, D.G., 2013. Load-dependent variations in knee kinematics measured with dynamic MRI. J. Biomech. 46, 2045–2052. doi:10.1016/j.jbiomech.2013.05.027

Whittington, B., Silder, A., Heiderscheit, B., Thelen, D.G., 2008. The contribution of passive-elastic mechanisms to lower extremity joint kinetics during human walking. Gait Posture 27, 628–634. doi:10.1016/j.gaitpost.2007.08.005

Zampeli, F., Ntoulia, A., Giotis, D., Tsiaras, V.A., Argyropoulou, M., Pappas, E., Georgoulis, A.D., 2012. Correlation between anterior cruciate ligament graft obliquity and tibial rotation during dynamic pivoting activities in patients with anatomic anterior cruciate ligament reconstruction: An in vivo examination. Arthrosc. - J. Arthrosc. Relat. Surg. 28, 234–246.

doi:10.1016/j.arthro.2011.08.285

Zavras, T.D., Race, A., Amis, A.A., 2005. The effect of femoral attachment location on anterior cruciate ligament reconstruction: Graft tension patterns and restoration of normal anterior-posterior laxity patterns. Knee Surgery, Sport. Traumatol. Arthrosc. 13, 92–100. doi:10.1007/s00167-004-0541-5

Zeller, B.L., McCrory, J.L., Kibler, W. Ben, Uhl, T.L., 2003. Differences in kinematics and electromyographic activity between men and women during the single-legged squat. Am. J. Sports Med. 31, 449–56. doi:10.1177/03635465030310032101

Chapter 4: Dynamic Imaging and Complementary Simulation Evidence that Graft Geometry Influences Tibiofemoral Kinematics, Cartilage Contact, and ACL Loading following ACL Reconstruction

Michael F. Vignos, Colin R. Smith, Joshua D. Roth, Jarred M. Kaiser, Geoffrey S. Baer, Richard Kijowski, Darryl G. Thelen

(This chapter is in review by the *American Journal of Sports Medicine*)

Abstract

Background: Graft placement is a modifiable and often discussed surgical factor in anterior cruciate ligament reconstruction (ACLR). However, the sensitivity of functional knee mechanics to variability in graft placement is not well understood.

Purpose: (1) Experimentally investigate correlations between ACL graft geometry and post-operative tibiofemoral mechanics.

(2) Computationally determine the causal relationships between graft geometry and functional tibiofemoral kinematics, cartilage loading, and ACL loading in simulated ACLRs.

Study Design: Controlled Laboratory Study

Methods: We tested eighteen subjects who were 1-4 years post-ACLR. We bilaterally assessed anterior laxity using a KT-1000, measured ACL geometry from magnetic resonance images (MRI), and characterized 3D tibiofemoral kinematics during active knee flexion-extension using dynamic MRI. Additionally, 500 virtual ACLRs were simulated by varying ACL footprint locations, graft stiffness, and initial tension within a computational knee model to account for common sources of surgical variability in ACLRs. We simulated laxity tests, active knee

extension, and walking with each virtual ACLR. Correlations between internal knee mechanics and ACL graft geometry were determined for both experimental and computational studies.

Results: A more vertical graft in the sagittal plane was experimentally correlated ($P<0.05$) with a greater laxity compliance index, and greater anterior tibial translation and internal tibial rotation during active knee extension. Similar causal relationships between a more vertical graft and increased compliance index, anterior translation, and internal rotation were predicted by the surgical simulation models, even when accounting for variations in graft stiffness and initial tension. These effects extended to simulations of walking, with a more vertical ACL graft inducing greater anterior tibial translation, ACL loading, and posterior migration of contact on the medial and lateral tibial plateaus.

Conclusions: This study provides empirical and complementary modeling evidence that functional post-operative knee mechanics are sensitive to graft geometry, especially the graft sagittal plane angle.

Clinical Relevance: Early onset osteoarthritis following ACLR is common. This study shows that post-operative cartilage loading is sensitive to graft angle; hence, variability in graft tunnel placement resulting in small deviations from the anatomic ACL angle might contribute to the elevated risk of early osteoarthritis following ACLR.

Key Terms: biomechanics, ACL reconstruction, osteoarthritis, anatomic graft placement

What is known about the subject: Abnormal tibiofemoral kinematics have previously been observed in ACL reconstructed knees, with some evidence this may be associated with graft tunnel placement.

What this study adds to existing knowledge: This study demonstrates that functional tibiofemoral kinematics, cartilage contact pressures, and ACL loading are sensitive to ACL graft angle. These graft geometry effects are substantial even in the presence of variations in other surgical factors, such as graft stiffness and initial tension.

1. Introduction

The placement of anterior cruciate ligament (ACL) graft tunnels is an important surgical factor in ACL reconstruction (ACLR) procedures. Tunnel placement determines the femoral and tibial graft footprints and, thus, is a primary determinant of graft angle in the frontal and sagittal planes. Many current ACLR techniques aim to position the graft within the native ACL footprints with the goal of restoring normal anterior and rotational laxities of the knee.[14,33,37,57] However, in practice, variability in arthroscopic techniques results in ACL graft footprints that deviate from the native ACL footprints.[2,39,45] As abnormal mechanics can contribute to instability and to the initiation and progression of cartilage damage patterns characteristic of osteoarthritis,[4,9,19,25] the effects of such surgical variability on internal knee mechanics must be well understood.

Dynamic imaging technologies have identified systematic abnormalities in kinematics and cartilage contact patterns in ACLR knees. For example, prior studies detected a bias toward external tibial rotation during active movement,[27,30,51] resulting in a posterior shift of contact on the tibial plateaus.[28] There is some evidence that graft geometry contributes to these asymmetries in ACLR knee mechanics.[1,41,53] However, a major challenge in experimental imaging studies is decoupling the effect of ACL graft geometry from other surgical factors, such as graft type,[54] stiffness,[50] and initial tension,[12,38] which may also influence knee behavior.

Probabilistic musculoskeletal modeling can be used to investigate the causal influence of multiple surgical factors on internal joint mechanics.[7,8,23,35] For example, Dhaher et al.[23] used a highly detailed knee model to simulate an ACLR using a bone—patellar tendon—bone autograft. This study found that anterior joint laxity is primarily dependent on tunnel placement and secondarily on graft initial tension. Additional modeling studies found that the ACL femoral attachment location, stiffness, and initial tension influence joint laxity and ACL loading under an anteriorly applied tibial load.[7,35] However, these previous studies did not provide a direct comparison to experimental measurements, and it remains unclear how these results under simple loading conditions relate to knee behavior during locomotion.

The purpose of this study was to use a coupled experimental and modeling approach to investigate the sensitivity of joint laxity and functional knee mechanics to ACL graft geometry, while accounting for surgical variability in graft stiffness and initial tension. Specifically, the first objective was to identify relationships between ACL graft footprint locations, graft angles, and tibiofemoral mechanics measured experimentally. The second objective was to determine the sensitivity of functional tibiofemoral kinematics, cartilage loading, and ACL loading to graft geometry metrics (i.e. footprint locations and angles) using simulated ACLRs with variations in graft footprint locations, stiffness, and initial tension.

2. Methods

2.1. Participants

Potential subjects were identified from a University of Wisconsin (UW) Health Sports Medicine Outcomes Program database. Eligible subjects were those who underwent a primary, unilateral ACLR within the past 1 to 4 years, had no concurrent ligament damage, no post-

operative complications, and no history of pain, injury, surgery, or inflammatory or crystalline-induced arthritis in the contralateral knee. Eighteen subjects agreed to participate and provided informed consent according to the UW Institutional Review Board-approved protocol (9 male, 9 female; 24.8±5.7 [mean ± standard deviation] years; 78.9 ± 16.5 kg; BMI, 24.1 ± 2.8; 20.2 ± 8.7 months post-surgery). ACL reconstructions were performed by four fellowship-trained sports medicine surgeons through independent tunnel drilling techniques. The graft type used for the ACLR was not controlled (9 bone—patellar tendon—bone grafts, 9 hamstrings tendon grafts). Three subjects had minor meniscal damage (1 subject had small, stable medial and lateral meniscal tears; 2 had small partial, lateral meniscectomies).

2.2. Clinical Assessment of Knee Anterior Laxity

Licensed physical therapists at the UW Health Sports Medicine Clinic assessed anterior laxity in the reconstructed and contralateral knees following each subject's clearance from post-surgery rehabilitation (9.2±3.5 months). Using a KT-1000 arthrometer, anterior tibial translation was measured under 67 N (15 lbs) and 89 N (20 lbs) of anterior load (Figure 1). The compliance index was computed as the difference in anterior tibial translation under these two loads.[3]

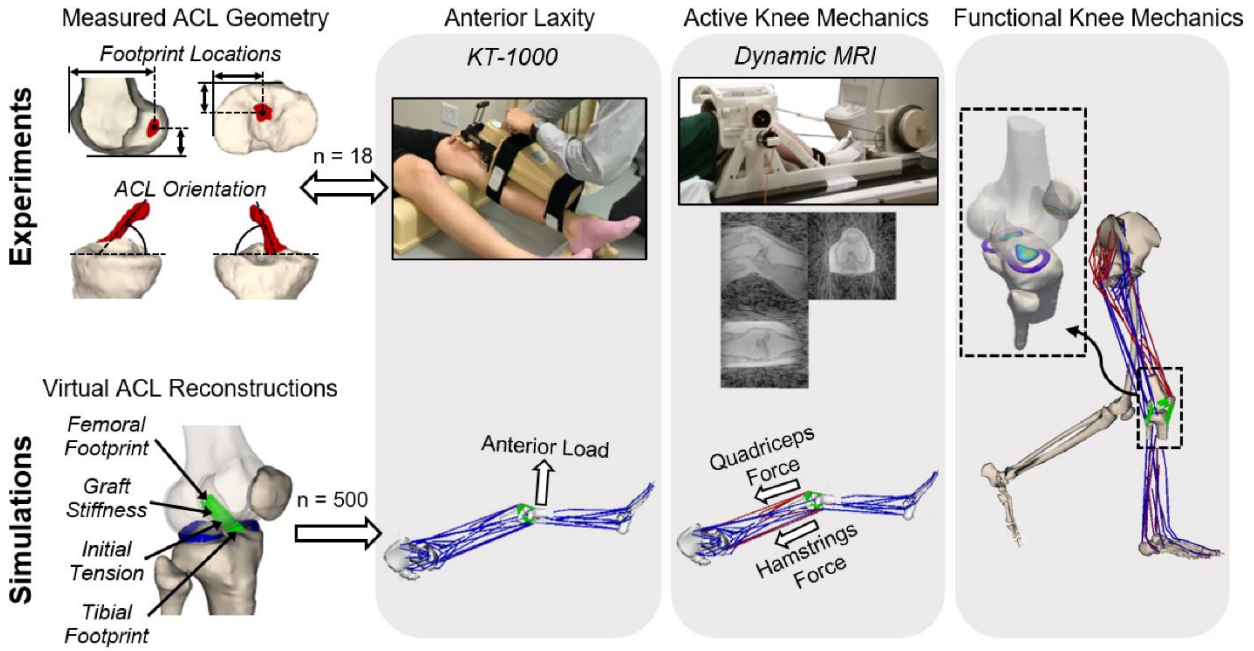

Figure 1: This study used complementary methods to experimentally (top row) and computationally (bottom row) determine the link between ACL graft geometry and post-operative knee mechanics. Experimentally, we measured the ACL graft and native ACL geometries of eighteen subjects from segmented MR images. We then correlated (as indicated by the two-way arrow) the ACL geometry metrics to knee anterior laxity measured using a KT-1000 arthrometer and tibiofemoral kinematics during active knee flexion-extension measured using dynamic MR imaging. Computationally, we performed 500 virtual ACLRs by varying the ACL femoral and tibial footprint locations, graft stiffness, and graft initial tension. We then simulated a KT-1000 assessment and active knee extension task with each virtual ACLR to determine the effect (as indicated by the one-way arrow) of ACL graft geometry on post-operative knee mechanics. The model-predicted effects of ACL graft geometry on anterior laxity and active knee mechanics were compared to those observed experimentally. Additionally, we simulated walking with each virtual ACLR to determine the effect of graft geometry on functional knee mechanics.

2.3. Magnetic Resonance Imaging

Each subject underwent a static bilateral magnetic resonance (MR) imaging protocol using an 8-channel phased array extremity coil (InVivo, Orlando, FL) within a 3.0T MR scanner (Discovery MR750, GE Healthcare, Waukesha, WI). An IDEAL-SPGR sequence (iterative least squares estimation of fat-water separation using a spoiled gradient recall-echo sequence) was used to obtain high-resolution images of the knee (in-plane resolution=0.37 x 0.37 mm; slice

thickness=0.9 mm). These IDEAL-SPGR images were manually segmented (MIMICS, Materialise Group, Leuven, Belgium) to create 3D models of the femoral and tibial bone geometries. A 3D FSE Cube sequence (fast spin-echo; in-plane resolution=0.39 x 0.39 mm; slice thickness=1.0 mm) was used to characterize ACL morphology. The 3D FSE Cube images were manually segmented to create models of the contralateral native ACL and ACL graft geometries. All models were smoothed and converted into triangular meshes (Geomagic Studio, 3D Systems, Rock Hill, SC). Anatomic coordinate systems were defined for the femoral and tibial bone models using an automated algorithm that determines the axes for each bone based on its geometric and inertial properties.[36] The bone and ACL models were subsequently co-registered to create subject-specific morphological knee models (Figure 1).

The native ACL and ACL graft footprints were identified as the intersections of the ACL meshes with the femoral and tibial bone meshes. We then computed the anatomic locations of the centroid of the femoral and tibial footprints (Figure 1). A cylinder was fit to the mid-substance of the ACL meshes and the ACL angles were computed as the relative angle between the long axis of the cylinder and the tibial plateau in the frontal and sagittal planes. The ACL angles were computed with the knee in the MRI scanning posture (approximately 10º knee flexion).

Dynamic MR imaging was performed bilaterally to characterize tibiofemoral kinematics during active movement. Subjects were positioned supine in the scanner with their lower leg secured to an inertial loading device[55] (Figure 1). Cyclic knee flexion-extension was voluntarily performed at 0.5 Hz, with the device inducing active quadriceps loading comparable to that seen in the weight-acceptance phase of gait.[55,56] Volumetric MR data was continuously acquired for five minutes using a SPGR sequence with vastly under-sampled isotropic projections (SPGR-VIPR; 1.5-mm isotropic resolution).[29] The SPGR-VIPR projections were sorted into 60 equally

spaced bins based on the lever arm angle measured via an MRI-compatible rotary encoder (Micronor Inc., Camarillo, CA). The sorted projections were reconstructed into 60 volumetric image frames throughout the flexion-extension motion cycle.[29]

Tibiofemoral kinematics were measured by registering the femoral and tibial geometries to the dynamic MR images at each frame of the motion cycle.[29] Tibiofemoral translations were defined as the three-dimensional position of the tibial reference frame relative to the femoral reference frame. Tibiofemoral orientation was defined by successive flexion, adduction, and internal rotation angles of the tibia relative to the femur.[26] Tibiofemoral kinematics were low-pass filtered with a cut-off frequency of 5 Hz. Kinematics metrics were defined as the tibiofemoral translations and rotations at peak knee flexion, which corresponds to the instance of peak quadriceps loading.[55]

2.4. Virtual ACL Reconstructions

A multibody knee model was used to predict the effects of ACL graft geometry on post-operative knee mechanics (Figure 1). The knee model was previously constructed from high-resolution MR images of a healthy adult knee.[32] The model includes representations of the femur, patella, tibia, and medial and lateral menisci connected by six degree-of-freedom tibiofemoral and patellofemoral joints. An elastic foundation formulation was used to compute cartilage-cartilage and cartilage-meniscal contact pressures.[48] Fourteen major knee ligaments and seven meniscal attachments were represented as bundles of ligament strands with their origins and insertions determined from the MR images. Ligament strands were defined as nonlinear springs characterized by their stiffness when taut and the ligament stretch when the knee was at full extension (i.e. reference strain). Stiffness parameters for individual ligaments were computed as the product of

the ligament cross-sectional area, as measured from MR images, and an assumed elastic modulus of 125 MPa.[18] Reference strains were adapted from previous studies.[43,44]

The knee model was incorporated into an existing lower-limb model with 44 muscles acting about the hip, knee, and ankle joints.[5] The combined model was implemented in the Software for Interactive Musculoskeletal Modeling (SIMM) with the Dynamics Pipeline (Musculographics, Inc., Santa Rosa, CA) and SD/Fast (Parametric Technology Corp., Needham, MA) used to generate the multibody dynamics equations of motion.[22] The model was previously validated by comparing simulated knee mechanics to tibiofemoral and patellofemoral kinematics measured via dynamic MR imaging performed on the same subject for which the knee model was constructed.[32] This validated model will subsequently be referred to as the native model.

A total of 500 virtual ACLRs were performed on the native model by randomly varying the ACL footprint locations, stiffness, and initial tension within bounds representative of those observed clinically.[15,34,52] The femoral footprint location in the anterior-posterior and superior-inferior directions and the tibial footprint location in the anterior-posterior and medial-lateral directions were randomly varied between ±5 mm from the native footprint locations. This range was selected to produce variability in ACL graft geometry comparable to that measured in the ACLR subjects. ACL stiffness was randomly varied between 150 N/mm and 750 N/mm, with this range defined based on the stiffness in the native model ±50%.[46] ACL initial tension at full knee extension was randomly varied between 0 N and 150 N.[34,52]

2.5. Simulated Movements

Each of the 500 virtual ACLRs and the native model were used in simulations of a KT-1000 laxity assessment, active isometric knee extension, and over-ground walking. The simulation

of the KT-1000 assessment consisted of a forward dynamic simulation with the knee flexion angle fixed at 20° and a point load applied to the tibia in the anterior direction (Figure 1). The load was applied 20 cm distal to the tibiofemoral joint line and was ramped from 0 N to 89 N to replicate the clinical assessment. We then extracted the anterior tibial translation under applied loads of 67 N and 89 N. These anterior translations were used to compute the compliance index of the virtual ACLRs and native model.

The active isometric knee extension simulation, which complemented the experimental dynamic MRI flexion-extension task, consisted of a forward dynamic simulation with the knee flexion angle fixed at 30°, and the quadriceps and hamstrings muscles activated to 15% and 5%, respectively (Figure 1). The 30° angle reflected the average peak knee flexion of subjects during the flexion-extension task. The muscle activations were equivalent to those observed at the time of peak ACL loading during simulated gait from the final portion of this study. These activations resulted in combined quadriceps and hamstrings muscle forces of 655 N and 130 N, respectively. At the end of each simulation, we extracted the tibiofemoral kinematics that resulted from the applied muscle loads.

Finally, we simulated the knee behavior over a full gait cycle during over-ground walking. Whole body kinematics and ground reaction forces were previously measured for the subject from which the knee model was generated.[32] The Concurrent Optimization of Muscle Activations and Kinematics (COMAK) simulation routine was used to calculate the muscle forces and internal knee mechanics (i.e. contact pressures and ligament forces) needed to generate the measured whole body dynamics and ground reactions at each frame of the gait cycle.[13,47] To resolve muscle redundancy, COMAK minimized the weighted sum of squared muscle activations.[13] These simulations provided predictions of secondary knee kinematics (i.e. 5 tibiofemoral degrees of

freedom aside from flexion, 6 patellofemoral degrees of freedom, and 12 meniscal degrees of freedom), ligament forces, and articular contact pressures throughout the gait cycle. For each of the 500 virtual ACLRs and the native model, we examined the tibiofemoral kinematics, the center of contact location (i.e. center of pressure) and contact pressure on the medial and lateral tibial plateaus, and the ACL force at the time of peak ACL loading.

2.6. Statistical Analysis

To experimentally determine the relationships between ACL graft geometry and post-operative knee laxity and tibiofemoral kinematics (objective 1), non-anatomic ACL graft geometry was assessed by computing side-to-side differences (reconstructed minus contralateral) in the ACL femoral and tibial footprint locations and the ACL angle in the frontal and sagittal planes for the ACLR subjects. Asymmetric knee mechanics were assessed by computing side-to-side differences (reconstructed minus contralateral) in the anterior laxity and tibiofemoral kinematics metrics. We then computed Spearman's correlation coefficients (R) between the non-anatomic ACL graft geometry metrics and the asymmetric knee mechanics metrics (α=0.05).

To computationally determine the sensitivity of post-operative knee mechanics to graft geometry, stiffness, and initial tension (objective 2), non-anatomic ACL geometry, stiffness, and initial tension were assessed by computing differences in these metrics between each of the 500 virtual ACLR models and the native knee model (virtual ACLR minus native). Abnormal knee mechanics were then assessed as differences in the anterior laxity metrics (KT-1000 simulation), differences in tibiofemoral kinematics (active knee extension simulation), and differences in tibiofemoral kinematics, cartilage contact location and pressures, and ACL loading (gait simulation) between each of the 500 virtual ACLR models and the native model (virtual ACLR minus native). We computed Spearman's correlation coefficients (R) between the abnormal knee

mechanics metrics and the non-anatomic ACL geometry, stiffness, and initial tension metrics to assess the effect of varying these surgical factors on knee mechanics. We then compared the predicted effect of graft geometry on knee mechanics from the KT-1000 and active knee extension simulations to the correlations derived from the experimental KT-1000 assessment and active knee flexion-extension, respectively (Figure 1). Additionally, we performed a least-squares linear regression between the non-anatomic ACL geometry, stiffness, and initial tension metrics and the abnormal knee mechanics metrics. The slope of the regression model (β) was used to assess the sensitivity of functional knee mechanics to non-anatomic ACL geometry, stiffness, and initial tension.

3. Results

Non-anatomic ACL graft geometry was significantly related to side-to-side differences in post-operative knee mechanics measured experimentally during laxity testing and active knee flexion-extension (Table 1). Specifically, a more vertical graft in the sagittal plane (i.e. a larger graft sagittal plane angle) was related to a greater compliance index during the KT-1000 assessment (Figure 2, P=0.049). During active knee extension, a greater graft sagittal plane angle was significantly correlated with greater anterior tibial translation (P=0.012), internal tibial rotation (P=0.024), and tibial adduction angle (P=0.034). Additionally, a more vertical graft in the frontal plane and a more superior femoral footprint location were significantly correlated with greater medial tibial translation (P=0.041 and P=0.014, respectively).

Table 1: Significant experimental (P<0.05) and corresponding simulated correlations between non-anatomic ACL graft geometry and side-to-side differences in knee laxity, kinematics, and cartilage contact metrics.

		ACL Angle (deg)				Femoral Footprint Location (mm)	
		Sagittal Plane		Frontal Plane		Superior	
		Exp. R	Sim. R	Exp. R	Sim. R	Exp. R	Sim. R
KT-1000 Measurement (mm)	Compliance Index	0.69	0.72	—	—	—	—
Tibiofemoral Rotations (deg)	Internal	0.53	0.33	—	—	—	—
	Adduction	0.51	0.34	—	—	—	—
Tibiofemoral Translations (mm)	Anterior	0.59	0.49	—	—	—	—
	Medial	—	—	0.49	0.88	0.58	0.45

ACLR simulations predicted relationships between ACL geometry and altered knee mechanics that were consistent with those observed experimentally (Table 1), thereby justifying the use of the simulations for a cause-effect interpretation of the clinical and MR imaging observations. During the simulated KT-1000 assessment, as in the clinical assessment, a more vertical graft in the sagittal plane was correlated with a greater compliance index (Figure 2, β=0.01 $^{mm}/_{deg}$). During active knee extension, as in the experimental flexion-extension motion, a more vertical graft in the sagittal plane was correlated with increased anterior tibial translation (β=0.12 $^{mm}/_{deg}$), internal tibial rotation (β=0.07 $^{deg}/_{deg}$), and tibial adduction (β=0.03 $^{deg}/_{deg}$). Additionally, a more vertical graft in the frontal plane and a more superior femoral footprint position led to greater medial tibial translation (β=0.04 $^{mm}/_{deg}$ and β=0.01 $^{mm}/_{mm}$, respectively).

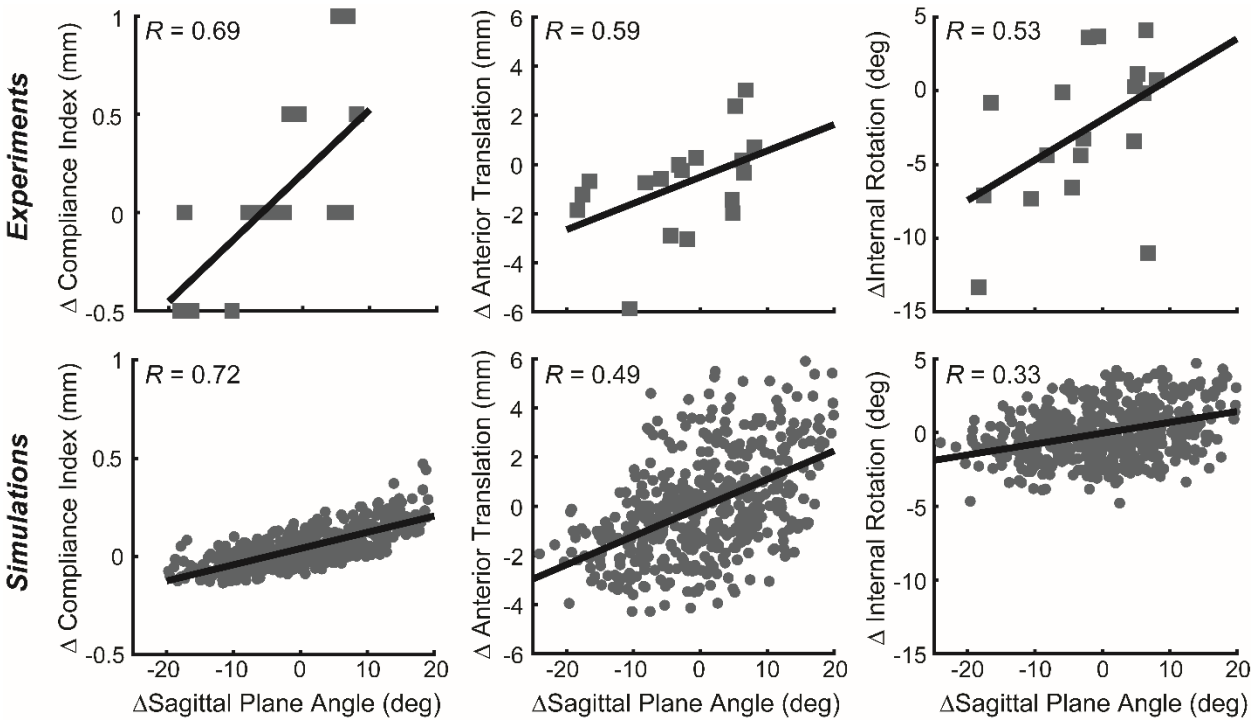

Figure 2: Correlations between post-operative tibiofemoral mechanics and sagittal plane graft angle measured experimentally (top row) and predicted by the model (bottom row). These scatter plots show representative examples of the agreement between experimental and simulation results. Both experiments and simulations show that a non-anatomic ACL sagittal plane angle leads to side-to-side differences in compliance index, anterior tibial translation, and internal tibial rotation during active knee extension. Similar agreement was observed between other ACL graft geometry metrics and knee mechanics metrics (Table 1).

The ACLR surgical simulations also provided insights into the sensitivity of knee mechanics during walking to ACL graft geometry, stiffness, and initial tension (Figure 3). At the time of peak ACL load, the model predicted that a more vertical graft in the sagittal plane and a more posterior tibial footprint location resulted in increased anterior tibial translation. In addition, a more vertical graft in the sagittal plane and a more anterior femoral footprint increased the peak ACL load. A greater ACL graft initial tension and stiffness led to an increase in the ACL force and a decrease in anterior tibial translation at the time of peak ACL load.

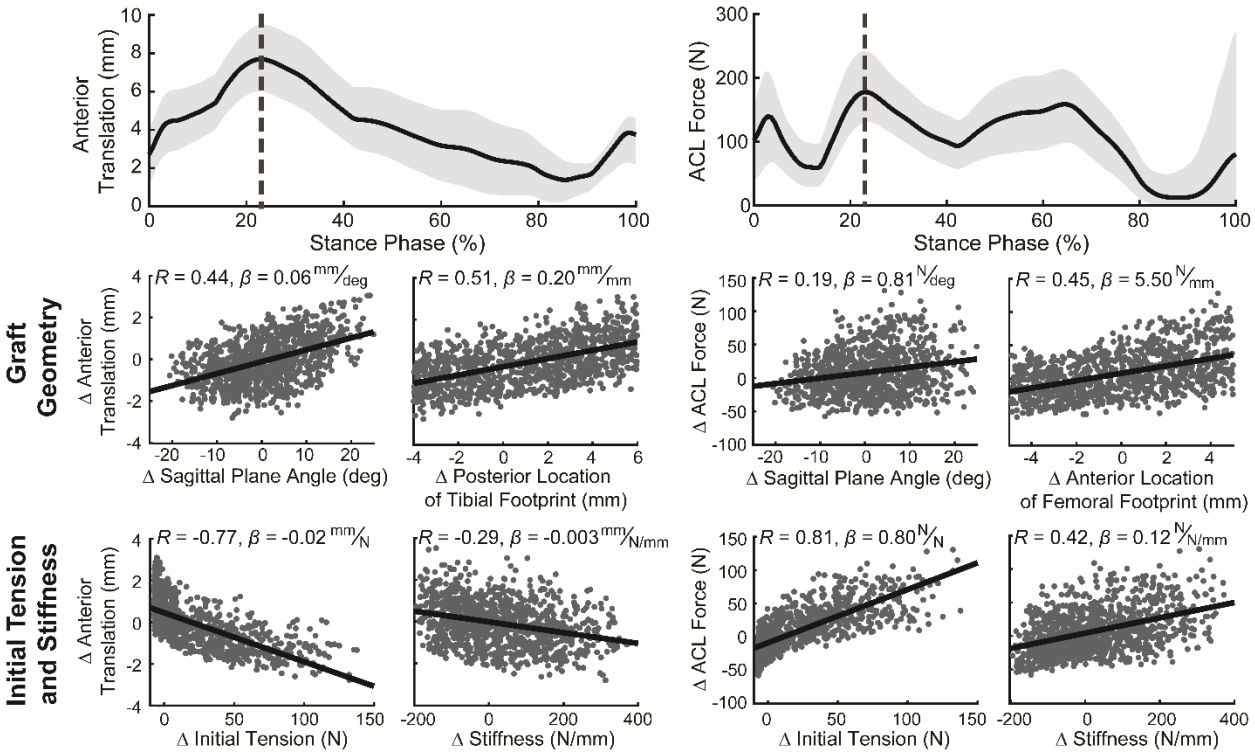

Figure 3: (top row) Plots show the mean (line) and the range between the 5 and 95 percentiles (light gray shaded region) for anterior tibial translation and ACL force during the stance phase of simulated walking for the 500 virtual ACLR with varying graft geometries, stiffnesses, and initial tensions. The scatter plots demonstrate the effect of ACL graft geometry (middle row) and graft initial tension and stiffness (bottom row) on anterior tibial translation and ACL force at the instance of peak ACL loading during stance (vertical dotted gray line in top plots). Each point in the scatter plots was computed relative to the native model (virtual ACLR minus native). Scatter plots also include the Spearman's correlation coefficient (R) and the coefficient of the least-squares linear regression (β) computed between the ACLR surgical factors and the internal knee mechanics metrics.

These effects of ACL geometry, stiffness, and initial tension on kinematics during walking extended to cartilage contact (Figure 4). During the stance phase, a more vertical graft in the sagittal plane led to a posterior migration in the center of pressure and an increase in the maximum contact pressure on the medial and lateral (R=-0.42, β=-0.04 $^{mm}/_{deg}$ and R=0.15, β=0.004 $^{MPa}/_{deg}$ respectively) tibial plateaus. Additionally, a more posterior tibial footprint led to a posterior migration in the center of pressure on the medial and lateral (R=-0.53, β=-

0.14 $^{mm}/_{mm}$) plateaus, an increase in contact pressure on the medial plateau, and a decrease in contact pressure on the lateral plateau (R=-0.15, β=-0.01 $^{MPa}/_{mm}$). A reduction in the graft initial tension and stiffness led to a posterior migration in the center of pressure on the medial and lateral (R=0.75, β=0.02$^{mm}/_{N}$ and R=0.31, β=0.002$^{mm}/_{N/mm}$, respectively) plateaus. Decreasing the graft initial tension and stiffness also led to an increase in the maximum contact pressure on the medial plateau and a decrease in the maximum contact pressure on the lateral plateau (R=0.8, β=0.005$^{MPa}/_{N}$ and R=0.46, β=0.0008$^{MPa}/_{N/mm}$, respectively).

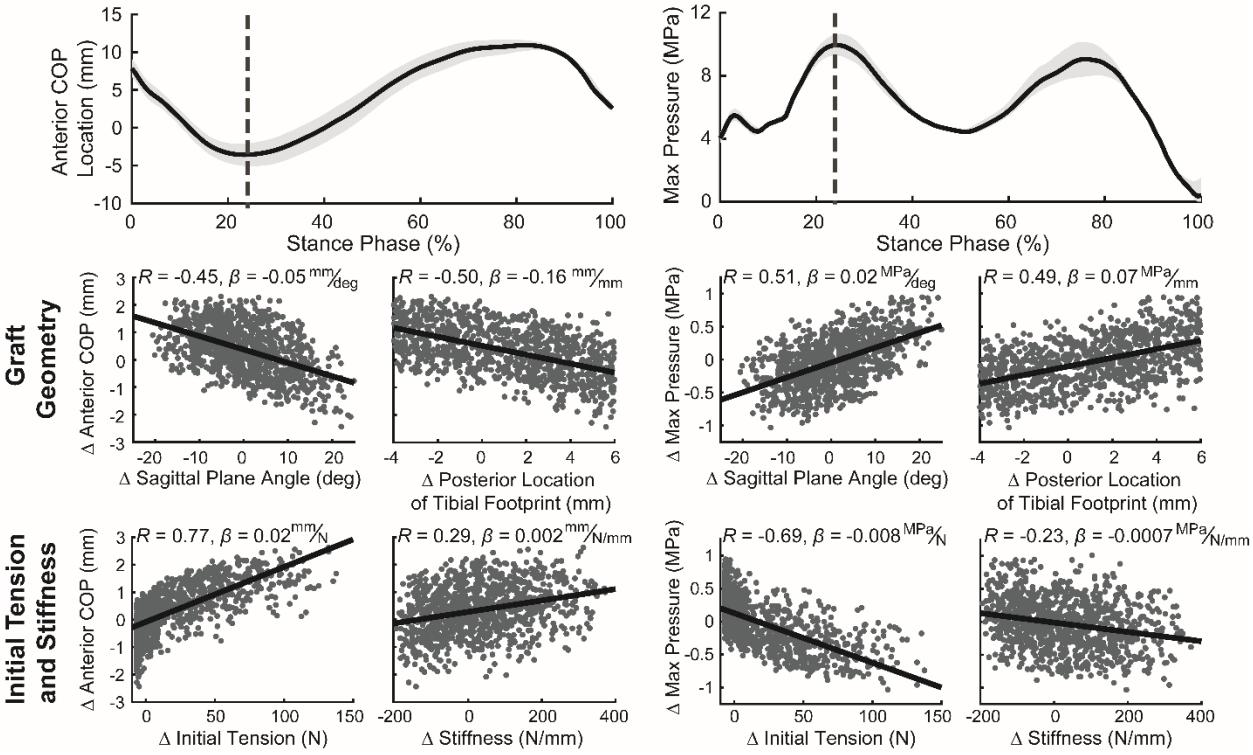

Figure 4: (top row) Plots show the mean (line) and the range between the 5 and 95 percentiles (light gray shaded region) for the anterior center of pressure (COP) location and the maximum contact pressure on the medial tibial plateau during the stance phase of simulated walking for the 500 virtual ACLRs. The scatter plots demonstrate the effect of ACL graft geometry (middle row) and graft initial tension and stiffness (bottom row) on the anterior COP location and maximum contact pressure on the medial tibial plateau at the instance of peak ACL loading during stance (vertical dotted gray line in top plots). Each point in the scatter plots was computed relative to the native model (virtual ACLR minus native). Scatter plots also include the Spearman's correlation coefficient (R) and the coefficient of the least-squares linear regression (β) computed between the ACLR surgical factors and the knee mechanics metrics.

4. Discussion

This study used a novel combination of dynamic MR imaging and computational models to investigate the influence of ACLR surgical factors on knee behavior during clinically relevant motions. Our results demonstrate that the placement of the graft in the sagittal plane is a primary geometric determinant of internal knee mechanics, with a more vertical graft inducing greater laxity, anterior tibial translation, and elevated cartilage contact pressure on the posterior aspect of the tibial plateau during walking. The effects of ACL graft geometry were notable even when other surgical factors (i.e. graft stiffness and initial tension) were simultaneously varied, indicating that graft geometry is a primary surgical factor affecting long-term joint behavior. To our knowledge, this is the first study to integrate both experiments and computational modeling to determine the effect of ACLR surgical factors on post-operative knee mechanics.

Optimal ACL graft placement has long been debated, with contemporary approaches tending to focus on the restoration of native ACL footprints (i.e. an anatomic graft placement).[16,40] This trend is supported by prior studies that have detected links between non-anatomic graft geometry and abnormal internal knee behavior. For example, a more vertical graft in the sagittal plane has been linked with greater anterior and rotational laxity[14,33] and larger anterior tibial translation, medial tibial translation, and internal rotation during a quasi-static lunge.[1] We observed similar results in this study, with a non-anatomic sagittal graft angle correlated with side-to-side differences in anterior laxity measures, and both anterior tibial translation and internal tibial rotation during active movement (Table 1). The causality of these relationships was confirmed with a probabilistic computational knee model, which predicted similar relationships between graft geometry, laxity, and tibiofemoral kinematics to those measured experimentally (Table 1 and Figure 2).

The consistency between experimental and modeling results provided confidence in extending the model to investigate the influence of surgical factors on knee mechanics during functional motion. We investigated over-ground walking, since altered cartilage loading during locomotion is considered to be one of the primary factors in initiating cartilage damage in ACLR knees.[19] To do this, we first randomly varied the femoral and tibial graft footprints to emulate the variability in tunnel placement present when surgeons attempt to restore native ACL footprints.[2,31] We simultaneously varied graft stiffness and initial tension to represent variations in graft properties and intraoperative tensioning.[15,34,52] Then, for each of the 500 virtual ACLRs, we simulated the internal knee mechanics that would arise during over-ground walking. These simulations again revealed a strong link between graft sagittal plane angle and functional knee mechanics, with a more vertical graft inducing greater anterior tibial translation, ACL loading, and contact pressure on the posterior tibial plateau (Figure 5). Both ACL stiffness and initial tension also affected the internal knee behavior, with lower stiffness and initial tension also resulting in greater anterior tibial translation and loading on the posterior tibial plateau (Figures 3 and 4).

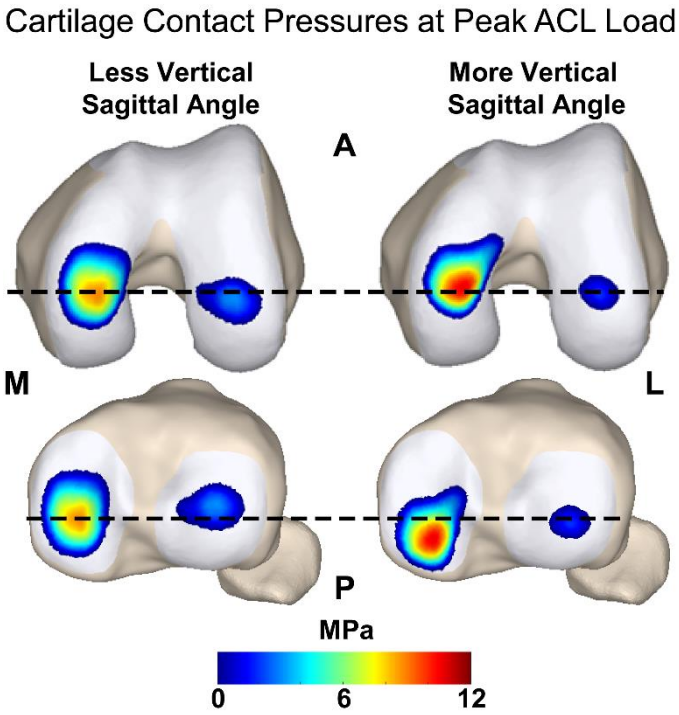

Figure 5: Representative cartilage contact pressures at the instance of peak ACL loading during simulated walking. A model with a less vertical sagittal graft angle (48º) is compared against a model with a more vertical sagittal graft angle (70º). The vertical graft resulted in larger anterior translation of the tibia relative to the femur. This manifested as the vertical graft leading to more anterior contact on the femur and more posterior contact on the tibial plateau. Additionally, a more vertical graft led to substantially greater contact pressure of the medial femoral and tibial cartilage surfaces.

The sensitivities of internal knee mechanics to variations in ACL graft geometry observed in this study may help in restoring common abnormalities seen in ACLR knees. Many studies have reported a bias towards external tibial rotation in ACLR knees during a range of tasks.[24,27,30,42,51] Further, a prior biplane fluoroscopy study of a quasi-static lunge found that ACLR knees exhibited a posterior-lateral shift in cartilage contact location on the tibial plateaus.[28] Our study suggests these biased kinematics and cartilage contact patterns could arise from biased ACL graft tunnel placements. In particular, we found that the graft sagittal plane angle was linked to asymmetries in external tibial rotation (Table 1) and anterior-posterior cartilage contact location (Figure 4). In

our surgical simulations, the sagittal plane graft angle was primarily influenced by the anterior and superior placement of the femoral footprint and the anterior placement of the tibial footprint (Figure 6). These findings suggest that reproducing the native graft sagittal plane angle through anatomical placement of the femoral and tibial graft footprints is critical to restore normative knee mechanics.

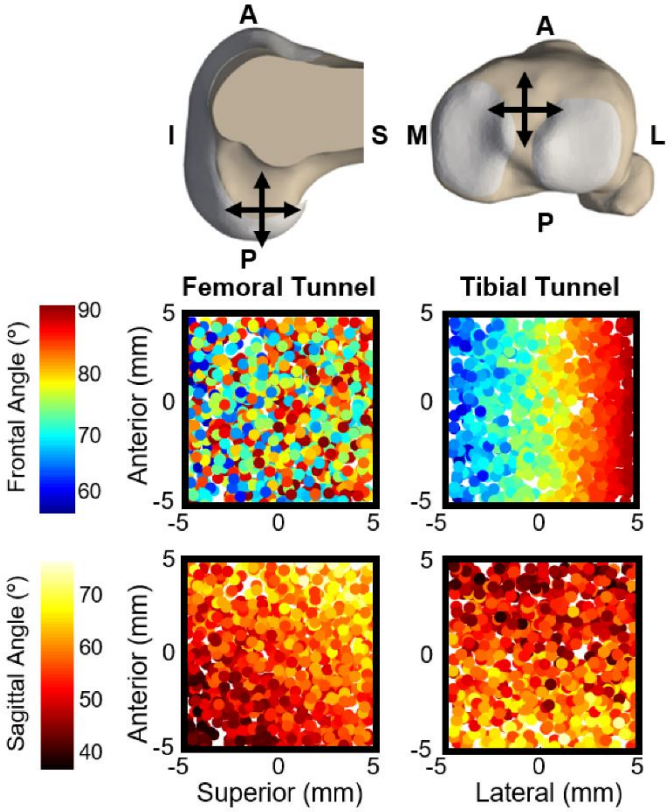

Figure 6: Composite image shows how changes to the femoral (top-left) and tibial (top-right) tunnel locations alter the frontal and sagittal plane angles of the ACL graft. Each dot in the four scatter plots represents the tunnel location in one of the 500 virtual ACLRs. The color of each dot indicates the resulting ACL graft angles measured with the knee in full extension, given the femoral and tibial tunnel locations of that virtual ACLR. From these scatter plots it is evident that femoral tunnel location does not systematically affect frontal plane angle of the graft. Femoral tunnel location does have a systematic effect on sagittal plane angle of the graft with a more posterior-inferior femoral tunnel resulting in a less vertical graft in the sagittal plane and a more anterior-superior femoral tunnel resulting in a more vertical graft in the sagittal plane. Tibial tunnel location systematically affects both frontal and sagittal plane angle of the graft.

Recent modifications to ACLR surgical techniques have focused on improving the accuracy of graft tunnel placement, thus allowing surgeons to more readily produce anatomic femoral and tibial graft footprints. Traditional transtibial graft placement typically produces femoral footprints an average of 8 to 9 mm from the center of the native femoral footprint.[2,31] Use of independent femoral and tibial tunnel drilling techniques (e.g. two-incision and accessory medial portal) has led to increased accuracy in tunnel placement,[40] with an average error of 3 mm in the femoral footprint location.[2] However, our findings suggest that errors in tunnel placement of this magnitude could still result in residual asymmetries in internal knee mechanics. Hence, further advancements in surgical technique, such as highly accurate placement of tunnels using computer-assisted and robotic guidance,[17,39] may be needed to fully restore normative mechanics.

Three limitations should be considered when interpreting the findings of this study. First, we did not control for graft type[54] or initial tension[12,38] in the experimental aspects of this study. To account for this, we randomly varied graft stiffness and initial tension, in addition to graft geometry, in the ACLR simulations. While the effects of stiffness and initial tension on simulated knee mechanics were qualitatively similar, initial tension had a relatively larger influence (Figures 3 and 4). However, it has previously been shown that graft stiffness and tension change following surgery due to graft relaxation and remodeling.[6,10,11] Hence, of the factors considered, graft geometry is the most controllable by surgeons over the long-term. Secondly, we did not simulate variations in muscle coordination strategies or walking dynamics, which have been shown to vary across ACLR patients[21] and can potentially influence *in vivo* knee behavior.[20] In future work, we plan to extend our study of ACLR surgical factors to include possible neuromuscular adaptations in walking behavior to gain insights into rehabilitation protocols for ACLR. Finally, we used a single knee model with fixed bone and cartilage geometry as segmented from MR images.

Previous studies have shown a link between variations in bone geometry and tibiofemoral kinematics.[49] Thus, this limitation may partially explain the reduced variation in knee kinematics observed in the surgical simulations, as compared to the experimental measurements (Figure 2). Advances in statistical shape modeling of the knee joint present exciting opportunities to systematically vary knee geometry,[49] and thus could be leveraged to better understand the interplay between bone geometry, ACLR surgical factors, and post-operative knee mechanics.

In conclusion, the findings of this study provide experimental and complementary simulation evidence that knee laxity, knee kinematics, cartilage contact, and ACL loading following ACLR are sensitive to surgical variability in ACL graft placement. This is potentially important to consider given the links between abnormal knee mechanics, cartilage degeneration, and early onset osteoarthritis in ACLR knees. Coupling these findings with future investigations to establish a threshold of acceptable altered cartilage loading could provide a better understanding of the accuracy in graft tunnel placement needed to improve long-term outcomes of ACLR.

References

1. Abebe E, Utturkar GM, Taylor DC, et al. The effects of femoral graft placement on in vivo knee kinematics after anterior cruciate ligament reconstruction. *J Biomech*. 2011;44(5):924-929. doi:10.1016/j.jbiomech.2010.11.028.
2. Abebe ES, Moorman CT, Dziedzic TS, et al. Femoral Tunnel Placement During Anterior Cruciate Ligament Reconstruction An In Vivo Imaging Analysis Comparing Transtibial and 2-Incision Tibial Tunnel–Independent Techniques. *Am J Sports Med*. 2009;37(10):1904-1911. doi:10.1177/0363546509340768.
3. Alford JW, Bach BR. Arthrometric Aspects of Anterior Cruciate Ligament Surgery

Before and After Reconstruction With Patellar Tendon Grafts. *Tech Orthop*. 2005;20(4):421-438. doi:10.1097/01.bto.0000190441.56526.92.

4. Anderst WJ, Tashman S. The association between velocity of the center of closest proximity on subchondral bones and osteoarthritis progression. *J Orthop Res*. 2009;27(1):71-77. doi:10.1002/jor.20702.
5. Arnold EM, Ward SR, Lieber RL, Delp SL. A Model of the Lower Limb for Analysis of Human Movement. *Natl Inst Heal*. 2011;38(2):269-279. doi:10.1007/s10439-009-9852-5.A.
6. Arnold MR, Lie DTT, Verdonschot N, De Graaf R, Amis AA, Van Kampen A. The remains of anterior cruciate ligament graft tension after cyclic knee motion. *Am J Sports Med*. 2005;33(4):536-542. doi:10.1177/0363546504269938.
7. Baldwin MA, Laz PJ, Stowe JQ, Rullkoetter PJ. Efficient probabilistic representation of tibiofemoral soft tissue constraint. *Comput Methods Biomech Biomed Engin*. 2009;12(6):651-659. doi:10.1080/10255840902822550.
8. Barry MJ, Kwon TH, Dhaher YY. Probabilistic musculoskeletal modeling of the knee: A preliminary examination of an ACL-reconstruction. *2010 Annu Int Conf IEEE Eng Med Biol Soc EMBC'10*. 2010:5440-5443. doi:10.1109/IEMBS.2010.5626511.
9. Beveridge JE, Heard BJ, Shrive NG, Frank CB. Tibiofemoral centroid velocity correlates more consistently with cartilage damage than does contact path length in two ovine models of stifle injury. *J Orthop Res*. 2013;31(11):1745-1756. doi:10.1002/jor.22429.
10. Beynnon BD, Uh BS, Johnson RJ, Fleming BC, Renstrom PA, Nichols CE. The elongation behavior of the anterior cruciate ligament graft in vivo. A long-term follow-up study. *Am J Sports Med*. 2001;29(2):161-166. doi:10.1177/03635465010290020801.

11. Blickenstaff KR, Grana WA, Egle D. Analysis of a Semitendinosus Autograft in a Rabbit Model. *Am J Sports Med*. 1997;25(4):554-559.

12. Brady MF, Bradley MP, Fleming BC, Fadale PD, Hulstyn MJ, Banerjee R. Effects of Initial Graft Tension on the Tibiofemoral Compressive Forces and Joint Position After Anterior Cruciate Ligament Reconstruction. *Am J Sports Med*. 2007;35(3):395-403. doi:10.1177/0363546506294363.

13. Brandon S, Smith CR, Thelen DG. Simulation of Soft Tissue Loading from Observed Movement Dynamics. In: *Handbook of Human Motion*. ; 2017. doi:1-34.10.1007/978-3-319-30808-1_172-1.

14. Brophy RH, Pearle AD. Single-Bundle Anterior Cruciate Ligament Reconstruction: A Comparison of Conventional, Central, and Horizontal Single-Bundle Virtual Graft Positions. *Am J Sports Med*. 2009;37(7):1317-1323. doi:10.1177/0363546509333007.

15. Brown CH, Wilson DR, Hecker AT, Ferragamo M. Graft-bone motion and tensile properties of hamstring and patellar tendon anterior cruciate ligament femoral graft fixation under cyclic loading. *Arthrosc - J Arthrosc Relat Surg*. 2004;20(9):922-935. doi:10.1016/j.arthro.2004.06.032.

16. Budny J, Fox J, Rauh M, Fineberg M. Emerging Trends in Anterior Cruciate Ligament Reconstruction. *J Knee Surg*. 2017;30:63-69.

17. Burkart A, Debski RE, McMahon PJ, et al. Precision of ACL tunnel placement using traditional and robotic techniques. *Comput Aided Surg*. 2001;6(5):270-278. doi:10.1002/igs.10013.

18. Chandrashekar N, Mansouri H, Slauterbeck J, Hashemi J. Sex-based differences in the tensile properties of the human anterior cruciate ligament. *J Biomech*. 2006;39(16):2943-

2950. doi:10.1016/j.jbiomech.2005.10.031.

19. Chaudhari AMW, Briant PL, Bevill SL, Koo S, Andriacchi TP. Knee kinematics, cartilage morphology, and osteoarthritis after ACL injury. *Med Sci Sports Exerc*. 2008;40(2):215-222. doi:10.1249/mss.0b013e31815cbb0e.

20. Chmielewski TL, Hurd WJ, Rudolph KS, Axe MJ, Snyder-mackler L. Perturbation Training Improves Knee Kinematics and Reduces Muscle Co-contraction After Complete Unilateral Anterior Cruciate Ligament Rupture. *Phys Ther*. 2005;85(8):740-754. doi:10.1093/ptj/85.8.740.

21. Ciccotti MG, Kerlan RK, Perry J, Pink M. An Electromyographic Analysis of the Knee During Functional Activities: II. The Anterior Cruciate Ligament-deficient and -reconstructed Profiles. *Am J Sports Med*. 1994;22(5):651-658. doi:10.1177/036354659402200513.

22. Delp SL, Loan JP. A Computational Framework For Simulating And Analyzing Human And Animal Movement. *Comput Sci Eng*. 2000:46-55. doi:10.1109/5992.877394.

23. Dhaher YY, Salehghaffari S, Adouni M. Anterior laxity, graft-tunnel interaction and surgical design variations during anterior cruciate ligament reconstruction: A probabilistic simulation of the surgery. *J Biomech*. 2016. doi:10.1016/j.jbiomech.2016.07.019.

24. Georgoulis AD, Papadonikolakis A, Papageorgiou CD, Mitsou A, Stergiou N. Three-dimensional tibiofemoral kinematics of the anterior cruciate ligament-deficient and reconstructed knee during walking. *Am J Sports Med*. 2003;31(1):75-79.

25. Griffin TM, Guilak F. The Role of Mechanical Loading in the Onset and Progression of Osteoarthritis. *Exerc Sport Sci Rev*. 2005;33(4):195-200. doi:10.1097/00003677-200510000-00008.

26. Grood ES, Suntay WJ. A joint coordinate system for the clinical description of three-dimensional motions: application to the knee. *J Biomech Eng*. 1983;105(2):136-144. doi:10.1115/1.3138397.

27. Hofbauer M, Thorhauer ED, Abebe E, Bey M, Tashman S. Altered Tibiofemoral Kinematics in the Affected Knee and Compensatory Changes in the Contralateral Knee After Anterior Cruciate Ligament Reconstruction. *Am J Sports Med*. 2014;42(11):2715-2721. doi:10.1177/0363546514549444.

28. Hosseini A, Van De Velde S, Gill TJ, Li G. Tibiofemoral Cartilage Contact Biomechanics in Patients after Reconstruction of a Ruptured Anterior Cruciate Ligament. 2012;(March):1781-1788. doi:10.1002/jor.22122.

29. Kaiser J, Bradford R, Johnson K, Wieben O, Thelen DG. Measurement of Tibiofemoral Kinematics Using Highly Accelerated 3D Radial Sampling. *Magn Reson Med*. 2013;69:1310-1316. doi:10.1002/mrm.24362.

30. Kaiser JM, Vignos MF, Kijowski R, Baer G, Thelen DG. Effect of Loading on In Vivo Tibiofemoral and Patellofemoral Kinematics of Healthy and ACL-Reconstructed Knees. *Am J Sports Med*. 2017;45(14). doi:10.1177/0363546517724417.

31. Kaseta MK, DeFrate LE, Charnock BL, Sullivan RT, Garrett WE. Reconstruction technique affects femoral tunnel placement in ACL reconstruction. *Clin Orthop Relat Res*. 2008;466(6):1467-1474. doi:10.1007/s11999-008-0238-z.

32. Lenhart RL, Kaiser J, Smith CR, Thelen DG. Prediction and Validation of Load-Dependent Behavior of the Tibiofemoral and Patellofemoral Joints During Movement. *Ann Biomed Eng*. 2015;43(11):2675-2685. doi:10.1007/s10439-015-1326-3.

33. Loh JC, Fukuda Y, Tsuda E, Steadman RJ, Fu FH, Woo SLY. Knee stability and graft

function following anterior cruciate ligament reconstruction: Comparison between 11 o'clock and 10 o'clock femoral tunnel placement. 2002 Richard O'Connor Award Paper Knee. *Arthrosc - J Arthrosc Relat Surg*. 2003;19(3):297-304. doi:10.1053/jars.2003.50084.

34. Mae T, Shino K, Matsumoto N, Hamada M, Yoneda M, Nakata K. Anatomical two-bundle versus Rosenberg's isometric bi-socket ACL reconstruction: A biomechanical comparison in laxity match pretension. *Knee Surgery, Sport Traumatol Arthrosc*. 2007;15(4):328-334. doi:10.1007/s00167-006-0172-0.

35. Mesfar W, Shirazi-Adl A. Biomechanics of changes in ACL and PCL material properties or prestrains in flexion under muscle force-implications in ligament reconstruction. *Comput Methods Biomech Biomed Engin*. 2006;9(4):201-209. doi:10.1080/10255840600795959.

36. Miranda DL, Rainbow MJ, Leventhal EL, Crisco JJ, Fleming BC. Automatic determination of anatomical coordinate systems for three- dimensional bone models of the isolated human knee. *J Biomech*. 2010;43(8):1623-1626. doi:10.1016/j.jbiomech.2010.01.036.

37. Musahl V. Varying Femoral Tunnels Between the Anatomical Footprint and Isometric Positions: Effect on Kinematics of the Anterior Cruciate Ligament-Reconstructed Knee. *Am J Sports Med*. 2005;33(5):712-718. doi:10.1177/0363546504271747.

38. Nicholas SJ, D'Amato MJ, Mullaney MJ, Tyler TF, Kolstad K, McHugh MP. A Prospectively Randomized Double-Blind Study on the Effect of Initial Graft Tension on Knee Stability After Anterior Cruciate Ligament Reconstruction. *Am J Sports Med*. 2004;32(8):1-6. doi:10.1177/0363546504265924.

39. Picard F, DiGioia AM, Moody J, et al. Accuracy in tunnel placement for ACL reconstruction. Comparison of traditional arthroscopic and computer-assisted navigation techniques. *Comput Aided Surg*. 2001;6(5):279-289. doi:10.1002/igs.10014.

40. Robin BN, Jani SS, Marvil SC, Reid JB, Schillhammer CK, Lubowitz JH. Advantages and Disadvantages of Transtibial, Anteromedial Portal, and Outside-In Femoral Tunnel Drilling in Single-Bundle Anterior Cruciate Ligament Reconstruction: A Systematic Review. *Arthrosc - J Arthrosc Relat Surg*. 2015;31(7):1412-1417. doi:10.1016/j.arthro.2015.01.018.

41. Scanlan SF, Andriacchi TP. Interactions Between Graft Placement, Gait Mechanics, and Premature Osteoarthritis Following Anterior Cruciate Ligament Reconstruction. *J Exp Clin Med*. 2011;3(5):207-212. doi:10.1016/j.jecm.2011.09.004.

42. Scanlan SF, Chaudhari AMW, Dyrby CO, Andriacchi TP. Differences in tibial rotation during walking in ACL reconstructed and healthy contralateral knees. *J Biomech*. 2010;43(9):1817-1822. doi:10.1016/j.jbiomech.2010.02.010.

43. Shelburne KB, Torry MR, Pandy MG. Contributions of Muscles, Ligaments, and the Ground-Reaction Force to Tibiofemoral Joint Loading During Normal Gait. *J Orthop Res*. 2006:1983-1989. doi:10.1002/jor.

44. Shin CS, Chaudhari AM, Andriacchi TP. The influence of deceleration forces on ACL strain during single-leg landing: A simulation study. *J Biomech*. 2007;40:1145-1152. doi:10.1016/j.jbiomech.2008.10.031.

45. Sirleo L, Innocenti M, Innocenti M, Civinini R, Carulli C, Matassi F. Post-operative 3D CT feedback improves accuracy and precision in the learning curve of anatomic ACL femoral tunnel placement. *Knee Surgery, Sport Traumatol Arthrosc*. 2018;26(2):468-477.

doi:10.1007/s00167-017-4614-7.

46. Smith CR, Lenhart RL, Kaiser J, Vignos MF, Thelen DG. Influence of Ligament Properties on Tibiofemoral Mechanics in Walking. *Journal of Knee Surgery*. 2015.

47. Smith CR, Vignos MF, Lenhart RL, Kaiser J, Thelen DG. The Influence of Component Alignment and Ligament Properties on Tibiofemoral Contact Forces in Total Knee Replacement. *J Biomech Eng*. 2016;138(c):1-10. doi:10.1115/1.4032464.

48. Smith CR, Won Choi K, Negrut D, Thelen DG. Efficient computation of cartilage contact pressures within dynamic simulations of movement. *Comput Methods Biomech Biomed Eng Imaging Vis*. 2016;1163(March):1-8. doi:10.1080/21681163.2016.1172346.

49. Smoger LM, Fitzpatrick CK, Clary CW, et al. Statistical Modeling to Characterize Relationships Between Knee Anatomy and Kinematics. *J Orthop Res*. 2015:1-11. doi:10.1002/jor.22948.

50. Suggs J, Wang C, Li G. The effect of graft stiffness on knee joint biomechanics after ACL reconstruction - A 3D computational simulation. *Clin Biomech*. 2003;18(1):35-43. doi:10.1016/S0268-0033(02)00137-7.

51. Tashman S, Collon D, Anderson K, Kolowich P, Anderst W. Abnormal Rotational Knee Motion During Running After Anterior Cruciate Ligament Reconstruction. *Am J Sports Med*. 2004;32(4):975-983. doi:10.1177/0363546503261709.

52. Tohyama H, Yasuda K. Significance of graft tension in anterior cruciate ligament reconstruction. Basic background and clinical outcome. *Knee Surg Sports Traumatol Arthrosc*. 1998;6 Suppl 1:S30-7. doi:10.1007/s001670050220.

53. Vignos MF, Kaiser JM, Baer GS, Kijowski R, Thelen DG. American Society of Biomechanics Clinical Biomechanics Award 2017: Non-anatomic graft geometry is linked

with asymmetric tibiofemoral kinematics and cartilage contact following anterior cruciate ligament reconstruction. *Clin Biomech*. 2018;56. doi:10.1016/j.clinbiomech.2018.05.008.

54. Webster KE, Feller JA. The knee adduction moment in hamstring and patellar tendon anterior cruciate ligament reconstructed knees. *Knee Surgery, Sport Traumatol Arthrosc*. 2012;20(11):2214-2219. doi:10.1007/s00167-011-1835-z.

55. Westphal CJ, Schmitz A, Reeder SB, Thelen DG. Load-dependent variations in knee kinematics measured with dynamic MRI. *J Biomech*. 2013;46(12):2045-2052. doi:10.1016/j.jbiomech.2013.05.027.

56. Whittington B, Silder A, Heiderscheit B, Thelen DG. The contribution of passive-elastic mechanisms to lower extremity joint kinetics during human walking. *Gait Posture*. 2008;27(4):628-634. doi:10.1016/j.gaitpost.2007.08.005.

57. Zavras TD, Race A, Amis AA. The effect of femoral attachment location on anterior cruciate ligament reconstruction: Graft tension patterns and restoration of normal anterior-posterior laxity patterns. *Knee Surgery, Sport Traumatol Arthrosc*. 2005;13(2):92-100. doi:10.1007/s00167-004-0541-5.

Chapter 5: Semi-automated Image Segmentation via Radial Projection to Assess Femoral, Tibial, and Patellar Cartilage Morphology

Michael F. Vignos, Isaac Loegering, Joshua D. Roth, Colin Smith, Wei Zha, Fang Liu, Richard Kijowski, and Darryl G. Thelen

(This chapter is prepared for submission to the *International Journal of Computer Assisted Radiology and Surgery*)

Abstract

Purpose: Assess the segmentation time, reproducibility, and accuracy of knee cartilage thickness maps created using semi-automated image segmentation via radial projections.

Methods: We acquired three-dimensional fast spin-echo (3D FSE Cube) magnetic resonance (MR) images (in-plane resolution: 0.31x0.31 mm, sagittal slice thickness: 1 mm) of three human knees at 3.0T. Three observers segmented the femoral, tibial, and patellar cartilage in each slice of the image sets, once manually and three times using the semi-automated method. The semi-automated method used a three-point radial line casting approach to identify the bone-cartilage interface and superficial cartilage surface boundary. The segmented slices were reconstructed into 3D cartilage geometries, and cartilage thickness was measured by projecting from the superficial cartilage surface to the bone-cartilage interface. Segmentation time, cartilage thickness measurements, and intra- and inter-observer reproducibility were compared between manual and semi-automated methods.

Results: There were no significant differences in thickness between semi-automated and manual segmentation methods for any of the cartilage surfaces, with an average difference of -0.07 ± 0.5 mm across all surfaces. Intra-observer reproducibility was high for the semi-automated method,

with average coefficients of variation for each observer ranging from 3-7%. Inter-observer reproducibility was similar between segmentation methods with similar average coefficients of variation (manual, 10 ± 4%; semi-automated, 11 ± 5%; p=0.4823) and intra-class correlation coefficients (manual, 0.91; semi-automated, 0.91) for each method. The semi-automated method reduced segmentation time by 27% on average, relative to a manual approach, with further time savings achievable by interpolating across images.

Conclusions: A radial projection cartilage segmentation method is shown to be efficient and sufficiently accurate for reconstructing cartilage geometries used in knee mechanics models, longitudinal studies of osteoarthritis, and the generation of large-scale databases needed for fully automated segmentation algorithms.

Keywords: MRI; knee cartilage; medical image segmentation; semi-automated segmentation; radial line casting; osteoarthritis

1. Introduction

Accurate assessment of cartilage morphology is important for modeling subject-specific joint mechanics [1, 2] and investigating the progression of osteoarthritis (OA) [3–7]. OA is a painful and debilitating degenerative joint disease affecting over 30 million adults in the United States [8]. OA commonly affects the knee and leads to long-term degeneration of the cartilage microstructure, and eventual thinning and loss of cartilage [9, 10]. It is increasingly recognized that cartilage tissue loading can influence the pathomechanics of OA [11–14] and, further, that joint morphology modulates joint mechanics [15]. Hence, there is now interest in using subject-specific loading information to tailor both conservative and surgical treatments of OA [16–18].

Radiography remains a standard for clinically assessing cartilage morphology. Plane radiographs can effectively identify cartilage thinning in moderate OA, but has poor sensitivity for detecting subtle changes in cartilage thickness over time [10]. Magnetic resonance (MR) imaging provides excellent contrast between soft tissues, allowing for the reconstruction of three-dimensional articular cartilage geometries [19, 20]. Such cartilage geometries can be incorporated into computational models to predict internal joint loading and deformation of cartilage tissue [21–24]. Further, cartilage thickness maps derived from cartilage geometries can be used to track disease- and treatment-related changes in cartilage morphology over time [3, 4].

Segmentation is a critical step in reconstructing articular cartilage geometries from MR images. Traditionally, 3D geometries are generated by manually segmenting the articular cartilage from each slice in a stack of images. However, this process is time-consuming and reliant on the user's experience level [25, 26], which makes large-scale investigations difficult. Automated cartilage segmentation methods have been proposed to reduce time and enhance consistency [4, 27–41]. Fully-automated methods, e.g. using atlas and deep learning-based algorithms, are

accurate and efficient [40, 41], but tend to require large training sets of data and have high computational costs [27–37, 40, 41]. Semi-automated methods enable the user to leverage automated algorithms, e.g. edge detection [42, 43] or region growing algorithms [44–47], to efficiently detect image features in stacks of images.

We recently proposed a semi-automated method that uses radial projections to detect cartilage tissue boundaries over the visible cartilage in an image slice [48]. To enable broad use of this radial projection algorithm, it is important to assess the efficiency, reproducibility, and cartilage thickness measurements and to compare to manual segmentation—the current gold-standard of MR image segmentation [4, 38–41]. Most prior evaluative studies have assessed accuracy of 2D segmentations of individual MR image slices [29, 30, 32–34, 40, 41]. However, this measure is insufficient for investigating the accuracy of 3D cartilage geometries and thickness maps that are important in computational models.

In this paper, we introduce a semi-automated cartilage segmentation method that uses radial projections and illustrate its use for assessing three-dimensional geometries of the femoral, tibial, and patellar cartilage. We then compare the efficiency, reproducibility, and cartilage thickness measurements of this semi-automated method to manual methods.

2. Methods

2.1. MR Imaging

MR imaging was performed on the dominant knee of one healthy male (34 years) and two healthy females (27 and 30 years) who had no history of prior knee pain, injury, or surgery. Subjects provided informed consent according to a University of Wisconsin-Madison Institutional Review Board-approved protocol. The MR imaging protocol consisted of a sagittal three-

dimensional intermediate weighted fast spin-echo sequence (3D FSE Cube); (in-plane resolution = 0.31 x 0.31 mm; slice thickness = 1.0 mm; number of slices = 96; imaging matrix = 384 x 384 x 96; repetition time = 2066.7 ms; echo time = 19.8 ms; flip angle = 90°; field of view = 14 cm; echo train length = 35; scan time = 6:48 min). Scans were performed on a 3.0T clinical MR scanner (Discovery MR750, GE Healthcare, Waukesha, WI) with an 8-channel phased-array extremity coil positioned around the knee (InVivo, Orlando, FL).

2.2. Semi-automated Segmentation Method

The articular cartilage of the femur, tibia, and patella were segmented from 3D MR images using a semi-automated radial-projection segmentation method implemented in MATLAB (Mathworks, Natick, MA) [48]. The segmented cartilage masks were used to generate 3D geometries, which were then used to create 3D thickness maps for each cartilage surface. The workflow for segmenting a single MR image slice consisted of the following steps: (1) manual selection of three seed points along the cartilage surface to compute a projection point, (2) automated detection of the cartilage boundary by radial line casting from the projection point defined in step 1, and (3) manual adjustment of the resulting mask when needed (Figure 1).These steps are discussed in detail in the following sections.

Step 1: Selection of Seed Points in a Image

The user was first asked to select three seed points along the visible cartilage in a counterclockwise fashion with the first (A) and third (C) points placed on the endpoints of the cartilage tissue (Fig. 1). A radial projection point was then computed and placed along the perpendicular bisector of the line that connected the two ends of the cartilage (Figure 1, line $\overline{AC}$). The length of the line connecting the cartilage endpoints was calculated and used to determine the

position of the projection point relative to $\overline{AC}$. The method for determining the position of the radial projection point differed slightly for femoral, tibial, and patellar cartilage surfaces being segmented (Figure 1).

Step 2: Radial Line Casting and Boundary Detection

Radial lines (i.e. rays) were then cast from the radial projection point (from step 1) toward the cartilage at uniform intervals from A to C (Figure 1). The image intensity along each radial line was then determined by interpolating the MR image. We then automatically identified the two points of maximum change in intensity along each ray. These two points generally correspond to 1) the edge of the deep cartilage surface reflecting the transition from bone to cartilage and 2) the edge of the superficial cartilage surface reflecting the transition from cartilage to surrounding tissue and synovial fluid. Contour points were then placed along these cartilage surface boundaries. The contour points on the inner and outer cartilage surfaces were checked to ensure the distance between each point and both its adjacent points did not exceed 1 cm—a heuristically defined threshold. If this threshold was exceeded for only one point in a local region, then this contour point was removed. If this threshold was exceeded for more than one point, then a B-spline curve was fit to this local region to smooth the contour points. This process iterated until the distance constraint was satisfied for all the contour points. A cubic B-spline curve was then fit to the final set of contour points to define the inner and outer cartilage contours.

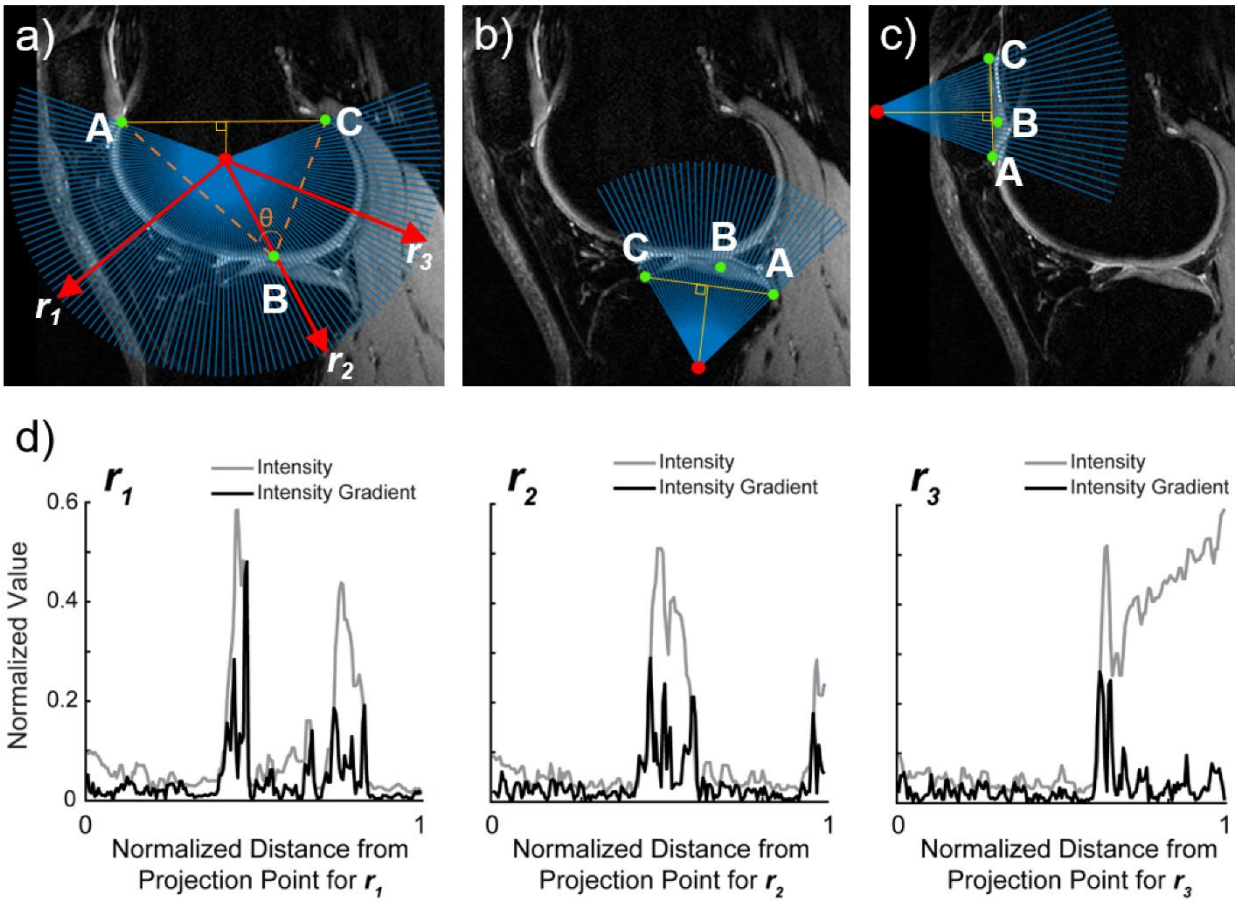

Figure 1: Semi-automated segmentation of each of the a) femoral, b) tibial, and c) patellar articular cartilage involved user selection of three seed points in a counterclockwise fashion with the first (A) and third (C) points placed on the endpoints of the cartilage. The second point (B) was selected along the cartilage surface and between the first and second points. A radial projection point (red dot) was then chosen along the perpendicular bisector of $\overline{AC}$. The length of $\overline{AC}$ (d_{AC}) was calculated and used to determine the position of the projection point relative to $\overline{AC}$. For the femoral cartilage (a), the central angle of the three seed points (θ) was first calculated. If $\theta < 90°$, the radial projection point was equidistant from the three seed points; if $90° \leq \theta < 180°$, the radial projection point was placed at 1.5 times d_{AC}; if $\theta \geq 180°$, the radial projection point was set at 0.5 times d_{AC}. These scale factors used for defining the radial projection point were determined empirically. For the relatively flat tibial (b) and patellar (c) cartilages, the radial projection points were positioned 1.5 and 2.5 times d_{AC}, respectively, from the midpoint of $\overline{AC}$ and along the perpendicular bisector of $\overline{AC}$. A series of radial lines were cast from the radial projection point toward the bone-cartilage interface at uniform intervals (1° for femur and tibia, 0.5° for patella) from point A to C. d) Plots show the normalized intensity and the normalized intensity gradient along three example radial lines (***r*₁**, left; ***r*₂**, middle; ***r*₃**, right) from the set of femoral radial lines shown in part a). These three example radial lines cross some of the interfaces commonly encountered by this radial projection algorithm (i.e. cartilage to fat, cartilage to cartilage, and

cartilage to muscle). For each radial line, the normalized intensity gradient was used to determine the location of the bone-cartilage interface and the superficial cartilage surface boundary

Step 3: Manual Checking of Contour Points

The user is then given the opportunity to inspect the cartilage contours generated in step 2. If the inner and outer cartilage boundaries look to have been accurately identified, then the user can approve the segmentation and move on to the next image. In cases where the user determines that there are regions where the contours deviate from the cartilage boundaries, the user is allowed to manually adjust the contour points. After manual editing, the cubic B-spline curve is re-fit to the contour points to generate the corrected cartilage contours.

Step 4 (optional): Interpolation of contours between slices

This semi-automated cartilage segmentation method provided two approaches for segmentation of an entire 3D MR image set: (1) segmenting each slice individually or (2) segmenting a subset of the image slices and then using contour interpolation. In the latter approach, interpolation was performed using both direct and indirect contour propagation. For both propagation techniques, a reference image slice was first defined as the segmented slice nearest the center of the image set. The contour on the reference image slice was then directly propagated to the target image slice using a feature tracking algorithm [49]. This algorithm propagated the cartilage contours from the reference slice to the adjacent slices sequentially until the target image slice was reached. Indirect propagation was performed by propagating the seed points from the reference to the target slice. The seed points were then used to perform radial line casting (step 2) and generate the cartilage contour on the target slice. The overlap of the contours generated from direct and indirect propagation was assessed by computing the Jaccard coefficient (Eq. 1) [50].

$$J(A,B) = 2\frac{|A \cap B|}{|A \cup B|}, \quad (1)$$

If the Jaccard coefficient was less than 0.5 (moderate overlap), then the user was prompted and given the option to accept or reject the interpolation.

Step 5: Creation of 3D Cartilage Thickness Maps

The final set of cartilage contours were then used to define the MR image voxels along the cartilage boundary. This was done by finding the voxel closest to each of the final contour points for each image slice. The cartilage boundary voxels were then connected into 3D isosurfaces and converted into triangular meshes (Figure 2). These resulting cartilage meshes were smoothed and decimated to a mesh density of 3.33 triangles/mm^2 (Geomagic, Research Triangle Park, NC). Cartilage thickness maps were computed from these meshes by projecting a normal vector from the center of each triangle on the superficial cartilage surface boundary (superficial surface) to the bone-cartilage interface (deep surface) and using the length of this vector as the cartilage thickness at that triangle (Figure 2).

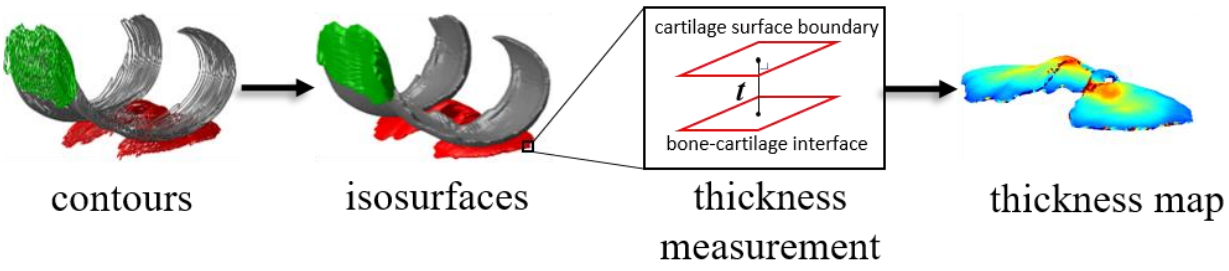

Figure 2: Workflow showing the generation of cartilage thickness maps from segmented contours. The superficial cartilage-surface boundary and the bone-cartilage interface were derived from the segmented contours of each MR image slice. 3D cartilage meshes were then constructed by generating isosurfaces from the contours. Cartilage thickness, ***t***, was calculated across each cartilage mesh to create thickness maps

2.3. Evaluation of Semi-Automated Segmentation Method

The semi-automated cartilage segmentation method was used to create 3D cartilage thickness maps of the articular cartilage of the femur, tibia, and patella from the 3D FSE Cube MR images of three knees. One experienced observer (O1, 50 knees segmented), one moderately trained observer (O2, 12 knees segmented), and one newly trained observer (O3, 3 knees segmented) segmented the knee cartilage of each of the three subjects. Each observer performed three semi-automated segmentations and one manual segmentation for each subject. The observers recorded the time required to perform each segmentation of the femoral, tibial, and patellar cartilage.

2.4. Efficiency of Segmentation Method

For the semi-automated and manual methods, the time required to segment the cartilage surfaces of the femur, tibia, and patella from each MR image set was recorded. These times were compared using a two-sample t-test.

2.5. Division of Cartilage Surfaces into Regions of Interest

Because cartilage morphology varies regionally, each of the femoral, tibial, and patellar cartilage meshes were split into regions of interest (ROIs) (Figure 4). The femur was divided into three ROIs: anterior, distal, and posterior. The tibia was divided into two ROIs: medial and lateral tibial plateaus. The patella was split into medial and lateral ROIs with the division running in the superior-inferior direction through the center of mass of the cartilage surface. Triangles along the boundary of each ROI were removed to analyze the regions of cartilage that experience the greatest

loads during functional movement and, thus, are most relevant when studying cartilage degeneration (Figure 4).

2.6. Comparison of 3D Cartilage Thickness Maps

For each ROI in the femoral, tibial, and patellar cartilage meshes, differences in the cartilage thickness maps generated using semi-automated segmentation and manual segmentation were computed (Fig. 3). To do this, the reference triangle for each triangle in the manual mesh was first computed by finding its nearest neighbor in the semi-automated mesh. The difference in the cartilage thickness was then computed for each of these triangle pairs, with a positive difference indicating a greater thickness in the semi-automatically segmented mesh [51]. The agreement between MR-derived cartilage thickness measurements from the two techniques was assessed for each ROI across all cartilage surfaces.

2.7. Intra- and Inter- Observer Reproducibility

Intra- and inter- observer reproducibility of the segmentation methods was determined by calculating the coefficients of variation (CVs) for the mean cartilage thickness within each ROI (Eq. 2).

$$CV = \frac{standard\ deviation\ of \bar{x}}{mean\ \bar{x}}, \tag{2}$$

where $\bar{x}$ is the set of mean cartilage thickness measurements for a given ROI. For intra-observer reproducibility, CVs were calculated for each observer across their three semi-automated segmentations. For inter-observer reproducibility, CVs were calculated for each segmentation method across the three observers. Inter-observer reproducibility was also assessed using intra-class correlation coefficients (ICC) [52, 53].

3. Results

Cartilage thickness maps generated from the semi-automated and manual segmentation methods showed similar thickness patterns throughout the cartilage (Figure 3), given that the average difference between these two segmentation methods across all triangles was -0.07 ± 0.5 mm. The largest average differences in thickness measurements occurred in the anterior region of the femoral cartilage (-0.2 ± 0.5 mm) and in the medial region of the patellar cartilage (0.2 ± 0.5 mm) (Figure 4). In general, the cartilage thickness measurements from these segmentation techniques were within 0.5 mm across each cartilage surface (Figure 5). There was a slight trend towards underprediction using the semi-automated method in thicker regions of the femoral and tibial cartilage.

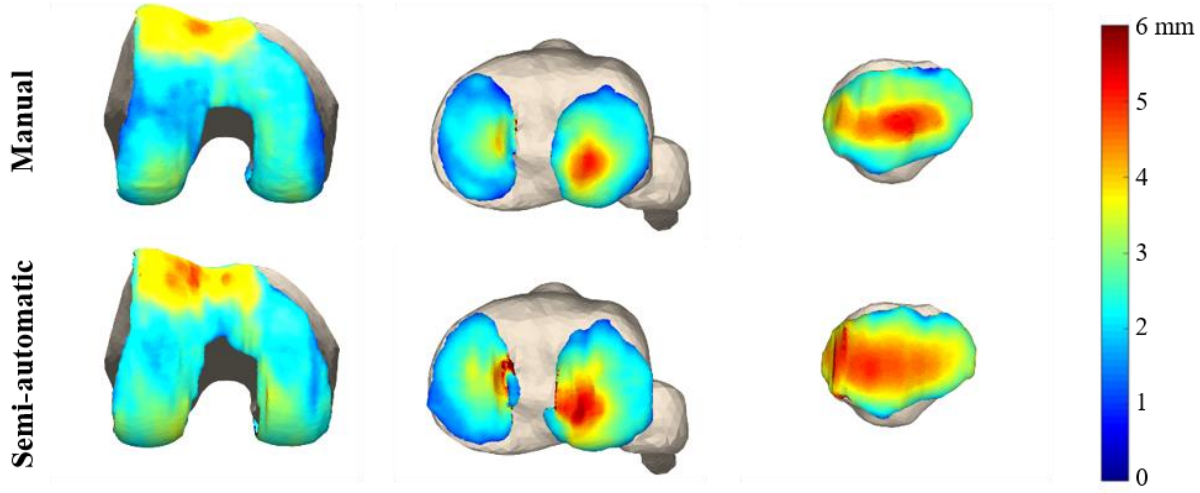

Figure 3: Representative cartilage thickness maps of the femur (left), tibia (middle), and patella (right) generated from manual (top) and semi-automated (bottom) segmentations of one subject's MR images performed by the same observer. Thickness maps generated using the semi-automated cartilage segmentation method were similar to those generated using manual segmentation. Similar patterns can be seen across the cartilage surfaces.

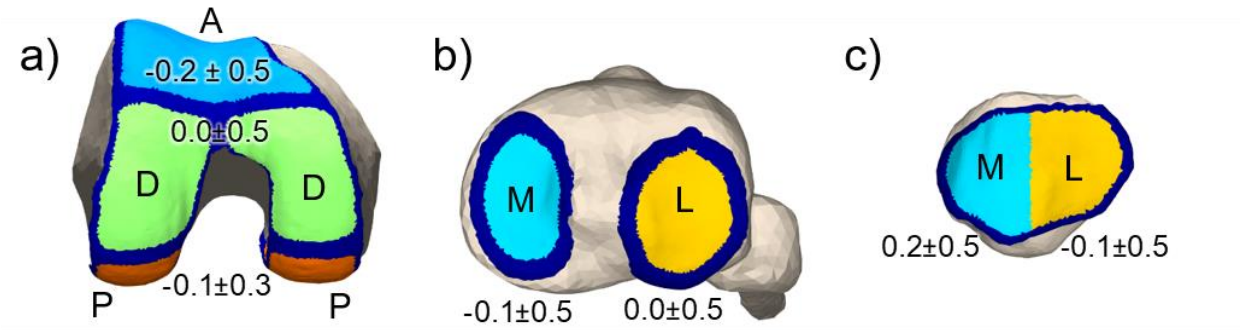

Figure 4: Regional analysis of cartilage thickness. For regional analysis of cartilage thickness, a) the femur was divided into anterior (A), distal (D), and posterior (P) regions of interest, and the b) tibia and c) patella were divided into medial (M) and lateral (L) regions. The difference (mean ± standard deviation in mm) between the semi-automated and manual thickness measurements is shown for each region. A positive difference indicates a greater cartilage thickness prediction by the semi-automated method

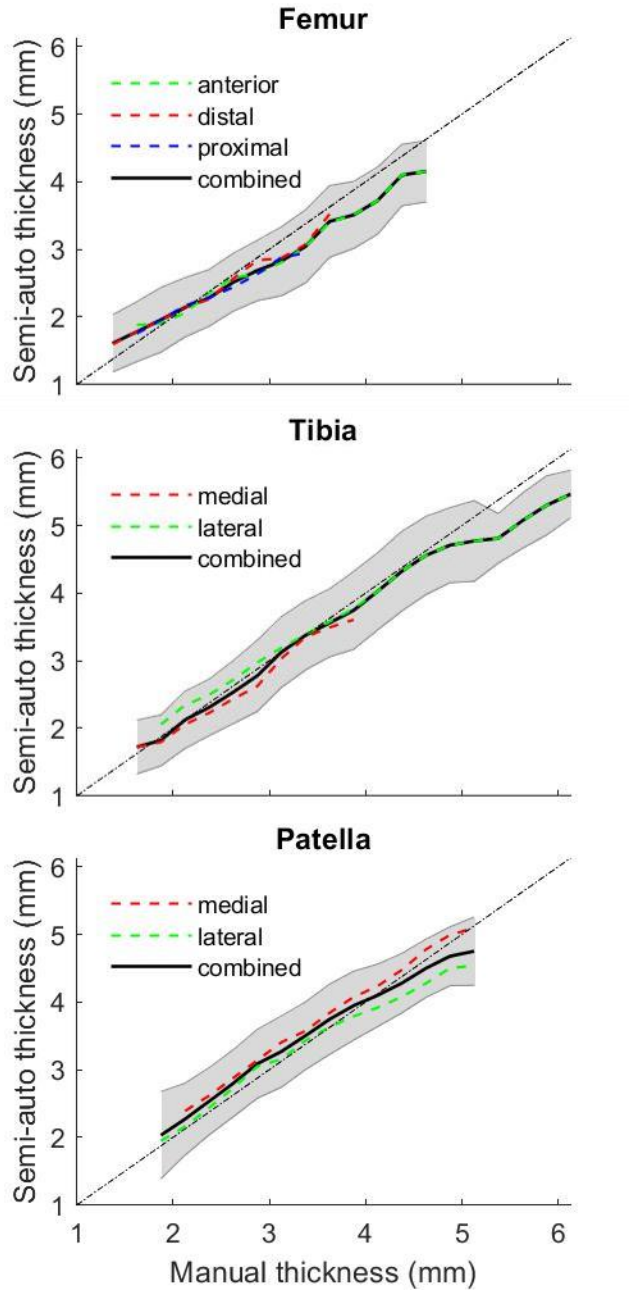

Figure 5: Plots of semi-automated segmentation vs. manual segmentation cartilage thickness measurements for each region of interest (dashed lines; mean) and combined (solid line; mean ± standard deviation) for each bone. The black dashed line in each plot shows perfect agreement between thickness measurements. Manual thickness measurements were grouped into 0.25 mm bins and the mean semi-automated thickness measurement for each bin was plotted. The thicker femoral cartilage and tibial cartilage falls only in the anterior and lateral regions, respectively; therefore, the region-specific (dashed) and combined (solid) lines overlap for the thicker femoral and tibial cartilage

The semi-automated segmentation method showed high reproducibility for measuring cartilage thickness. The average CV calculated for each ROI across all semi-automated segmentation trials showed a high degree of intra-observer reproducibility for each observer with O1 (experienced) and O2 (moderately experienced) showing slightly better reproducibility than O3 (inexperienced) (Table 1). Inter-observer reproducibility was comparable between methods with average CVs of 10 ± 3.7% and 11 ± 5.2% for manual and semi-automated methods ($p=0.4823$), respectively, and intra-class correlation coefficients of 0.91 for both methods (Table 2).

Table 1: Intra-observer reproducibility results. Average coefficient of variation (CV) (mean ± standard deviation), thickness, and standard deviation (SD) across all regions of interest for the semi-automated segmentations performed by observers O1, O2, and O3

	O1	**O2**	**O3**
Average CV (%)	3.0 ± 1.5	3.0 ± 1.6	7.2 ± 3.5
Average thickness (mm)	3.0 ± 0.84	2.4 ± 0.85	2.6 ± 0.83
Average SD (mm)	0.09 ± 0.05	0.08 ± 0.05	0.18 ± 0.08

Table 2: Inter-observer reproducibility results. Average coefficient of variation (CV) (mean ± standard deviation), thickness, and standard deviation (SD) and interclass correlation coefficients (ICC) across all regions of interest for the manual and semi-automated segmentations performed by observers O1, O2, and O3

	Manual	**Semi-Automated**
Average CV (%)	10 ± 3.7	11 ± 5.2
Average thickness (mm)	2.6 ± 0.84	2.7 ± 0.85
Average SD (mm)	0.28 ± 0.09	0.29 ± 0.11
ICC	0.91	0.91

The proposed semi-automated method resulted in a shorter average segmentation time than manual segmentation for an entire knee (semi-automated: 22 ± 6 sec/slice, manual: 30 ± 12 sec/slice, $p = 0.0185$). Additionally, segmentation time for each of the individual articular cartilage surfaces was shorter with the semi-automated method (Table 3).

Table 3: Segmentation times (mean ± standard deviation) for each bone across all subjects, observers, and trials

	Femur	**Tibia**	**Patella**
Semi-automated (sec/slice)	11 ± 3.5	6.0 ± 1.5	5.1 ± 1.6
Manual (sec/slice)	14 ± 5.8	9.7 ± 3.4	6.5 ± 3.2

4. Discussion

Growing interest in subject-specific joint modeling has escalated the need for more efficient and accurate cartilage segmentation methods given that manual segmentation is time-consuming and its accuracy is dependent on the experience of the observer [25, 26]. In this paper, we introduced a semi-automated segmentation method that uses a three-point radial line casting approach to reconstruct 3D articular cartilage morphology and generate cartilage thickness maps. We show that this method produces cartilage thickness maps with comparable accuracy and reproducibility to manual techniques, while reducing the time needed to segment images. The cartilage geometries can be directly incorporated in computational models of joint mechanics [54], and may also find utility for tracking changes in cartilage thickness in longitudinal studies of osteoarthritis.

Our semi-automated segmentation technique reduced segmentation time by 27% on average. The time savings can be furthered by not segmenting every slice in a stack of images, a technique previously shown to result in no reduction in accuracy or precision when every other slice is segmented [55]. While fully-automated cartilage segmentation methods could conceivably eliminate all manual user time [40, 41], these techniques need a pre-established database. Hence, our semi-automated method could provide a more efficient approach to segment images for this training database.

Our study assessed the accuracy of the newly developed cartilage segmentation method by comparing cartilage thickness measurements generated using the semi-automated and manual segmentation methods. In general, the cartilage thickness measurements generated with these techniques were within 0.5 mm (Figure 5), which is slightly greater than the in-plane image resolution (0.31 mm) which may reflect the lower limit for the segmentation accuracy. Notably, there was no bias in the semi-automated thickness predictions with only a slight trend towards

underprediction in the thickest cartilage regions (>5 mm). These thickest regions correspond to portions of the tibial and femoral cartilage surface that are in contact when the knee is in the MR scanning posture (approximately full extension). Determining the boundary of these cartilage surfaces in contact regions presents a segmentation challenge and, thus, may partially explain this trend in underestimation. Errors in cartilage thickness measurements may also result from inaccurate delineation of the bone-cartilage interface and the superficial cartilage surface boundary, which can occur in both manual and semi-automatic segmentations. Manual segmentation of the bone-cartilage interface is particularly prone to errors due to the low contrast between bone and the deep zone of cartilage in MR images [4]. Similarly, synovial fluid located near the superficial cartilage surface boundary can result in ambiguous boundaries. These sources of error may be minimized by the proposed semi-automated method since it uses objective measures of pixel intensity gradients to find the bone-cartilage interface and superficial cartilage surface boundary. The semi-automated method provides an additional advantage by allowing users to adjust misidentified contour points in regions of low image contrast. The higher average thickness measurements of O1 compared to the other observers (Table 2) may be the result of this observer adjusting the contour points based on previous segmentation experience.

We found intra-observer reproducibility for the semi-automated cartilage segmentation method comparable to that reported for manual segmentation methods [38], with the observers with the most knee cartilage segmentation experience (O1 and O2) exhibiting the best reproducibility. However, the observer with the least segmentation experience (O3) exhibited the highest variations in cartilage thickness measurements across repeat segmentations. These differences demonstrate that the proposed method still benefits from use by more experienced observers, especially during the optional manual correction of the contour points. The coefficients

of variation (CVs) for inter-observer reproducibility were higher than for intra-observer reproducibility, which agrees with previous findings [38]. Both CVs and intra-class correlation coefficients showed that both semi-automated and manual methods produced similar agreement across observers. This finding is important for large-scale investigations of cartilage morphology because it gives greater confidence in cartilage thickness measurements obtained by a wide-range of observers using this semi-automated segmentation method.

It is notable that our semi-automated algorithm was suitable for reconstructing femoral, tibial, and patellar cartilage morphologies given that all geometries are needed to model joint mechanics. The technique can readily be extended to other joints, e.g. hip, shoulder and ankle, with a simple modification of the radial projection point (Fig. 1). Our current study tested the segmentation algorithm on MRI images obtained from a 3D FSE Cube sequence, which has previously been shown to accurately capture knee cartilage morphology [56] and is readily available on clinical MR scanners. The semi-automated algorithm is likely suitable for other MR sequences that provide good contrast between cartilage and neighboring tissues.

In conclusion, we have developed and validated a new semi-automated cartilage segmentation method that uses a novel three-point radial line casting algorithm to identify the bone-cartilage interface and the superficial cartilage surface boundary of the knee articular cartilage from MR images. The semi-automated cartilage segmentation method was shown to provide accurate and repeatable measurements of cartilage morphology that may be suitable for use in computational joint mechanics models, longitudinal studies of OA progression, and generation of large-scale databases for fully automated segmentation algorithms.

Acknowledgements

The authors gratefully acknowledge the contributions of Kwang Won Choi, Jarred Kaiser, and Chihwa Song. This material is based upon work supported by the National Science Foundation Graduate Research Fellowship Program under Grant No. DGE-1747503 and the National Institutes of Health (EB015410). Any opinions, findings, and conclusions or recommendations expressed in this material are those of the author(s) and do not necessarily reflect the views of the NSF or NIH. Support was also provided by the Graduate School and the Office of the Vice Chancellor for Research and Graduate Education at the University of Wisconsin-Madison with funding from the Wisconsin Alumni Research Foundation.

References

1. Gerus P, Sartori M, Besier TF, Fregly BJ, Delp SL, Banks SA, Pandy MG, D'Lima DD, Lloyd DG (2013) Subject-specific knee joint geometry improves predictions of medial tibiofemoral contact forces. J Biomech 46:2778–2786 . doi: 10.1016/j.jbiomech.2013.09.005
2. Lenaerts G, De Groote F, Demeulenaere B, Mulier M, Van der Perre G, Spaepen A, Jonkers I (2008) Subject-specific hip geometry affects predicted hip joint contact forces during gait. J Biomech 41:1243–1252 . doi: 10.1016/j.jbiomech.2008.01.014
3. Eckstein F, Burstein D, Link TM (2006) Quantitative MRI of cartilage and bone: degenerative changes in osteoarthritis. NMR Biomed 19:822–854
4. Eckstein F, Cicuttini F, Raynauld J-P, Waterton JC, Peterfy C (2006) Magnetic resonance imaging (MRI) of articular cartilage in knee osteoarthritis (OA): morphological assessment. Osteoarthr Cartil 14:46–75

5. Favre J, Erhart-Hledik JC, Chehab EF, Andriacchi TP (2016) Baseline ambulatory knee kinematics are associated with changes in cartilage thickness in osteoarthritic patients over 5 years. J Biomech 49:1859–1864 . doi: 10.1016/j.jbiomech.2016.04.029

6. Favre J, Erhart-Hledik JC, Blazek K, Fasel B, Gold GE, Andriacchi TP (2017) Anatomically Standardized Maps Reveal Distinct Patterns of Cartilage Thickness With Increasing Severity of Medial Compartment Knee Osteoarthritis. J Orthop Res 35:2442–2451 . doi: 10.1002/jor.23548

7. Wirth W, Hunter DJ, Nevitt MC, Sharma L, Kwoh CK, Ladel C, Eckstein F (2017) Predictive and concurrent validity of cartilage thickness change as a marker of knee osteoarthritis progression: Data from the osteoarthritis initiative. Osteoarthr Cartil 25:2063–2071 . doi: 10.1016/j.joca.2017.08.005

8. Barbour KE, Helmick CG, Boring M, Brady TJ (2017) Vital Signs: Prevalence of Doctor-Diagnosed Arthritis and Arthritis-Attributable Activity Limitation — United States, 2013–2015. MMWR Morb Mortal Wkly Rep 66:246–253 . doi: 10.15585/mmwr.mm6609e1

9. Litwic A, Edwards MH, Dennison EM, Cooper C (2013) Epidemiology and burden of osteoarthritis. Br Med Bull 105:185–199 . doi: 10.1093/bmb/lds038

10. Amin S, LaValley MP, Guermazi A, Grigoryan M, Hunter DJ, Clancy M, Niu J, Gale DR, Felson DT (2005) The relationship between cartilage loss on magnetic resonance imaging and radiographic progression in men and women with knee osteoarthritis. Arthritis Rheumatol 52:3152–3159

11. Griffin TM, Guilak F (2005) The Role of Mechanical Loading in the Onset and Progression of Osteoarthritis. Exerc Sport Sci Rev 33:195–200 . doi: 10.1097/00003677-200510000-00008

12. Beveridge JE, Heard BJ, Shrive NG, Frank CB (2013) Tibiofemoral centroid velocity correlates more consistently with cartilage damage than does contact path length in two ovine models of stifle injury. J Orthop Res 31:1745–1756 . doi: 10.1002/jor.22429
13. Anderst WJ, Tashman S (2009) The association between velocity of the center of closest proximity on subchondral bones and osteoarthritis progression. J Orthop Res 27:71–77 . doi: 10.1002/jor.20702
14. Buckwalter JA, Anderson DD, Brown TD, Tochigi Y, Martin JA (2013) The Roles of Mechanical Stresses in the Pathogenesis of Osteoarthritis: Implications for Treatment of Joint Injuries. Cartilage 4:286–294 . doi: 10.1177/1947603513495889
15. Smoger LM, Fitzpatrick CK, Clary CW, Cyr AJ, Maletsky LP, Rullkoetter PJ, Laz PJ (2015) Statistical Modeling to Characterize Relationships Between Knee Anatomy and Kinematics. J Orthop Res 33:1620–1630 . doi: 10.1002/jor.22948
16. Mootanah R, Imhauser CW, Reisse F, Carpanen D, Walker RW, Koff MF, Lenhoff MW, Rozbruch SR, Fragomen AT, Dewan Z, Kirane YM, Cheah K, Dowell JK, Hillstrom HJ (2014) Development and validation of a computational model of the knee joint for the evaluation of surgical treatments for osteoarthritis. Comput Methods Biomech Biomed Engin 17:1502–1517 . doi: 10.1080/10255842.2014.899588
17. Gardiner BS, Woodhouse FG, Besier TF, Grodzinsky AJ, Lloyd DG, Zhang L, Smith DW (2016) Predicting Knee Osteoarthritis. Ann Biomed Eng 44:222–233 . doi: 10.1007/s10439-015-1393-5
18. Liukkonen MK, Mononen ME, Klets O, Arokoski JP, Saarakkala S, Korhonen RK (2017) Simulation of subject-specific progression of knee osteoarthritis and comparison to experimental follow-up data: Data from the osteoarthritis initiative. Sci Rep 7:1–14 . doi:

10.1038/s41598-017-09013-7

19. Roemer FW, Crema MD, Trattnig S, Guermazi A (2011) Advances in imaging of osteoarthritis and cartilage. Radiology 260:332–354
20. Guermazi A, Niu J, Hayashi D, Roemer FW, Englund M, Neogi T, Aliabadi P, McLennan CE, Felson DT (2012) Prevalence of abnormalities in knees detected by MRI in adults without knee osteoarthritis: population based observational study (Framingham Osteoarthritis Study). Bmj 345:e5339
21. Lenhart RL, Kaiser J, Smith CR, Thelen DG (2015) Prediction and Validation of Load-Dependent Behavior of the Tibiofemoral and Patellofemoral Joints During Movement. Ann Biomed Eng 43:2675–2685 . doi: 10.1007/s10439-015-1326-3
22. Guess TM (2012) Forward dynamics simulation using a natural knee with menisci in the multibody framework. Multibody Syst Dyn 28:37–53 . doi: 10.1007/s11044-011-9293-4
23. Kiapour A, Kiapour AM, Kaul V, Quatman CE, Wordeman SC, Hewett TE, Demetropoulos CK, Goel VK (2014) Finite Element Model of the Knee for Investigation of Injury Mechanisms : Development and Validation. J Biomech Eng 136:1–14 . doi: 10.1115/1.4025692
24. Andriacchi TP, Briant PL, Bevill SL, Koo S (2006) Rotational Changes at the Knee after ACL Injury Cause Cartilage Thinning. Clin Orthop Relat Res 442:39–44 . doi: 10.1097/01.blo.0000197079.26600.09
25. Yushkevich PA, Piven J, Hazlett HC, Smith RG, Ho S, Gee JC, Gerig G (2006) User-guided 3D active contour segmentation of anatomical structures: significantly improved efficiency and reliability. Neuroimage 31:1116–1128
26. Stammberger T, Eckstein F, Michaelis M, Englmeier KH, Reiser M (1999) Interobserver

reproducibility of quantitative cartilage measurements: Comparison of B-spline snakes and manual segmentation. Magn Reson Imaging 17:1033–1042 . doi: 10.1016/S0730-725X(99)00040-5

27. Tamez-Peña JG, Farber J, Gonzalez PC, Schreyer E, Schneider E, Totterman S (2012) Unsupervised segmentation and quantification of anatomical knee features: data from the Osteoarthritis Initiative. IEEE Trans Biomed Eng 59:1177–1186
28. Liu J, Udupa JK (2009) Oriented active shape models. IEEE Trans Med Imaging 28:571–584
29. Suzuki K (2012) Pixel-based machine learning in medical imaging. Int J Biomed Imaging 1–18 . doi: 10.1155/2012/792079
30. Koo S, Gold GE, Andriacchi TP (2005) Considerations in measuring cartilage thickness using MRI: factors influencing reproducibility and accuracy. Osteoarthr Cartil 13:782–789
31. Cohen ZA, Mccarthy DM, Kwak SD, Legrand P, Fogarasi F, Ciaccio EJ, Ateshian GA (1999) Knee cartilage topography, thickness, and contact areas from MRI: in-vitro calibration and in-vivo measurements. Osteoarthr Cartil 7:95–109
32. Zhou Z, Zhao G, Kijowski R, Liu F (2018) Deep Convolutional Neural Network for Segmentation of Knee Joint Anatomy. Magn Reson Med 1–12 . doi: 10.1002/mrm.27229
33. Liu F, Zhou Z, Jang H, Samsonov A, Zhao G, Kijowski R (2018) Deep convolutional neural network and 3D deformable approach for tissue segmentation in musculoskeletal magnetic resonance imaging. Magn Reson Med 79:2379–2391 . doi: 10.1002/mrm.26841
34. Fripp J, Crozier S, Warfield SK, Ourselin S (2010) Automatic segmentation and quantitative analysis of the articular cartilages from magnetic resonance images of the knee. IEEE Trans Med Imaging 29:55–64

35. Ye T, Cui X, Kim H (2015) Fully automated segmentation of cartilage from magnetic resonance images using improved 3D shape context and active shape model. Osteoarthr Cartil 23:A301–A302 . doi: https://doi.org/10.1016/j.joca.2015.02.546

36. León M, Escalante-Ramirez B (2013) Segmentation of knee cartilage by using a hierarchical active shape model based on multi-resolution transforms in magnetic resonance images. Proc SPIE - Int Soc Opt Eng 8922: . doi: 10.1117/12.2035534

37. Solloway S, Hutchinson CE, Waterton JC, Taylor CJ (1997) The use of active shape models for making thickness measurements of articular cartilage from MR images. Magn Reson Med 37:943–952

38. Pang J, Li P, Qiu M, Chen W, Qiao L (2015) Automatic articular cartilage segmentation based on pattern recognition from knee MRI images. J Digit Imaging 28:695–703

39. Zhang K, Deng J, Lu W (2011) Segmenting human knee cartilage automatically from multi-contrast MR images using support vector machines and discriminative random fields. In: 18th IEEE International Conference on Image Processing (ICIP). IEEE, Brussels, Belgium, pp 721–724

40. Yin Y, Zhang X, Williams R, Wu X, Anderson DD, Sonka M (2010) LOGISMOS—layered optimal graph image segmentation of multiple objects and surfaces: cartilage segmentation in the knee joint. IEEE Trans Med Imaging 29:2023–2037

41. Yu HJ, Chang A, Fukuda Y, Terada Y, Nozaki T, Yoshioka H (2016) Comparison of semi-automated and manual segmentation of knee cartilage. Osteoarthr Cartil 24:S311 . doi: https://doi.org/10.1016/j.joca.2016.01.560

42. Lorigo LM, Faugeras O, Grimson WEL, Antipolis S, Kikinis R (1998) Segmentation of Bone in Clinical Knee MRI Using Texture-Based Geodesic Active Contours. In: Wells

WM, Colchester A, Delp S (eds) Medical Image Computing and Computer-Assisted Intervention - MICCAI ’98. MICCAI 1998. Lecture Notes in Computer Science, vol 1496. Springer, Berlin, Heidelberg, pp 1195–1204

43. Lynch JA, Zaim S, Zhao J, Stork A, Peterfy CG, Genant HK (2000) Cartilage segmentation of 3D MRI scans of the osteoarthritic knee combining juser knowledge and active contours. Proc SPIE 3979, Med Imaging 2000 Image Process 925–935 . doi: 10.1117/12.387758

44. Freixenet J, Muñoz X, Raba D, Martí J, Cufí X (2002) Yet Another Survey on Image Segmentation: Region and Boundary Information Integration. In: Heyden A, Sparr G, Nielsen M, Johansen P (eds) Computer Vision — ECCV 2002. ECCV 2002. Lecture Notes in Computer Science, vol 2352. Springer, Berlin, Heidelberg, pp 408–422

45. Saad NM, Abu-Bakar S, Muda S, Mokji M, Abdullah A (2012) Automated Region Growing for Segmentation of Brain Lesion in Diffusion-weighted MRI. Proc Int MultiConference Eng Comput Sci 1:1–4 . doi: 10.13140/2.1.2036.0321

46. Hojjatoleslami SA, Kittler J (1998) Region growing: A new approach. IEEE Trans Image Process 7:1079–1084 . doi: 10.1109/83.701170

47. Wu J, Poehlman S, Noseworthy MD, Kamath M V. (2009) Texture Feature based Automated Seeded Region Growing in Abdominal MRI Segmentation. J Biomed Sci Eng 2:1–8 . doi: 10.1109/BMEI.2008.352

48. Won Choi K, Song C, Kijowski R, Thelen DG (2016) Systems and methods for semi-automated segmentation of medical images. 1–8

49. Messerli A, Grinsted A (2015) Image georectification and feature tracking toolbox: ImGRAFT. Geosci Instrumentation, Methods Data Syst 4:23–34 . doi: 10.5194/gi-4-23-

2015

50. Tustison NJ, Gee JC (2009) Introducing Dice, Jaccard, and Other Label Overlap Measures To ITK. Insight J

51. Koo S, Giori NJ, Gold GE, Dyrby CO, Andriacchi TP (2009) Accuracy of 3D cartilage models generated from MR images is dependent on cartilage thickness: laser scanner based validation of in vivo cartilage. J Biomech Eng 131:121004

52. Koo TK, Li MY (2016) A guideline of selecting and reporting intraclass correlation coefficients for reliability research. J Chiropr Med 15:155–163

53. McGraw KO, Wong SP (1996) Forming inferences about some intraclass correlation coefficients. Psychol Methods 1:30–46

54. Baldwin MA, Langenderfer JE, Rullkoetter PJ, Laz PJ (2010) Development of subject-specific and statistical shape models of the knee using an efficient segmentation and mesh-morphing approach. Comput Methods Programs Biomed 97:232–240 . doi: 10.1016/j.cmpb.2009.07.005

55. Hunter DJ, Niu J, Zhang Y, Totterman S, Tamez J, Dabrowski C, Davies R, Le Graverand M-PH, Luchi M, Tymofyeyev Y, Beals CR (2009) Change in cartilage morphometry: a sample of the progression cohort of the Osteoarthritis Initiative. Ann Rheum Dis 68:349 . doi: 10.1136/ard.2007.082107

56. Chen CA, Kijowski R, Shapiro LM, Tuite MJ, Davis KW, Klaers JL, Block WF, Reeder SB, Gold GE (2010) Cartilage morphology at 3.0 T: Assessment of three-dimensional magnetic resonance imaging techniques. J Magn Reson Imaging 32:173–183

Conclusions and Future Directions

This thesis aimed to directly assess the link between abnormal knee mechanics and early signs of cartilage degeneration in ACLR knees and, then, to investigate the effect of ACLR surgical factors on post-operative knee mechanics. This was achieved by first assessing the link between quantitative MR relaxation parameters measured via a mcDESPOT sequence and cartilage mechanical properties. The associations found in this investigation provided confidence in using this quantitative MR sequence to track changes in cartilage health in ACLR knees. As discussed in Chapter 1, an additional motivation of this study was to investigate the potential to use the mcDESPOT sequence as a non-invasive method of assessing cartilage mechanical properties. While the observed link between mcDESPOT relaxation parameters and cartilage properties provides promise for this application, further work is needed to assess the robustness and accuracy of this relationship. Fortunately, this work is already moving forward with more cadaveric cartilage resections being imaged, along with additional testing techniques (i.e. unconfined compression and microindentation) being used to characterize mechanical properties and histology and biochemical analyses being used to assess macromolecular content of the cartilage tissue. These data will be used to further assess the accuracy of this link between mcDESPOT relaxation parameters and cartilage mechanical properties and to determine if this relationship is subject-specific. Additionally, the findings in Chapter 1 suggest that, regardless of how many samples are tested, there will still be some variability in cartilage mechanical properties assessed using quantitative MR imaging. The next step in this work is to use the probabilistic modeling techniques discussed in Chapter 4 to assess the variability in computational model predictions as a result of variability in cartilage properties. This will provide an understanding of the confidence bounds for the predictions of this modeling framework.

This thesis then investigated the commonly cited theory that abnormal knee mechanics following ACLR initiate cartilage degeneration. We found that abnormal cartilage contact was linked to progressive changes in cartilage composition, which provides support for this theory. It is interesting that most of the changes in cartilage contact and composition were observed on the medial tibial plateau, which is the same region in which OA development most commonly occurs in this population [1]. However, it is important to note that these findings are associative and do not indicate a cause-effect relationship between knee mechanics and changes in cartilage health. It is well-known that there are a cascade of additional changes that occur within the knee joint following an ACL injury and subsequent ACLR that may also contribute to cartilage degeneration, including acute cartilage damage sustained at injury [2], subchondral bone bruising [3], and inflammation within the joint capsule [4, 5]. Thus, future work is needed to assess the interaction between these changes and altered cartilage contact mechanics in the progression of OA. This will likely require a well-controlled model of cartilage degeneration and altered knee mechanics. Therefore, a combination of animal models and high-fidelity cartilage models may be necessary to investigate the causal link between altered knee mechanics and the development of OA following ACLR.

This thesis then determined that variability in ACL graft tunnel placement leads to altered knee mechanics during both simple and functional movements. These studies (Chapters 3 and 4) were motivated by the findings of Chapter 2, given that Chapter 2 showed that altered knee mechanics may initiate cartilage degeneration in ACLR knees. However, to further assess the link between ACL graft tunnel placement and cartilage degeneration, the next step is to investigate the relationship between ACL graft geometry (from Chapters 3 and 4) and longitudinal changes in cartilage composition (from Chapter 2). This will allow for a more direct assessment of the link

between ACLR surgical technique and long-term cartilage health. Additionally, through the use of probabilistic surgical simulations, we determined that additional ACLR surgical factors (i.e. graft stiffness and initial tension) also influence post-operative knee mechanics. Using these surgical simulations, we can begin to assess the interaction between these surgical factors to determine an ideal approach to restoring normative knee mechanics with current ACLR techniques.

The final chapter of this thesis assessed the accuracy, reproducibility, and efficiency of a semi-automated technique for the segmentation of knee articular cartilage in comparison to manual segmentation. This study provided confidence in the cartilage contact measurements of the other chapters of this thesis, given that this segmentation algorithm was commonly used to generate the cartilage models for each ACLR subject. Inaccurate segmentation of the articular cartilage would lead to large errors in the contact measurements. Thus, this study confirmed that this semi-automated segmentation method was appropriate for our application.

In the final chapter, we also concluded that this semi-automated segmentation algorithm was faster than the gold-standard of manual segmentation. While statistically true, the difference between the speed of these techniques may not be noticeable unless one is performing a large volume of segmentations. Truly, the future of MR image segmentation lies in fully-automated techniques, the most promising of which utilize machine-learning and deep-learning based algorithms [6, 7]. These techniques can produce complete knee segmentations within a few seconds with accuracy comparable to manual techniques. However, these fully-automated algorithms require large amounts of training data and are not currently widely available. Thus, this semi-automated segmentation method may be a useful option for efficiently generating the training data needed for fully-automated techniques or for researchers that only need to segment a small number of knees. Additionally, in collecting and analyzing the data for this thesis we generated a

large number of segmented MR images that can be used as a training data set for these fully-automated algorithms. I am currently in the process of applying one of these algorithms [6] to our data to mitigate the need for manual segmentation by future members of our lab.

While this thesis provides insight into the development of OA following ACLR, these findings open the question of the next steps in attempting to mitigate the risk of OA and improving long-term outcomes of this patient population. In Chapters 3 and 4, we showed that small variations in tunnel placement can lead to relatively large shifts in knee mechanics. The next step in this work to assess the sensitivity of cartilage health to these shifts in knee mechanics. Understanding this sensitivity is necessary to determine the accuracy needed in graft placement to mitigate the risk of cartilage degeneration following ACLR. The data used in Chapter 2 could be used to initially investigate this sensitivity given that bilateral differences in graft geometry can be assessed for each subject and coupled with longitudinal measures of cartilage composition. However, it is important to note that experienced, fellowship-trained surgeons are highly accurate in graft placement with 'errors' of 2 to 3 mm with independent tunnel drilling techniques [8, 9]. To further improve the accuracy of tunnel placement it may be necessary to explore use of robot-assisted or computer-navigated surgical techniques, which have become more common in orthopedic applications with the adoption of robot-assisted joint replacements. While an expensive option, data such as those presented in this thesis are beginning to show that restoring normative knee mechanics during an ACLR may help reduce the risk of OA and, thus, reduce the financial burden associated with the current incidence of OA. Additionally, we have begun to investigate the link between ACL graft tunnel 'grading' performed by surgeons of different experience levels and post-operative knee mechanics (Appendix A). Data such as these may serve as an additional

training tool for surgeons, to provide a more clear relationship between decisions made during surgery and patient outcomes.

In conclusion, this thesis couples longitudinal *in vivo* assessments of knee mechanics and cartilage composition with probabilistic surgical simulations to conclude that optimal graft tunnel placement is critical to restore normative knee mechanics and, thus, to mitigate the risk of OA following ACLR. This is the first study to provide a direct link between abnormal *in vivo* cartilage contact and early signs of cartilage degeneration in ACLR knees. Further, this is also the first study to couple experimental measurements and computational model predictions to assess the effect of ACLR surgical factors on post-operative knee mechanics. Given the ever-advancing technologies for assessing joint mechanics and cartilage health and recent trends towards patient-specific medicine, I am excited to follow future modifications and improvements for the treatment of ACL injuries.

References

1. Barenius B, Ponzer S, Shalabi A, et al (2014) Increased risk of osteoarthritis after anterior cruciate ligament reconstruction: a 14-year follow-up study of a randomized controlled trial. Am J Sports Med 42:1049–57 . doi: 10.1177/0363546514526139
2. Bolbos RI, Ma CB, Link TM, et al (2008) In vivo T1rho quantitative assessment of knee cartilage after anterior cruciate ligament injury using 3 Tesla magnetic resonance imaging. Invest Radiol 43:782–788 . doi: 10.1097/RLI.0b013e318184a451; 10.1097/RLI.0b013e318184a451
3. Johnson DL, Bealle DP, Brand Jr. JC, et al (2000) The effect of a geographic lateral bone bruise on knee inflammation after acute anterior cruciate ligament rupture. Am J Sport

Med 28:152–155 . doi: 10.1177/03635465000280020301

4. Elsaid KA, Fleming BC, Oksendahl HL, et al (2008) Decreased lubricin concentrations and markers of joint inflammation in the synovial fluid of patients with anterior cruciate ligament injury. Arthritis Rheum 58:1707–1715 . doi: 10.1002/art.23495
5. Marks PH, Donaldson MLC (2005) Inflammatory Cytokine Profiles Associated With Chondral Damage in the Anterior Cruciate Ligament-Deficient Knee. Arthrosc J Arthrosc Relat Surg 21:1342–1347 . doi: 10.1016/j.arthro.2005.08.034
6. Liu F, Zhou Z, Jang H, et al (2018) Deep convolutional neural network and 3D deformable approach for tissue segmentation in musculoskeletal magnetic resonance imaging. Magn Reson Med 79:2379–2391 . doi: 10.1002/mrm.26841
7. Zhou Z, Zhao G, Kijowski R, Liu F (2018) Deep Convolutional Neural Network for Segmentation of Knee Joint Anatomy. Magn Reson Med In Press:1–12 . doi: 10.1002/mrm.27229
8. Abebe ES, Moorman CT, Dziedzic TS, et al (2009) Femoral Tunnel Placement During Anterior Cruciate Ligament Reconstruction An In Vivo Imaging Analysis Comparing Transtibial and 2-Incision Tibial Tunnel–Independent Techniques. Am J Sports Med 37:1904–1911 . doi: 10.1177/0363546509340768
9. Robin BN, Jani SS, Marvil SC, et al (2015) Advantages and Disadvantages of Transtibial, Anteromedial Portal, and Outside-In Femoral Tunnel Drilling in Single-Bundle Anterior Cruciate Ligament Reconstruction: A Systematic Review. Arthrosc - J Arthrosc Relat Surg 31:1412–1417 . doi: 10.1016/j.arthro.2015.01.018

Appendix A: Association between Surgeon Graft Tunnel Grading and Tibiofemoral Kinematics following ACL Reconstruction: A Preliminary Investigation

Following anterior cruciate ligament reconstruction (ACLR) surgeons will commonly 'grade' the quality of their graft tunnel placement. This is typically done by obtaining anterior-posterior (AP) and lateral radiographs of the patient's reconstructed knee and assessing if the location at which the tunnel enters the joint capsule is 'anatomic'. Since the location of the native ACL footprint is unknown, 'anatomic' is typically defined as the expected location of the native ACL footprint based off bony landmarks within the radiograph. While this practice of grading ACLR graft tunnels is not currently standardized, it is commonly done by many surgeons as a means of assessing the quality of their tunnel placement. We previously found that variations in graft tunnel placement affect post-operative knee mechanics. Thus, we sought to investigate the link between ACL graft tunnel grading and tibiofemoral kinematics.

In this preliminary investigation, we used data previously collected on 18 subjects that underwent a primary, unilateral ACLR and were reported in Chapter 3 (9 male, 9 female, 24.8 ± 5.7 yrs, 78.9 ± 16.5 kg, 20.2 ± 8.7 months post-op, 9 bone-patellar tendon-bone grafts, 9 hamstrings tendon grafts). Briefly, bilateral static and dynamic magnetic resonance (MR) images were collected for each subject and used to measure tibiofemoral kinematics during active, loaded knee flexion-extension. We then computed the tibiofemoral kinematics at peak knee flexion. We then had two orthopedic surgeons (surgeon 1: 12 years as a fellowship-trained sports medicine surgeon; surgeon 2: 2 years as a fellowship-trained sports medicine surgeon) grade the femoral and tibial tunnel graft placement of each subject. Given that this was a preliminary investigation, the surgeons graded the tunnel placement using the static MR images, as opposed to the more common approach of using radiographs. We used a grading system to reflect how well the graft tunnel footprint matched the native ACL footprint to standardize the grading across surgeons (Figure 1).

Since these MR images were collected post-ACLR, the native ACL footprint was no longer visible. Thus, we allowed each surgeon to use his own method for assessing the location of the native ACL footprint. We then computed the Pearson's correlation coefficients between the graft tunnel grade and the absolute side-to-side differences (reconstructed minus contralateral) in tibiofemoral kinematics at peak knee flexion ($\alpha = 0.05$).

The absolute side-to-side differences in anterior tibial translation and internal tibial rotation were significantly correlated with femoral tunnel score when grouping the tunnel grading of both surgeons together (Figure 2). However, when analyzing the femoral tunnel scores of each surgeon independently, we observed a significant correlation between femoral tunnel score and abnormal anterior tibial translation and internal tibial rotation for only the more experienced surgeon (i.e. surgeon 1) (Figure 3). A trend towards significance was observed for the correlation between abnormal anterior tibial translation and femoral tunnel score for the less experienced surgeon (i.e. surgeon 2). No correlation was observed between abnormal internal tibial rotation and femoral tunnel score for surgeon 2.

The ACL graft tunnel grading of the more experienced surgeon was more strongly linked to post-operative tibiofemoral kinematics, than that of the less experienced surgeon. This finding may reflect a link between greater experience and an improved understanding of ideal graft placement based off landmarks in a static MR image. However, it is unknown how this finding translates to the assessment of ideal graft placement during arthroscopic tunnel drilling. Additionally, this finding may reflect a potential opportunity to provide training to less experienced surgeons in the grading of ACL graft tunnels. By providing feedback to surgeons on subjects with large bilateral differences in tibiofemoral kinematics, but tunnels scored as 'good', we may be able to close the gap in understanding the link between tunnel placement and patient

outcomes. This approach may also allow us to develop a standardized approach to grade ACL graft tunnel placement. However, future work is need to assess the link between graft tunnel grading and post-operative kinematics across a wider range of surgeons and experience levels.

Name: _____ Date: _____

Years as a fellowship trained surgeon: _____

ACL Reconstruction Tunnel Location Assessment:

Please assess how well the femoral and tibial tunnel footprints match the native ACL footprints for each patient.
1 = tunnel footprint is completely outside of the native ACL footprint.
3 = center of the tunnel footprint aligns with the outer edge of the native ACL footprint.
5 = center of the tunnel footprint perfectly aligns with the native ACL footprint.

	Femoral Tunnel Footprint Location									**Tibial Tunnel Footprint Location**									
	Tunnel footprint Native ACL footprint									Tunnel footprint Native ACL footprint									
Patient	**1**		**2**		**3**		**4**		**5**	**1**		**2**		**3**		**4**		**5**	
1	☐	☐	☐	☐	☐	☐	☐	☐	☐	☐	☐	☐	☐	☐	☐	☐	☐	☐	☐
2	☐	☐	☐	☐	☐	☐	☐	☐	☐	☐	☐	☐	☐	☐	☐	☐	☐	☐	☐
3	☐	☐	☐	☐	☐	☐	☐	☐	☐	☐	☐	☐	☐	☐	☐	☐	☐	☐	☐
4	☐	☐	☐	☐	☐	☐	☐	☐	☐	☐	☐	☐	☐	☐	☐	☐	☐	☐	☐
5	☐	☐	☐	☐	☐	☐	☐	☐	☐	☐	☐	☐	☐	☐	☐	☐	☐	☐	☐
6	☐	☐	☐	☐	☐	☐	☐	☐	☐	☐	☐	☐	☐	☐	☐	☐	☐	☐	☐

Figure 1: Graft tunnel grading system used by surgeons. The system ranged from 1 to 5 points, with 5 indicating an ideal tunnel placement and 1 indicating a poor tunnel placement. During grading, we allowed surgeons to assign a score to the femoral and tibial tunnels independently in 0.5 point increments.

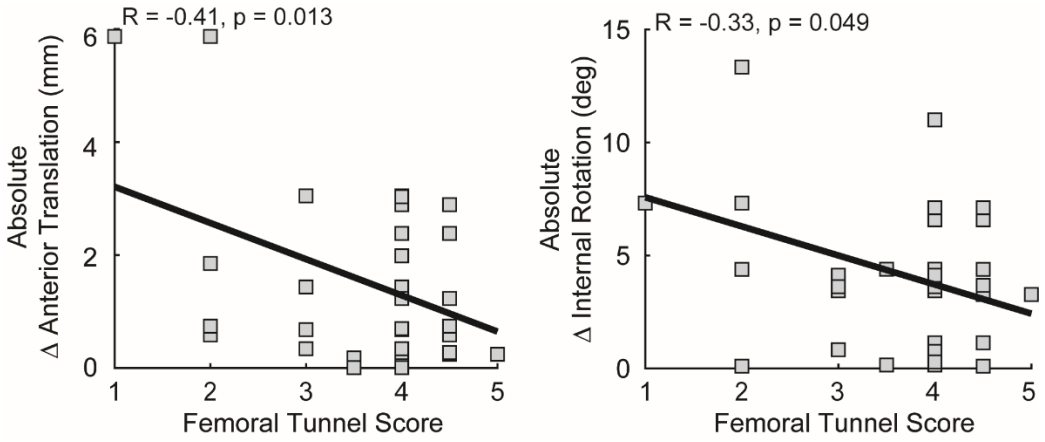

Figure 2: Scatter plots show the correlation between abnormal tibiofemoral kinematics and the femoral tunnel scores for both surgeons. The absolute side-to-side difference in anterior tibial translation and internal tibial rotation were correlated with the femoral tunnel score when grouping the scores for both surgeons.

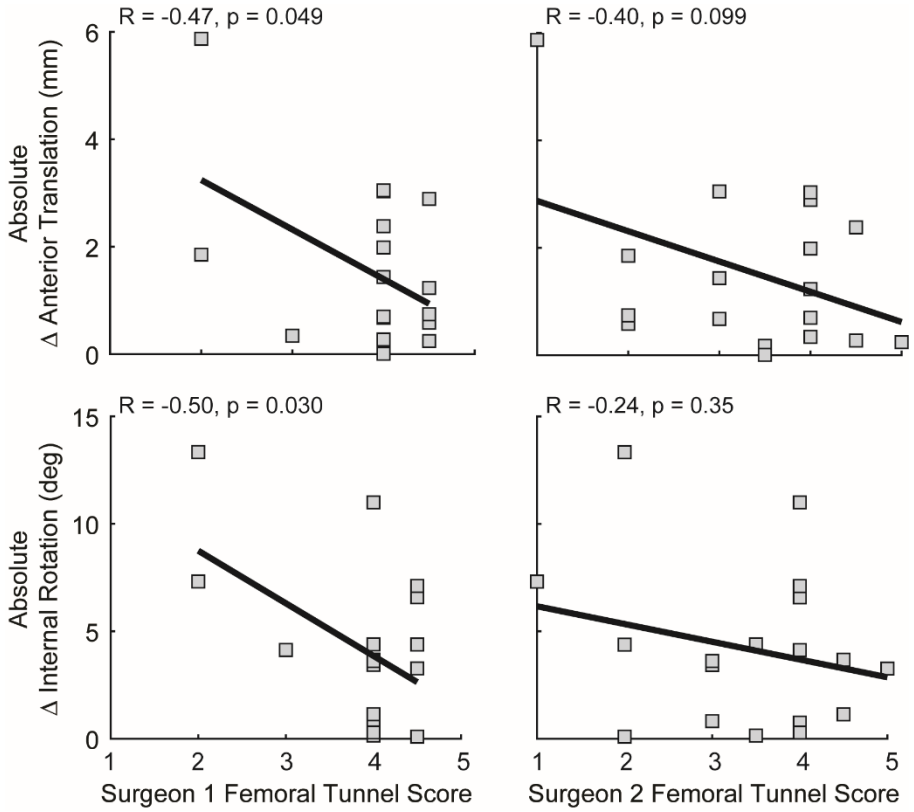

Figure 3: Scatter plots show the correlation between abnormal tibiofemoral kinematics and the femoral tunnel score for each surgeon. The absolute side-to-side difference in anterior tibial translation and internal tibial rotation were significantly correlated with the femoral tunnel score for the more experienced surgeon (i.e. surgeon 1). However, only a trend towards significance was observed between the absolute side-to-side difference in anterior tibial translation and the femoral tunnel score for the less experienced surgeon (i.e. surgeon 2).